Concrete pavement prediction life model based on electrical response of concrete-CNTs sensors under fatigue loading

Doctoral Dissertation
Doctoral Program in Department of Environment, Land and Infrastructure Engineering

Concrete pavement prediction life model based on electrical response of concrete-CNTs sensors under fatigue loading

By

Mostafa Adresi

******

Supervisor(s):
Prof. A. ,Hassani
Prof. G. ,Lacidogna
Dr. P. ,Antonaci

Doctoral Examination Committee:
Prof. A. ,Kavussi, Referee, University of Tarbiat Modares
Prof. S. M. ,Asgharzadeh , Referee, University of Tarbiat Modares
Prof. J. M. ,Tulliani, Referee, Politecnico di Torino
Prof. G. ,Ventura, Referee, Politecnico di Torino

Politecnico di Torino
2017

Declaration

I hereby declare that the contents and organization of this dissertation constitute my own original work and does not compromise in any way the rights of third parties, including those relating to the security of personal data.

Mostafa Adresi

2017

* This dissertation is presented in partial fulfillment of the requirements for **Ph.D. degree** in the Graduate School of Politecnico di Torino (SCUDO).

I would like to dedicate this thesis to my loving parents and wife

Acknowledgment

I would like to express the deepest appreciation to my supervisors, Professors Abolfazl Hassani, Giuseppe Lacidogna and Dr. Paola Antonaci, who have the attitude and the substance of a genius: they continually and convincingly conveyed a spirit of adventure in regard to research and scholarship, and an excitement in regard to teaching. Without their guidance and persistent help this dissertation would not have been possible.

I would like to thank my PhD board members, Professor Ali Yazdian and Professor Mohammad Reza Soleimani, whose work demonstrated to me how I can solve the technical and educational problems and guide me to gain my goal.

In addition, a thank you to Professor Jean Marc Tulliani, who invited me to Politecnico di Torino as sabbatical student and gave me a chance to continue my study in double degree program. During my life in Torino, he helped me more than a formal regulation and he was my really best friend, so this is my great pleasure to thank him a lot. I thank the Politecnico di Torino and Tarbiat Modares University and their staff for their help to finish this dissertation. I also thank Mr. Gharashi and Mr. Di Vasto for their help as testing lab instructors. Finally, I would also like to thank to Dr. Mohammad Javad Zarif the Foreign Minister of the Islamic Republic of Iran and Italian Ministry of Education, which helped me to continue my study in Italy.

Abstract

Structural Health Monitoring (SHM) of important infrastructures such as Portland cement concrete pavements plays a key role in pioneer societies, to guarantee the optimum usability and performance of the infrastructure system. As an example, this is imperative to appraise the destruction level in Portland cement concrete pavements along time as to plan their maintenance with proper actions at the right time. Based on this premise, the goal of this study is to extend an extensive feasibility study to set up a novel approach for SHM of Portland cement concrete pavements and remaining life estimation, based on self-sensing concrete-CNTs sensors added with multi-walled carbon nanotubes (CNTs). The concrete-CNTs sensors are applied as piezoresistive sensors (i.e. to collect information such as weight and species of passing vehicles), or as destruction identification sensors (i.e. to detect crack propagation in the Portland cement concrete pavement). For casting the concrete-CNTs sensors, some parameters are important, such as the number of CNTs, species of surfactant, dispersion quality etc. In this research, the dispersion quality of multi-walled carbon nanotubes in the aqueous phase and cement matrix was experiment examined using Ultraviolet-Visible Spectrophotometry (UV-VIS), Scanning Electron Microscopy (SEM) and mechanical experiments for compressive and flexural strength. The outcomes demonstrated that a new specific surfactant composition (sodiumdodecylbenzene sulfonate (SDS) and superplasticizer carboxylate base (SP-C) with the ratio of 1:9 respectively) could disperse MWCNTs around 64% more than other surfactant combinations indicated in the previous studies while this has enough compatibility with the concrete to omit antifoam in the mixing process and maintain the concrete mechanical specifications pretty constant. To appraise the influences of the main parameters affecting concrete-CNTs sensors function, diverse criteria in static and dynamic loading patterns were defined such as sensitivity of the sensor (Se), the standard deviation of the prediction error, repeatability (Re), cross-correlation (CC) and hysteresis (SSE). The dynamic criteria such as sensitivity, internal repeatability, cross-correlation and hysteresis declared that the dispersion energy levels for the dispersion of MWCNTs have a major impact on enhancing the function of the sensor rather than the number of CNTs. The repeatability criterion, contrariwise, showed that the number of MWCNTs has a major impact on the function of the sensor compared to the dispersion quality (dispersion energy level) of MWCNTs. Consequently, both parameters have to be regarded as relevant. The overall outcomes showed that the sensors fabricated with 0.15 wt% CNTs, superplasticizer and SDS as a surfactant using the maximum dispersion energy level (ultrasonic bath for 2 hours and 90 minutes of ultrasonic probing) have the best function in both static and dynamic load mode. To explore the influences of traffic loads on the

pavement, concrete-CNTs sensors were experiment examined under various value of dynamic loads. The outcomes demonstrated that the maximum exterior load applied on the sensor (Fmax) is linearly correlated to the maximum response of the sensor (Smax) via a constant coefficient tagα/tagβ, in which tagα is defined as the slope of the Force vs. Time graph and tagβ is defined as the slope of the Sensor's response vs. Time curve. So, this can be concluded that the application of the indicated concrete-CNTs sensors for piezoresistive applications is feasible and the sensors can appraise the load with of high-goodness of fit (R2adj.> 0.99). In addition, to study the response of the concrete-CNTs sensor under the traffic loading, fatigue experiments were run. An alternative data processing log(G)-log(N) was applied instead of traditional S-log(N) fatigue graphs (Goodman curves), based on the electrical sensor response with a linear regression approach and the outcomes were verified by statistical tests. In this research, the concept of G has been defined for the first time as the slope of a sensor's response that reflects the destruction created in a pavement because of one pass of vehicle load. Based on these findings, two various types of remaining life models for Portland cement concrete pavements were proposed.

Keywords: Remaining life, Fatigue, Portland cement concrete pavement, Carbon nanotubes, self-sensing concrete, Sensor.

Contents

List of Figures

List of Tables

Chapter 1 Research Statement

1.1 Subject description

The aim of this study is to seek the possibility of developing a new approach to Portland cement concrete pavement health monitoring. As a new method, this can eliminate the problems in the current non-destructive testing methods which are applied to appraise the adequacy of pavement structures. The main object of this study is to obtain a more precise control of Portland cement concrete pavement structural adequacy with fewer problems, applying the best solution at the best time for pavement maintenance.

1.2 Purposes of research

1) Producing the self sensing specification in Portland cement concrete pavement to appraise the adequacy of structural Portland cement concrete pavement.
2) Construction of a destruction identification concrete-CNTs sensor with high sensitivity and proper performance.
3) Investigation of the engineering specifications of concrete material containing carbon nanotubes.
4) A model to determine the remaining fatigue life of Portland cement concrete pavement using the electrical resistance that could eliminate the risk of pavement distress and increment management performance in the timely recognition and repair the damage.
5) Increasing the managing ability of critical infrastructure after the crisis by the SHM system based on concrete-CNTs sensor response.

1.3 Assumptions

1) A mix design, a carbon nanotube type, approach of manufacturing and an aggregate species will be considered for making concrete samples.
2) All experiments will be performed after 28 days curing both in humid and in dry situations.

3) The fatigue experiments for simulating accelerate destruction propagation will be run by laboratory-scale experiments using the standard three-point-bending fatigue test.

1.4 Limitations

1) The maximum size of aggregate applied to cast concrete-CNTs sensor \ will be limited to 9.5 mm.
2) To omit the temperature impact on concrete-CNTs sensor response, the experiment temperature will be set to 25 °C on average. Also, to omit internal moisture on cement-based sensor response, all cement-based sensors will be dried in the oven after curing process at 80 °C for 8 days.
3) Based on previous literature, the fatigue experiment frequency does not affect fatigue results. Nevertheless, the fatigue experiments will be run at a constant frequency and load mode.
4) Based on our lab instrumentation potential, our limitation in time and budget to do this research, the goal of this study can be neither to cast specimens and test them in real situations nor validate the lab experiment outcomes by performing full-scale experiments in real situations.

Chapter 2 Literature review

2.1 Abstract

In this chapter, the previous study of some important topics such as various methods for qualified dispersion of Multi-walled carbon nanotubes (MWCNTs) in an aqueous phase and cement matrix to cast concrete-CNTs sensor is investigated. The next step, application of various types of concrete-CNTs sensors are remarked and to gain the goal of this study to apply destruction identification concrete-CNTs sensor for monitoring of the structural adequacy of Portland cement concrete pavement, the fatigue fundamentals are inquired as laboratory approach. To model the concrete-CNTs sensor response to appraise the destruction propagation, the backgrounds in various studies are assayed.

2.2 Introduction

2.2.1 Dispersion of multi-walled carbon nanotubes

In recent years, the application of multifunctional cementitious composites has led to notable improvements in the construction and transport industry (Nasibulin *et al.*, 2013). As regards, tensile strength, modulus of elasticity and thermal and electrical conductivity of MWCNTs are far superior to those of ordinary fibers, they have received much attention in the preparation of multifunctional cementitious composites multifunctional (Khare and Bose, 2005; Coleman *et al.*, 2006; SIXUAN, 2012). The challenge of efficient and properly uniform dispersion of MWCNTs in the mixture is because of the natural propensity of agglomeration of MWCNTs and their high surface activity (Xin Jiang, Torsten L. Kowald, Thorsten Staedler, 2006; Yazdanbakhsh, 2012). Although the issue of efficient dispersion of MWCNTs in the concrete mixtures has been inquired in many studies, there are some difficulties to gain the efficient dispersion of

MWCNTs (Nasibulin *et al.*, 2013). as regards water plays an imperative role in preparing cementitious materials reinforced with MWCNTs, a convenient solution for making cementitious materials containing MWCNTs is to homogeneously disperse MWCNTs in aqua phase before their composition with the cement (Gopalakrishnan, Bjorn Birgisson and (Eds.), 2011). One of the most common mechanical methods for dispersing MWCNTs in aqua phase is the application of an ultrasonic device. The ultrasonic approach is not adequate to uniformly disperse MWCNTs in aqua phase (Gopalakrishnan, Bjorn Birgisson and (Eds.), 2011), but this can be applied as a complement to the chemical approach (Konsta-Gdoutos, Metaxa and Shah, 2010). One of the most widely applied methods for the efficient dispersion of MWCNTs in aqua phase is the application of surfactants so that the establishment of MWCNTS agglomerates is prohibited and MWCNTs are uniformly dispersed in aqua phase (Gopalakrishnan, Bjorn Birgisson and (Eds.), 2011; Nasibulin *et al.*, 2013). This non-covalent approach is straightforward and classically applied to disperse both organic and inorganic particles in aqueous solutions (Vaisman, Wagner and Marom, 2006). The concentration of surfactant and species of interaction with this are known to play a notable role in the phase behaviour of classical colloids (Rosen and Kunjappu, 2012) as well as multi-walled carbon nanotubes (Cui *et al.*, 2003; Shvartzman-Cohen *et al.*, 2004). Basically, surfactants because of electrostatic and steric repulsion forces prohibit the establishment of MWCNTs agglomerates (Luo, Duan and Li, 2009). According to this, the scientists have attempted to promote dispersion of MWCNTs in aqua phase using various surfactant materials including sodium dodecylbenzenesulfonate (NaDDBS), Sodium deoxycholate (NaDC), Triton X-100 (TX100), Gum Arabic (AG) and Cetyltrimethylammonium bromide (CTAB) (Chen *et al.*, 2011). They came to the conclusion that the NaDDBS and TX100 with a mixing ratio of 3:1 respectively, by weight of cement and with the concentration of 0.02 grams per mL show the best dispersion ability (Han, Yu and Kwon, 2009; Han *et al.*, 2015). to reduce MWCNTs aggregative propensity in water, the ionic surfactants, Sodium Dodecyl Sulfate (SDS) (Hilding *et al.*, 2003; Dyke and Tour, 2004; O'Connell *et al.*, 2010) and dodecyl-benzene sodium sulfonate (NaDDBS) (Tan and Resasco, 2005; Camponeschi *et al.*, 2006) were commonly applied . The high dispersive performance of NaDDBS (Islam *et al.*, 2003) and even better performance of Dowfax surfactant (anionic alkyldiphenyl-oxide disulfonate) that has twice the charge of NaDDBS and a di-benzene group (Tan and Resasco, 2005) is mainly because of the benzene ring along the surfactant. Also, Aerosol OS surfactant (sodium diisopropylnaphthalene sulfonate) presented higher fractions of individual tubes compared to the

outcomes obtained with NaDDBS and Dowfax surfactants, as confirmed by UV–vis spectroscopy analysis (Tan and Resasco, 2005). In another study run by Sharifi et al., they applied SDS and Dodecyltrimethylammonium bromide (DTAB) with a mixing ratio of 9:1 respectively, by weight of cement and with the concentration of 8 mMol/L to disperse MWCNTs in aqua phase. They reported this composition as the best composition for dispersing MWCNTs in aqua phase compared to other surfactants (Sharifi, 2012; Sohrabi and Nayeri, 2014).

It should be noted that the surfactant creates foam when making concrete that may cause problems for the cement hydration and concrete mechanical properties. So, MWCNTs being well-dispersed in aqua phase is not adequate to boost concrete specifications as well and the impact of surfactants on the specifications and stability of cementitious materials should be investigated (Han *et al.*, 2015). According to this, scientists figure out that the excessive amounts of NaDDBS and TX100/SDS in the mixture have a negative impact on the hydration of cement and may cause more trapped air in the concrete (Ibarra, Gaitero and Campillo, 2005; Gopalakrishnan, Bjorn Birgisson and (Eds.), 2011). The primary additives compatible with concrete and appliedreseaas a surfactant in the process of dispersing MWCNTs in aqua phase are the water-reducing additives, plasticizers and polycarboxylate superplasticizers capable of facilitating the properly uniform dispersion of MWCNTs and prohibiting unwanted voids in the cement matrix and subsequently in concrete (Ibarra, Gaitero and Campillo, 2005). The researchers have demonstrated that using the ultrasonic method, a small number of MWCNTs can be dispersed in aqua phase containing 5 wt% superplasticizer (Gopalakrishnan, Bjorn Birgisson and (Eds.), 2011). Shah et al. achieved an efficient dispersion of MWCNTs with diverse lengths and concentrations in cementitious materials by employing polycarboxylate-based superplasticizers (Shah *et al.*, 2009; Konsta-Gdoutos, Metaxa and Shah, 2010). In the meantime, Han et al. reported that the efficient dispersion of MWCNTs by means of superplasticizers can be assigned to their double-dispersion impact on MWCNTs/CNFs (carbon nanofibers) and cement particles (Han, Ding and Yu, 2015).

In this research, the influence of diverse surfactants on the dispersion of MWCNTs in the water and on the concrete function is investigated. A new composition as surfactant compatible with concrete is presented and provides the best dispersion of MWCNTs whereas the concrete mechanical specifications remain constant. This will help also to cast a concrete-CNTs sensor with the same mechanical specifications as conventional concrete and will cause a cast concrete-

CNTs sensor that can appraise structural and mechanical specifications of plain concrete(Adresi *et al.*, 2016). The optimum dose of the new surfactant composition is calculated using UV-visible spectroscopy and turbidimetry to evaluate the dispersion quality of MWCNTs in the aqueous phase. The mechanical specifications of the concrete such as compressive and flexural strength have been selected as the concrete function criteria to explain the impact of MWCNTs dispersion quality and surfactant interaction on the concrete composition and hydration process compared to the plain concrete.

2.2.2 Concrete sensors

A sensor is a device that is capable of identifying the probability or the value of changes and presenting them as a relevant output (typically electrical or optical signal) (Wilson, 2005). The self sensing concrete is caste via enhancement of functional fillers (carbon nanotubes, etc.) into plain concrete to increment its ability to sense stress, strain or destruction in itself (Han, Yu and Ou, 2015). As the concrete is stressed, the contact between the fillers and the cement matrix is affected, thereby affecting its electrical resistance. Strain, stress, crack and destruction are detected via estimation of the electrical resistance (Shi and Chung, 1999; Saafi, 2009; Han *et al.*, 2011). Making materials electrically conductive may be possible in many various ways such as creating piezoresistive sensors with the ability to measure stress-strain or load-displacement data (Qu and Han, 2008; Gopalakrishnan, Bjorn Birgisson and (Eds.), 2011) or creating sensors with the ability to measure data on the extent of destruction to the concrete (Bontea et al. 2000; Han et al. 2015; Han, Ding, et al. 2015). The precision of a sensor is evaluated by some function criteria such as sensitivity, repeatability, linearity, hysteresis, etc. (Wilson, 2005). To gain precise concrete sensors, the functional fillers need to be truly dispersed in concrete via an efficient process to produce a vast conductive network inside the concrete (Han, Ding, et al. 2015). The electrical specifications of self sensing concrete depend on many parameters including the type, amount, surface activity and the dispersion quality of CNTs, the species and number of surfactant, and the composition of cement matrix as well as the mechanical specifications of cementitious materials reinforced with MWCNTs (Han, Ding, et al. 2015; Wang et al. 2002). Azhari, evaluated the sensing function of carbon fiber and multi-walled carbon nanotubes (CNTs) cement-based sensors with various carbon fibers/ MWCNTs ratios under uniaxial compression and modeled the relationship between the fractional change in electrical resistance and compressive stress (Azhari and Banthia, 2012). Han et al.

cast cement-based stress/strain sensors using carbon fiber and carbon black and evaluated the function parameters (e.g. input, output, sensitivity, linearity, repeatability and hysteresis) (Han, 2006). Han et al. cast CNT-filled cement-based sensors and appraised their performances with some criteria under various loading rate. They remarked that the cement-based sensors with 0.1% MWCNTs have stable and reversible piezoresistive responses. The relationship between input (compressive stress) and output (change in electrical resistance) of the cement-based sensors was linear. The cast cement-based sensors had favorable function parameters such as sensitivity of 0.911 kΩ/MPa, linearity of 7.16%, repeatability of 1.53% and hysteresis of 7.24% as the input of cement-based sensors was from 0 to 10 MPa (Han *et al.*, 2011). Sun et al. developed cement-based strain sensors with high strength and self sensing ability. The outcomes demonstrated that the concrete-CNTs sensors with 0.5% brass-coated steel fibers had high compressive strength over 120 MPa. Their piezoresistivity showed little noise, indicating the resistance of the concrete-CNTs sensors varied smoothly with the strain. Also, after oven-drying, the repeatability and sensitivity of the piezoresistivity highly improved (Sun *et al.*, 2014). Galao et al. cast carbon nanofibers (CNF) cement composites with various CNFs quantity. They proved the sensitivity of these CNF composites by gage parameter as function criterion to sense their own destruction under various variables, such as cement pastes curing age, current density, loading rate or maximum stress applied (Galao *et al.*, 2014). Ubertini et al. examined a specific concrete-CNTs sensor containing 2% MWCNTs, which were dispersed by 15 min of sonication with a 225 W ultrasound device equipped with a probe series, under various loading situations. They adopted two-probe measurement configuration that provided good quality of the measurements. In this particular configuration, increments in the distance between active electrodes resulted in an increment of the strain sensitivity of the cement-based sensor and reduce of signal-to-noise ratio. The cement-based sensor also showed a non-linear input-output behaviour, with some hysteresis (Ubertini *et al.*, 2014). Jian et al. studied the sensing behaviour of carbon fiber-concrete with 0.5, 0.7, 0.9, and 1.1 wt% of carbon fiber under dynamic compression loading pattern. The outcomes showed that 0.7 and 0.9 wt% of carbon fiber cement-based sensor have the highest sensitivity and the best repeatability (Huali, Huicai and Jinwei, 2003). Wen et al. believe that the ability of the concrete-CNTs sensor is significantly dependent on its electrical conductivity that is highly affected by MWCNTs quantity (Wen and Chung, 2007). Lue et al. compared the electrical conductivity of the conventional cement matrix with the electrical conductivity of cement pastes containing 0.2 wt% multi-walled carbon nanotubes dispersed with 5 various surfactants. They

figure out that the electrical resistance of nanocomposites reduces by increasing the number of MWCNTs (Luo, Duan and Li, 2009). Azhari inquired the impact of various types and amounts of CNTs, and the composition of MWCNTs and carbon fibers on the electrical conductivity of nanocomposites. They figure out that the hybrid cement-based sensors, containing a composition of 15 wt% carbon fibers and 1 wt% carbon nanotubes, provided a better quality signal, improved reliability and increased sensitivity over cement-based sensors carrying 15 wt% carbon fibers alone (Azhari and Banthia, 2012). Han et al. (Han, Yu and Ou, 2015) showed that the dispersion of functional fillers in a concrete matrix directly affects the conductive network inside the composite, and thus the electrical resistance of the composite. So, the better the dispersion quality, the more reproducible sensing specifications are. Sonication has been recognized as the key step in the manufacturing process, that mostly affects strain sensitivity of CNTs. therefore, the duration of the whole dispersion process is important (Materazzi, Ubertini and D'Alessandro, 2013; Ubertini *et al.*, 2014). Konsta Gdoutos et al. reached a relatively high electrical conductivity in the cement matrix by adding 0.1 wt% MWCNTs to the cement matrix and enhancing the dispersion quality of MWCNTs (Konsta-Gdoutos, Metaxa and Shah, 2010). The previous study shows that a range of MWCNTs from 0.1 wt% to 1 wt% was applied to cast concrete sensor. This high variation in MWCNTs quantity is related to many parameters such as quality of MWCNTs and their aspect ratio, species of dispersion composition and the amount of dispersion energy applied by types of sonication systems, concrete materials species and moisture quantity in concrete, etc., that all affect cement-based sensor sensitivity and other qualification criteria.

The previous studies show that there are no definite function criteria to appraise the cement-based sensor response. So, in this research, the diverse function criteria such as the sensitivity of the cement-based sensor, the standard deviation of the prediction error, the repeatability, the cross-correlation and the hysteresis were defined to appraise the performance and precision of the cement-based sensors. Also, many studies emphasized on the influences of MWCNTs ratio and dispersion quality on the conductivity of concrete sensors. However, they did not focus on function criteria. So, the function of CNT-filled cement-based sensors was inquired at various MWCNTs quantity and various MWCNTs dispersion energy levels (dispersion quality) under static and dynamic loading regime.

2.2.3 Concrete sensors application

Structural health monitoring (SHM) focused on continuously monitoring and evaluating the qualification of structural systems such as Portland cement concrete pavement(Azhari and Banthia, 2012). The Sensors are the devices that are capable to identify the probability or the value of parametric changes and presenting them as a relevant output (typically electrical or optical signal)(Wilson, 2005). Therefore, sensors play a key role as important part of SHM system. A new generation of sensors is known by embedded concrete sensors, that are multifunctional materials combining both mechanical specifications and functional applications(Galao *et al.*, 2014). They can disclose a self sensing ability by adding various types of conductive fillers such as multi-walled carbon nanotubes (CNTs), so, they can provide real-time data on the situation of Portland cement concrete pavement measuring parameters like displacement, strain (piezoresistive cement-based sensor(Han and Ou, 2007; Xiao, Li and Ou, 2011; Baoguo Han *et al.*, 2012; Du, Quek and Pang, 2013; Han, Yu and Ou, 2014; Kim, Park and Lee, 2014; Konsta-Gdoutos and Aza, 2014; Sun *et al.*, 2014; Han *et al.*, 2015)), they can monitor destruction propagation (damage identification cement-based sensor(Bontea, Chung and Lee, 2000; Wen and Chung, 2006; Saafi, 2009; Sun, Yu and Han, 2014; Han, Ding and Yu, 2015)) or they can be applied as weight in motion (WIM) detector in concrete highway(Shi and Chung, 1999; Han, Yu and Kwon, 2009; Yu and Kwon, 2009; Han, Ding and Yu, 2015).

The concept of destruction sensing in composites based upon the carbon fiber reinforcements was pioneered by Schulte and co-workers (see Refs. [1–4]). The basic idea of this method is in the application of conductive carbon fibers as the electric current carrier and the measurement of resistivity change in the fiber direction because of fiber fractures or in the transverse direction because of the separation of fiber contacts [5]. destruction sensing mechanism begins at the yielding point, corresponding to the material's plastic zone, and can be seen on irreversible changes in the electrical resistivity (Galao *et al.*, 2014).

A material's strain sensing capacity defined as the response of the volumetric electrical resistivity (proportional and reversible) because of its strain state. If a longitudinal compressive stress is exerted the electrical resistance in that direction is diminished. However, if the material is upon tension then the impact will be the inverse. This application of cement composites is called piezoresistivity and applied as structural service state monitoring, room occupancy control or vehicle weighing in different types of pavements (Galao *et al.*, 2014). Checking the

weighing of vehicles such as trucks has been necessitated to avoid destruction to highways because of overweight vehicles (Shi and Chung, 1999).

The piezoresistive cement-based sensor is capable of detecting the applied forces to the structure based on the changes in the electrical resistance that is emanated from the tunneling conduction impact of CNTs. The tunneling conduction arises in the small amounts of MWCNTs (Li, Wang et al. 2007, Gopalakrishnan, Birgisson et al. 2011, Han, Sun et al. 2013), but the destruction identification cement-based sensor operates based on the contacting conduction of CNTs. This means that by increasing the number of MWCNTs in concrete matrix, the three-dimensional contacting network of MWCNTs is formed (Gopalakrishnan, Birgisson et al. 2011, Han, Ding et al. 2015).

Han et al. developed a self sensing pavement with piezoresistive multi-wall CNTs (MWCNTs) reinforced cement-based materials and inquired the feasibility of using self sensing pavement for traffic monitoring with vehicular wheel loading tests. They figure out that the vehicular wheel loads can cause a remarkable change in electrical resistance. So, traffic flow monitoring and even possible identification of various vehicular wheel loadings can be identified by measuring the electrical resistance of the cement composites(Han, Yu and Kwon, 2009; Gopalakrishnan, Bjorn Birgisson and (Eds.), 2011). In this research, the probes were steel bar located in the top and botom of pavement layer and were perpendicular to vehicle load direction.

Yu et al. (Yu and Kwon, 2012) cast two CNT-based self sensing concrete sensors, a pre-cast cement-based sensor and a cast-in-place cement-based sensor, that were integrated into a concrete experiment section at the Minnesota Road study Facility with two mesh electrodes arranged in top and bottom of the pavement. identification outcomes of a truck passing at low and higher speeds have shown that abrupt changes arised in the voltage signal graphs when the truck passes over the cast-in-place and pre-cast MWCNT concrete sensors so that each peak indicates a passing wheel.(Yu and Kwon, 2012)

Wen and Chung inquired the behaviour of strain and destruction self sensing in carbon fiber cement matrix under flexure. The oblique resistance (i.e., volume resistance in a direction between the longitudinal and through-thickness directions) increases upon loading and is a good indicator of both destruction and strain. The surface resistance on the compressive side reduces upon loading and is

a good indicator of strain. The surface resistance on the tensile side increases upon loading and is a good indicator of destruction (Wen and Chung, 2006).

Galao et al. evaluate both strain and destruction sensing specifications on carbon nanofiber cement composites. They experiment strain sensing under the flexural setup on the material's elastic range. After the first set of elastic tests, the same specimens were gradually loaded up to material's failure. At the same time, both strain and resistivity were evaluated. The aim of these experiments was to prove the sensitivity of these CNF composites to sense their own damage. The outcomes showed that the cement-based sensors can detect load and destruction truly simultaneously(Galao *et al.*, 2014).

Chung et al. presented that self-monitoring concrete containing short carbon fibers (0.5% or 1.0% by weight of cement) is efficient for traffic monitoring and weighing in motion (WIM). The resistance reduces reversibly with increasing stress up to 1 MPa and is independent of speed factor up to 55 mph (Shi and Chung, 1999).

Azhari et al. extend two types of cement-based sensors, one with carbon fibers(15% wt) alone and the other having both fibers and multi-walled carbon nanotubes(15% wt CF and 1% wt MWCNT). They model the cement-based sensor response with regression technique with a hyperbolic trend and explain that cement-based sensor response consists of linear, nonlinear including propagation of microcracks, and failure zones. They remarked that their response is both nonlinear and rate-dependent. However, given the loading rate, the imposed material strains can be predicted from fractional changes in the cement-based sensor resistivity via a unique nonlinear calibration curve.(Azhari and Banthia, 2012)

In this research, we intend to focus on modeling the concrete-CNTs sensor electrical response under three points flexural test set up with sinousial loading pattern as a proper simulation for vehicle wheel loading. this means that once embedded in Portland cement concrete pavement under traffic loading, theconcrete-CNTs sensor can work as destruction identification cement-based sensor and can monitor the weight of the passing vehicles too. In the destruction identification cement-based sensor, normally probes are cast around the specimen and parallel to the exterior force direction, but for weight detection, the cement-based sensor setup is the same as the concrete piezoresistive sensor, in which the probes are up and down of the cement-based sensor, perpendicular to the exterior

force direction. So, research map is combining these two types of cement-based sensor in one sensor schema and measuring both exterior loads and destruction propagation under repeated loads during the loading process.

2.2.4 Concrete fatigue

Many civil infrastructures are often subject to repetitive dynamic loads. Examples of such dynamic loads include machine vibration, sea waves, wind action and automobile in traffic. The exposure to repeated loading outcomes in a steady reduction in the stiffness of the structure, that may eventually cause fatigue failure (Lee and Barr, 2004). Fatigue may be defined as a process of progressive, permanent interior structural changes in a material subjected to repeated loading. In concrete, these changes are mainly associated with the progressive growth of internal microcracks, that outcomes in a notable increment of irrecoverable strain. At the macro level, this will disclose itself as changes in the material's mechanical specifications (Lee and Barr, 2004).

The mechanism of fatigue failure in concrete or mortar matrix can be categorized into three different stages (Horii, B and Pallewatta, 1992). The first stage includes the weak zones within the concrete or mortar matrix and is termed defect initiation. The second stage is characterized by a slow and progressive growth of the intrinsic defects to a critical size and is generally known as microcracking. In the final stage, when an adequate number of impermanent cracks have formed, a continuous or macro crack will develop, eventually leading to failure.

Fatigue loading is usually categorized into two parts (36-RDL, 1984) i.e. low-cycle and high-cycle dynamic loading. Low-cycle loading involves the application of a few load cycles at high stress levels. On the other hand, high cyclic loading is characterized by a large number of cycles at lower stress levels. in the case of static tests, various loading arrangements have been applied in fatigue testing, including compression, tension and bending tests. The most common approach to fatigue testing, by far, is via flexural tests.

Various approaches have been applied in the fatigue life assessment of structural elements. A widely accepted method for engineering practice especially thickness design is based on empirically derived S–N graphs, also known as Wöhler curves. The stress-fatigue life graphs, such as S-N curves, shown in Figure 1. These graphs were developed from experiments on 6 x 6 in. (152 x 152

mm) conventional concrete beams loaded at the third points of a 60 in. (1.52 m) span (Hanson *et al.*, 1997). The experiments were run at the rate of 450 cycles per min. This concrete mix with a water-cement ratio (W/C) of 0.52 provided an average compressive strength of 5000 psi (34.5 MPa) in 28 days. The age of the fatigue test specimens at the time of testing ranged from 150 to 300 days. In Figure 1, the vertical axis is the ratio of the maximum stress, (applied stress (Smax) to the static strength (MOR)). In this case, Smax is the calculated flexural tensile stress, and the static strength is the modulus of rupture stress, f_r,. The abscissa is the number of cycles up to failure, plotted on a logarithmic scale (Hanson *et al.*, 1997).

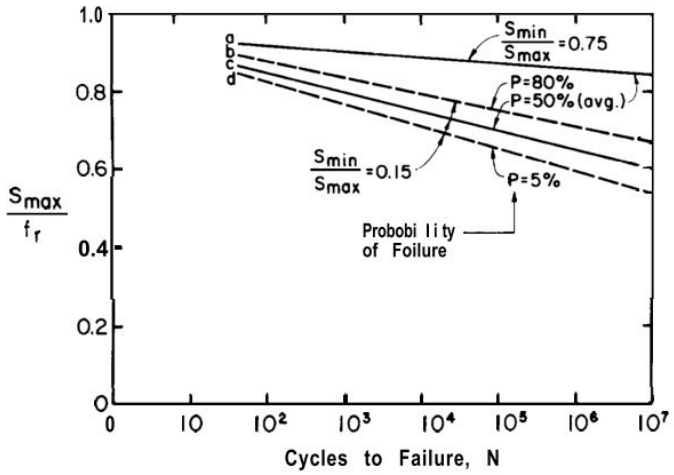

Figure 1- Fatigue strength of conventional concrete beams(Hanson *et al.*, 1997).

In addition, the influences of minimum stress in the loading cycle may be demonstrated in so-called Goodman graphs or Smith graphs, that are also known as constant life graphs in the analyses of metals (Sendeckyj, 2001). Design for fatigue may be facilitated by application of a modified Goodman graph, as explained in Figure 2. This graph is based on the fact that the fatigue strength of conventional concrete is essentially the same whether the mode of loading is tension, compression, or flexure. The graph also incorporates the influence of the range of loading. For the zero minimum stress level, the maximum stress level of the concrete can withstand for one million cycles without any failure is taken conservatively as 50 percent of the static strength. As the minimum stress level is increased, the stress range that the concrete can withstand reduces. The linear reduce stress range with increasing minimum stress has been demonstrated, at least approximately, by many investigators(Hanson *et al.*, 1997).

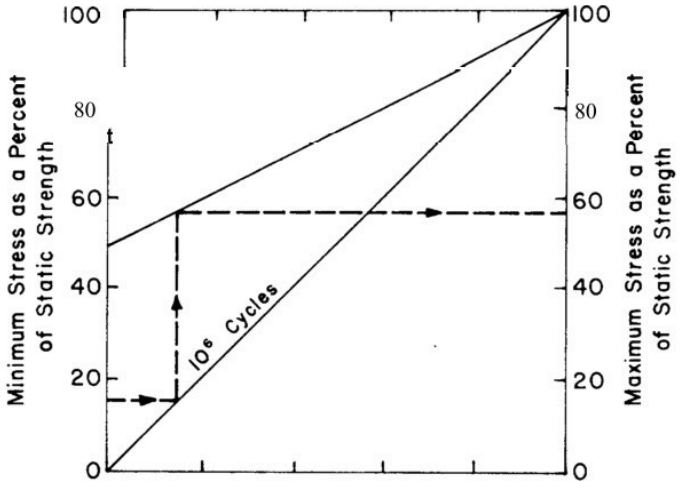

Figure 2- Fatigue strength of conventional concrete in tension, compression or flexure(Hanson *et al.*, 1997).

The enhancement of fibre reinforcement has been figure out to have a dual impact on the dynamic behaviour of concrete. Fibres are able to bridge micro cracks and retard their growth, thereby enhancing the composite's function under dynamic loading. On the other hand, the presence of fibres increases the pore and initial micro crack density, resulting in strength reduces. The overall outcome of these two competing influences depends significantly on the fibre content (Lee and Barr, 2004). The main advantage of the enhancement of fibres in the concrete matrix is increased the ability to absorb energy. Increasing the fibre quantity and aspect ratio increases the number of energy spent on crack growth under fatigue load (Chang and Chai, 1995). The main fibre parameter influencing the fatigue function of FRC seems to be the fibre quantity. On the other hand, the aspect ratio and fibre species is secondary in importance (Mailhot *et al.*, 2001).

To date, there is no standard procedure for carrying out fatigue experiments on conventional concrete or fibre reinforced concrete (FRC). Strictly speaking, fatigue data obtained from a particular experimental setup cannot be directly compared to data obtained from various loading configurations (Kolluru *et al.*, 2000). However, S–N graphs are plotted using strength (or stress) values that are made dimensionless by relating them to the static strength. The dimensionless term, S, in part omit influences such as specimen shape, water–cement ratio, species and grading of aggregates, concrete strength, curing situation, moisture situations and age at loading etc. Dimensionless S–N graphs are thought to

represent as close as possible the true behaviour of concrete under fatigue loading (Hsu, 1984).

Lee et. al. compare diverse studies in flexural fatigue experiments on conventional concrete and SFRC have been extensively studied (Raithby, 1979; Chang and Chai, 1995; Zhang, Phillips and Wu, 1997; Singh and Kaushik, 2000; Mailhot *et al.*, 2001) as presented in Figure 3.

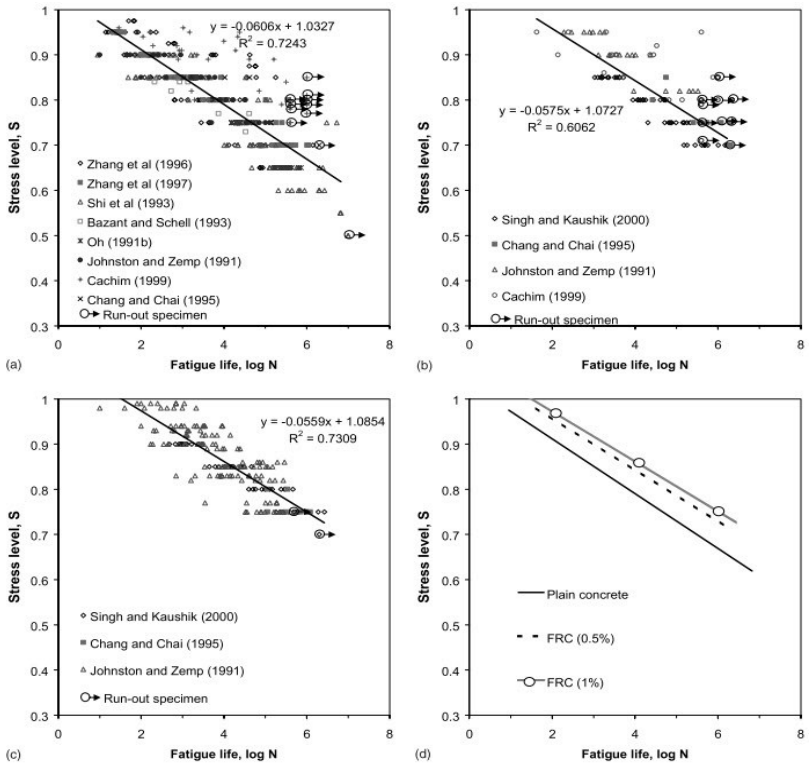

Figure 3- (a) S–N graph for conventional concrete under flexural loading; (b) S–N graph for SFRC (0.5% fibre content) under flexural loading; (c) S–N graph for SFRC (1.0% fibre quantity) under flexural loading; (d) comparison between S–N graphs for plain and SFRC (0.5% and 1.0% fibre quantity) under flexural loading(Lee and Barr, 2004).

Figure 3(a) presents the S–N graph for conventional concrete under flexural loading. Similarly, Figure 3(b) and (c) give the S–N graphs for SFRC containing 0.5% and 1.0% of fibres under flexural loading respectively. Finally, Figure 3(d) compares the linear regression lines for all three experiment outcomes in flexure (Lee and Barr, 2004). There are diverse combinations of loading frequency, load sequencing, matrix composition, experiment configuration etc. that can be expected to change the behaviour of FRC under fatigue loads. Nevertheless, the

outcomes show that the inclusion of fibres can advantage the fatigue function of concrete. However, the quantitative nature of this advantage is difficult to determine. this appears that only a marginal advantage comes from fibre addition because the additional defects introduced by fibre enhancement outweigh the benefits (Lee and Barr, 2004).

Newly, scientists have paid more attention to the fatigue behaviour of concrete pavement. On the other hand, heavy traffic flow and heavier vehicles load, force the concrete pavement subject to increment value and cycles of fatigue stresses. Hence, new types of concrete containing nano-particles have been applied to boost the fatigue performance. Li et. al. applied both nano-TiO_2 and nano-SiO_2 as the additives in concrete to study its flexural beam fatigue performance. The experiment outcomes shows that the fatigue lives of concretes containing nano-particles trace the double-parameter Weibull distribution. The flexural beam fatigue of concretes which is containing nano-particles, is improved significantly and the sensitivity of their fatigue lives to the change of stress is also improved (Li, Zhang and Ou, 2006).

2.2.4.1 Fatigue model types

Numerous scientists have published fatigue data, usually from repeated load flexural beam tests. In general, when the number of load levels causing failure is drawn against the ratio of applied flexural tensile stress to flexural tensile strength, the data trace specific trend within a relatively narrow band. Figure 4 involves a set of flexural beam experiment data. consider that a specification of concrete in fatigue test set up is extremely sensitive to load level, presented by Y-axis in Figure 4 (Griffiths and Thom, 2007).

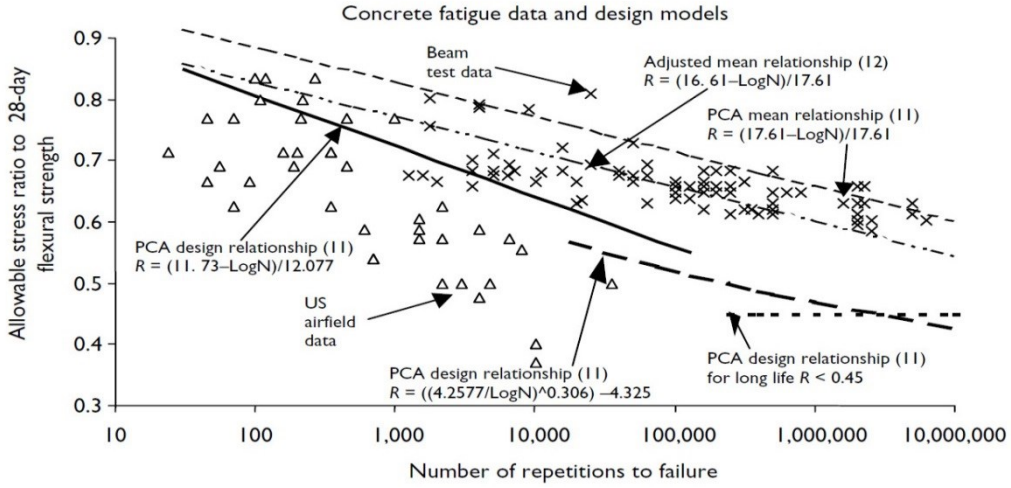

Figure 4- Fatigue data and design models(Griffiths and Thom, 2007).

Also, NCHRP 1-37A presented the fatigue model to appraise the allowable number of load applications as Equation 1 (NCHRP1-37A, 2004).

Equation 1

$$LogN_{i,j,k,l,m,n} = C_1 \left(\frac{M_R}{\sigma}\right)^{C_2}_{i,j,k,l,m,n} + 0.4371$$

where

N = allowable number of load applications in PCC (The applied number of load applications ($n_{i,j,k,l,m,n}$) is the actual number of axle composition k of load level L that passed via traffic path n under each situation (age, season, and temperature difference)).

M_R = modulus of rupture, psi.

σ = critical stress calculated using axle composition k of load level L that passed via traffic path n under a given set of situations (age, season, and temperature difference).

C_1, C_2 = calibration constants.

The allowable number of load applications is the number of load cycles at that fatigue failure is expected (corresponding to 50 percent slab cracking) and is a function of the exerted stress and concrete strength. The allowable number of load

applications is specified using the fatigue model in equation 2 (NCHRP1-37A, 2004).

2.2.4.2 Miner model to appraise destruction level

Most of the study reporting on the fatigue specifications of concrete has been limited to constant-magnitude loading. This, however, rarely arises in practice, and a typical loading history will contain stress levels of varying magnitude, various number of cycles, loading sequences and perhaps intermediate rest periods. In analyzing the effect of complicated loading histories, the classical hypothesis of linear accumulative destruction called Palmgren-Miner, is widely applied (Zhang, Phillips and Wu, 1997).

The outcomes of a variable-magnitude fatigue experiment may conveniently be demonstrated by the 'Miner number' (M) in Equation 2. A well-known hypothesis originally indicated the fatigue destruction because of n_i cycles of load to a stress level S_i at that N_i cycles would cause failure is n_i/N_i. The total destruction resulting from repeated loading at s + 1 various stress levels (ie. with s 'steps' or changes of stress) will be (Bennett, 1980):

$$\sum_{i=1}^{i=S+1} \frac{n_i}{N_i} = M \qquad \text{Equation 2}$$

The summation M is denominated the Miner sum, and according to the Palmgren-Miner hypothesis fatigue failure should arise when M attains a value of unity.

2.2.5 Prediction of destruction by concrete sensors

Pavement health monitoring system plays a key role in pavement management systems. Early repair and maintenance scheduling increment the safe operation and in-service function of pavement. This can be achieved via an precise and consistent monitoring of pavement situation. destruction arises when concrete structures are under dynamic loading and destruction monitoring of structures is valuable for hazard mitigation. In general, the destruction sensing that is a key role in pavement health monitoring can be categorized into exterior evaluation technologies (containing most traditional approaches) and in situ pavement cement-based sensors (Xue *et al.*, 2014). Besides, there are abundant non-

destructive evaluation (NDE) methods for the assessment of the behaviour of pavements and other infrastructures (Behnia, Chai and Shiotani, 2014). The in-situ pavement health monitoring can be performed by attached or embedded destruction sensors, such as optical fibres, acoustic sensors and etc. However, these type of sensors have limited application duo to high cost, low durability, and limited sensing volume and spatial resolution. A new approach of detecting destruction in real time by electrical resistance has been indicated (Chung, 1995; Chen and Chung, 1996; Fu and Chung, 1996; Chen and Liu, 2007) that is based on the concept that destruction causes irreversible change in electrical resistance, while elastic strain causes reversible change in electrical resistance (Chen and Liu, 2007).

Carbon fibre-reinforced concrete (CFRC) consisting of insulating cement matrix and conducting carbon fibre is well known to show a large variation in electrical resistance. Using this species of concrete as sensor in pavement enables real time identification of destruction in concrete structures with simple and inexpensive electrical equipment (Chen and Liu, 2007). This species of concrete is attractive not only for its low drying shrinkage, high flexural strength, high tensile strength, high flexural toughness and high tensile ductility (Chen and Chung, 1996), but also for its ability to sense its own strain and destruction (Chen and Chung, 1993, 1996; Chung, 1995; Bontea, Chung and Lee, 2000; Wen and Chung, 2002). The self-monitoring ability is associated with the change in electrical resistivity upon strain or damage. Reversible strain in the elastic regime causes the resistivity to change reversibly, while destruction causes the resistivity to increment irreversibly. The strain sensing ability stems from the slight (< 1 pm) pull-out of the crack-bridging conducting carbon fiber upon deformation and the consequent increment in the resistivity. The destruction sensing ability stems from fiber breakage and crack propagation, both of that cause the resistivity to increment irreversibly. Without the fibers, crack opening is not restrained and the resistivity increases only at fracture(Fu *et al.*, 1997).

Many studies were run by Chan and Han, independently upon destruction mechanism of concrete sensor. They categorised the destruction to minor and major. The major destruction can be seen by visual inspection but the minor one is because of degradation of structural properties(Bontea, Chung and Lee, 2000). They funded that under the fatigue dynamic loading, although the fractional changes in electrical resistant baseline reduce was clear and monotonic, this was not linear with cycle number. They remarked that this reduce is attributed to destruction of the cement matrix separating adjacent fibres at their junction. This

destruction promoted the chance for adjacent fibres to touch one another, thereby causing the baseline reduce. Nevertheless, this provides an indication of the extent of destruction in the regime of slight damage(Bontea, Chung and Lee, 2000; Wen and Chung, 2006; Chen and Liu, 2007; Galao *et al.*, 2014; Sun, Yu and Han, 2014; Han *et al.*, 2015; Han, Ding and Yu, 2015). Chung et.al. examined CFRC specimens under dynamic compression and evaluated their strain and electrical response. Figure 5 reports the outcomes for loading in that the stress magnitude increased cycle by cycle to a maximum (more than 90% of the compressive strength) and was held at the maximum for numerous cycles (Figure 5(b)). The strain magnitude (Figure 5(a)) increased along with the stress magnitude, but continued to increment after the stress magnitude had reached. The resistance increased as the stress increased in each cycle by cycle. The baseline resistance increased significantly cycle by cycle and continued to increment after the stress magnitude had reached its maximum.

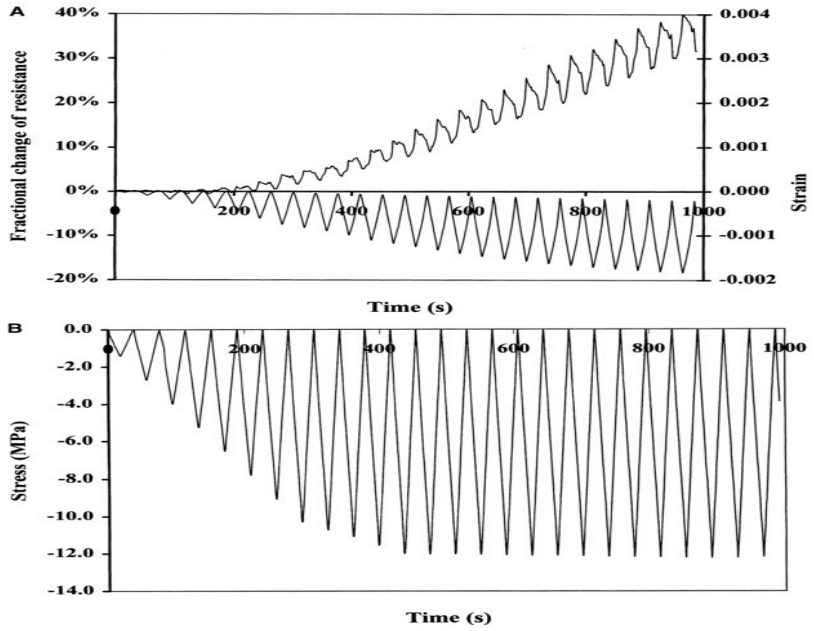

Figure 5- fractional change in resistance, strain(a) and stress (b)during repeated compressive loading stress magnitudes up to >90% of the compressive strength and then with the stress magnitude fixed at the maximum(Bontea, Chung and Lee, 2000).

They claimed that the resistance increment showed the occurrence of damage. Also, they mentioned that the major stress magnitude, the larger and the less reversible is the damage-induced resistance increase(Bontea, Chung and Lee, 2000).

They believed that at low-stress magnitude, the baseline resistance reduce irreversibly and gradually cycle by cycle. This is the same as the impact reported in Ref. (Fu and Chung, 1996) and is attributed to matrix destruction and consequent enhancement of the chance of adjacent fibers to touch one another. At the high stress magnitude, this baseline resistance reduce is overshadowed by the damage-induced resistance increase, the occurrence of that cycle by cycle as the stress magnitude increment causes the baseline resistance to increment irreversibly (Figure 5) (Bontea, Chung and Lee, 2000). This two opposing baseline influences caused the baseline to have positive, zero or negative slope.

Chapter 3 Materials and Methodology

3.1 Materials

In this research, multi-walled carbon nanotubes (MWCNT) obtained from Research Institute of Petroleum Industry (RIPI) was applied; their specifications are given in **Table 1** and their diameters are shown in Figure 6. to appraise the various surfactants impact on dispersion quality of MWCNTs in the aqueous phase, the number of MWCNTs was assumed constant at the value of 0.05 wt% that was applied in many previous studies to prepare smart concrete (Parveen, Rana and Fangueiro, 2013). Figure 7 summarizes aggregate grading specification for concrete. The applied mix design is shown in **Table 2**. Species II Portland cement was obtained from Abyek Cement Company. To disperse CNTs in the aqua mixture, various types of surfactants were applied (**Table 3**). In addition, 0.02 wt% Tributyl phosphate made by Sigma-Aldrich Co. was applied as a defoamer. A dark brown solution of polycarboxylate-based superplasticizer (Sarapush construction chemical manufacture) with a 36% solid quantity and had a density of 1.1 g/cm^3 was applied for workability purpose. SP-C are composed by a methoxy-polyethylene glycol copolymer (side chain) grafted with a methacrylic acid copolymer (main chain). The carboxylate group -COO−Na$^+$ dissociates in water, providing a negative charge along the SP-C backbone.

Table 1- specifications of MWCNTs

Type of additive	***Characteristic (Research Center)***	***MWCNTs diameter (nm)***	***MWCNTs length (μm)***	***Tensile strength (GPa)***	***Purity***	***Specific gravity***	***Electrical conductivity (Ohm-cm)***
CNT	MWCNT (Research Institute of Petroleum Industry)	10-20	10 ± 3	About 100	$\geq 95\%$	About 1.5	$< 10^{-2}$

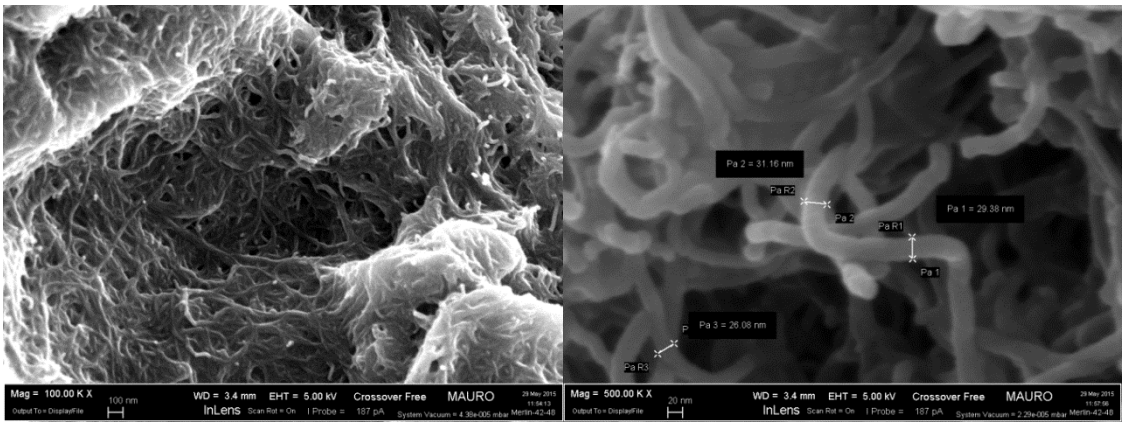

Figure 6- MWCNTs SEM image and their measured diameres

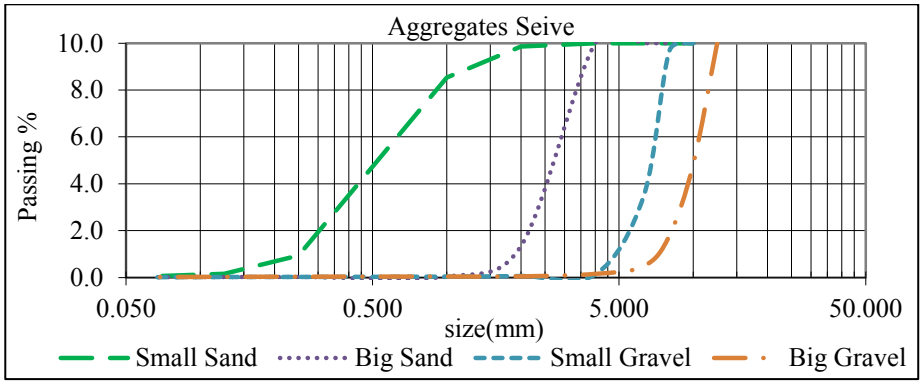

Figure 7- various aggregate grading experiment outcomes (ASTMC136/C136M-14, 2014)

Table 2- Mix design

Mix design	*Cement*	*Small sand**	*Big sand**	*Small Gravel**	*Big Gravel**	*Water*	*W/C*
Percentage	15.34	39.58	6.96	23.19	7.72	7.21	0.47
kg/m3	380	980.40	172.40	574.42	191.22	178.60	

* Sand and gravel are silica based.

Table 3- The optimum dose of various combinations of surfactant

Surfactant	*manufacturer*	*purity*	*Dosage (gr/mL)*
SDS/DTAB(9:1) (Sharifi, 2012; Sohrabi and Nayeri, 2014)	Sigma-Aldrich	SDS≥98% DTAB≥98%	SDS =2.272, DTAB =.2524
SDS**	Sigma-Aldrich	≥98%	SDS =2.524
NaDDBS (Han, Yu and Kwon, 2009)	Merck Group	---	NaDDBS=4.88
TX-100/NaDDBS(3:1) (Chen *et al.*, 2011)	Merck Group	---	TX-100=6.672, NaDDBS=2.224
TX-100/NaDDBS(2.25:1)**	Merck Group	---	TX-100=5.004, NaDDBS=1.668
Superplasticizer (0.4 wt*%)(Sun, Yu and Han, 2014)	Sarapouch Co.	≥97%	superplasticizer=0.0098
Superplasticizer (0.5 wt*%)**	---	≥97%	superplasticizer=0.0123
Superplasticizer (0.7wt*%)**	---	≥97%	superplasticizer=0.0173

Superplasticizer/ SDS(9:1)**	---	SDS≥98% superplasticizer≥97%	SDS=0.0014, superplasticizer=0.0123

*: Weight of cement applied per cubic meter of concrete (wt).
**: These combinations were examined for further research.

According to recent researches, the destruction identification concrete-CNTs sensors can be manufactured with two or four probes (Han, Ding and Yu, 2015). In this research, the cement-based sensors with two copper probes (Kim et al. 2014; Han, Ding, et al. 2015) with the dimensions 5 cm×3.6 cm and the electrical resistance of 2.15 nΩm were applied to ensure electrical conductivity between both sides of the concrete sensor.

3.2 Methodology

SDS/MWCNT and NaDDBS/MWCNT solutions were prepared by mixing 0.05wt% MWCNTs with an aqueous individual surfactant solution at concentration 2.254, 4.88 (gr/mL) respectively. Also mixtures of NaDDBS/TX-100 and SDS/DTAB at concentrations 8.896, 2.524 (gr/mL) respectively were prepared. Then 0.05wt% MWCNTs was added to each mixed solution. All solutions were stirred for 10 min with a magnetic stirrer (model, WIFESTEER MSH-20B) and then sonicated for 130 min with an ultrasonic cleaner set (model NISONIX 3000) at an average power of 275 W. The temperature was controlled during sonication to prohibit warming of the solutions. Subsequently, the solutions were centrifuged for 10 min at 8000 rpm to remove the bigger clusters. The result shows that the supernatant was truly separated from the sediment after centrifugation stage. After 24h resting, the characterization of MWCNs solutions was performed (see Figure 8). UV–vis absorption spectra were recorded using a Shimadzu-2100 UV–visible spectrophotometer (model, Japan) with a matched pair of glass cuvettes, 1 cm in optical path length, placed in a thermostated cell holder. The final samples were diluted to three times their original volume with pure water to reduce the original darkness of solution for UV-vis test. Given that the absorption spectrum of MWCNTs is in the 500-700 nm wavelength range, the UV-vis experiment can be applied to appraise the dispersion of MWCNTs in the water (Vaisman, Wagner and Marom, 2006; Luo, Duan and Li, 2009). The UV experiment scaled from 0 to 5 where the maximum value means the dispersion quality is at the maximum and the minimum value means the dispersion quality is low. The UV experiment was run at the wavelength of 650 nm. Finally, the outcomes obtained from the UV-vis experiment and the turbidimetry that is the process of measuring the loss of intensity of transmitted light because of the scattering impact of particles suspended in it, were compared to determine the best surfactant for the uniform and efficient dispersion of MWCNTs in the aqueous phase.

The cement was added to the mixer containing water and MWCNTs with high-speed turning ability (3600 rpm – Pars-Khazar Co.) to be uniformly mixed. After adding the aggregate to

the mixer, the concrete was placed in pre-oiled molds (Figure 9) and by applying appropriate vibration, any air that may have been trapped was released.

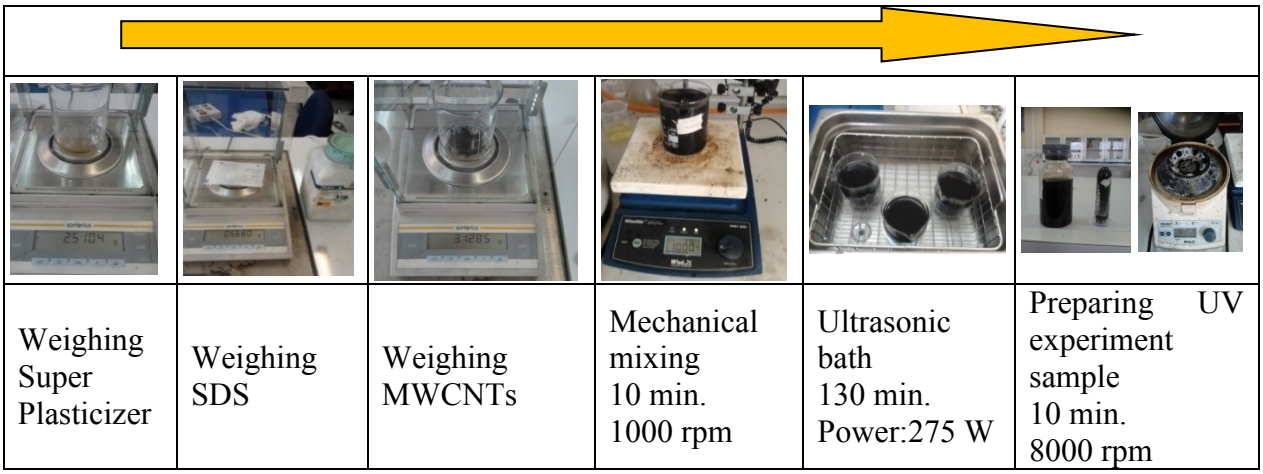

Weighing Super Plasticizer	Weighing SDS	Weighing MWCNTs	Mechanical mixing 10 min. 1000 rpm	Ultrasonic bath 130 min. Power:275 W	Preparing UV experiment sample 10 min. 8000 rpm

Figure 8- Dispersion of MWCNTs in the aqueous phase.

Concrete specimens were removed from the molds after 24 hours and cured in aqua phase at 25 °C for 28 days (Astm:C192/C192M-13, 2013). To appraise the impact of various surfactants on dispersion quality with constant number of MWCNTs (0.05% wt) under static loading regime, The 3 specimens were examined for compressive (5×5×5 cm) and 3 other for flexural (4×4×16 cm) stress in accordance with ASTM C39 and ASTM C78 standards, respectively (ASTMC39/C39M-04a, 2004; ASTM C78, 2012). SEM images that were captured with ZEISS SUPRA™ 40 Field Emission Scanning Electron Microscope (FESEM), were also applied to appraise the dispersion quality of the MWCNTs in the concrete.

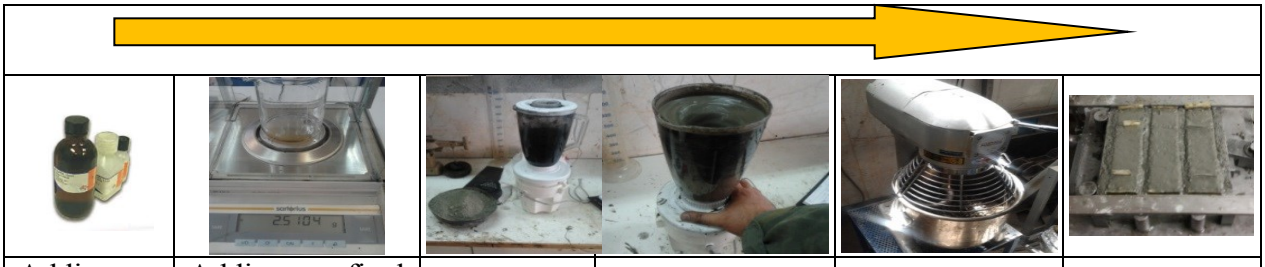

Adding antifoam in step 1	Adding final number of superplasticizer	Mechanical mixing	Mixing cement 3 Min.	Mixing aggregate	Molding

Figure 9- Dispersion of MWCNTs in cement and cast the cement-based sensor.

After finding the proper surfactant composition to disperse MWCNTs in concrete, other experiments were run to estimate the proper number of MWCNTs to gain consistent concrete-CNTs sensor with conventional concrete with same mix design. This is the critical point to produce a cement-based sensor, that has same specifications with conventional concrete embedded in to appraise its specifications near real situation. To appraise the cement-based sensor function and to investigate the efficient parameters during

manufacturing to gain consistent cement-based sensor to plain concrete, the experiment process designed as presented in **Table 4**.

As this is presented in table 4, various parameters may be affected on cement-based sensor function such as various types of surfactant composition, diverse dispersion energy levels applying to the aqueous phase for increasing dispersion quality and various numbers of MWCNTs were inquired to cast various cement-based sensors. To appraise the impact of each parameter on cement-based sensor response, some criterion were defined and each experiment was run with three specimens (4×4×16 cm) under static and dynamic loading regime.

Table 4- study process and experiment approach

Loading regime	Surfactant	Energy level	Amount of MWCNTs by weight of cement(wt) (volume fraction (%))					Criteria
Static	Superplasticizer (SP)	L			0.15 (0.21)	0.1 (0.14)	0.05 (0.07)	Sensitivity of the sensor (Se) Standard deviation of the prediction error
	Superplasticizer +SDS(SPS)	L	0.25 (0.35)	0.2 (0.28)	0.15 (0.21)	0.1 (0.14)	0.05 (0.07)	
Dynamic	Superplasticizer +SDS(SPS)	VL			0.15 (0.21)	0.125 (0.18)	0.1 (0.14)	Internal and exterior repeatability of the sensor (Re) Sensitivity of the sensor (Se) Cross-correlation (CC) Hysteresis (SSE)
		L						
		H						

Very Low energy level (**VL**): Ultrasonic bath for one hour, Low energy level (**L**): Ultrasonic bath for two hours, high energy level (**H**): Ultrasonic bath for two hours + 90 minutes of probe ultrasonic

Figure 10 explains the way in which the flexural experiment was conducted. To run low cycle fatigue experiment to appraise cement-based sensor function under dynamic loading pattern, each of the cement-based sensors was loaded by sinusoidal forces with various magnitudes (from 0.2 to 0.7 and 0.2-1.2 kN) in the linear region of concrete stress-strain graph (the applied force is less than 50% of the ultimate force). The experiments were run four times for each cement-based sensor, and the outcomes are shown in the related graphs and expressed in form of average and standard deviation.

After determination of proper mix design to manufacture concrete-CNTs sensor consistent with conventional concrete mechanical properties. This mix design includes the composition of superplasticizer and the SDS with a mixing ratio of 9:1 respectively and 0.15% wt MWCNTs with conventional concrete mix design. to perform unlimited dynamic fatigue experiments and study around destruction propagation in Portland cement concrete pavement and its remaining life, 6 samples (10×10×40 cm) at each stress levels (S) (70%,

80% and 90%) to the final stress (MOR), were loaded under sinusoidal dynamic load pattern with frequency of 7.5 Hz and stress ratio (R = 0.25) up to failure.

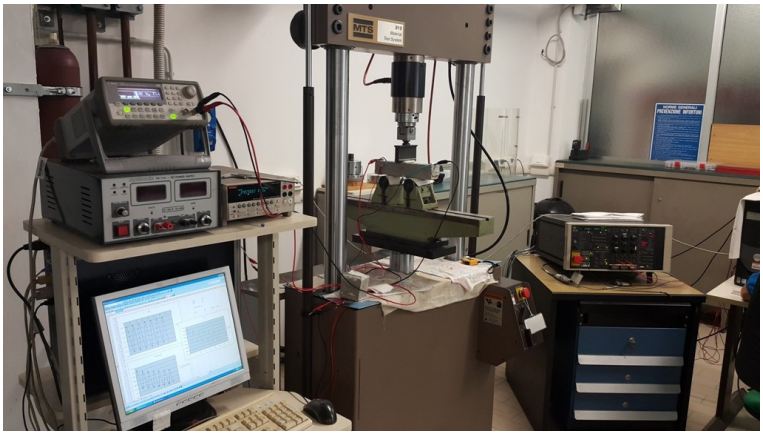

Figure 10- Three-point bending experiment under static and dynamic loading

According to Figure 11, to simulate the situation of pavement slab under vehicle wheel load, the concrete-CNTs sensors were placed in the conventional concrete beam with the same concrete mixture design. For investigation of the dynamic response of cement-based sensors, the cement-based sensors were examined by MTS experiment equipment. The experiment was carried out pursuant to ASTM C78 that is the base for static loading(ASTM C78, 2012).

To model the cement-based sensor response to evaluate exterior load and calibrate the cement-based sensors for weight in motion detector, they were examined under various dynamic loading magnitudes according to **Table 5** and the relationship between maximum load and maximum fractional changes in resistance was investigated.

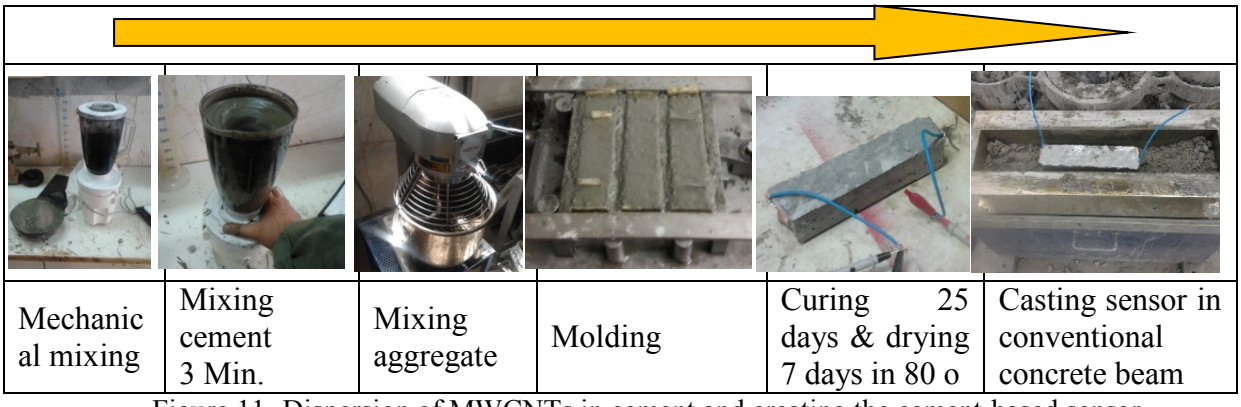

Figure 11- Dispersion of MWCNTs in cement and creating the cement-based sensor

Table 5- Research process and experiment method

Loading pattern	Surfactant	Amount of MWCNTs (%)	loading magnitude(KN)				
Dynamic	SDS/SP	0.15	0.5	0.7	1.3	2	3

3.2.1 Proper electrical circuit for concrete sensor

Generally based on previous literature, two types of circuit consist of direct current (DC), alternative current (AC)(Vossoughi, 2004; Hou and Lynch, 2005; Galao *et al.*, 2014; D'Alessandro *et al.*, 2016) combine with two types of electrode schemes consist of two probes(Fu *et al.*, 1997; Chung, 1998; Wen and Chung, 2001; Baeza *et al.*, 2013; Han, Yu and Ou, 2015), and four probes set up have been applied in concrete sensors. Although the two-probe approach has simpler measurement circuit compared with the four-probe method, the four-probe approach is preferred to the two-probe approach because this can omit the contact resistance between electrodes and concrete-CNTs sensor (Qu and Han, 2008; Han, Ding and Yu, 2015; Han, Yu and Ou, 2015).

Use of direct current circuit cause seeing the resistance varied along time because of polarization effect. The polarization cause variable potential (Vp) over the time opposes the electrical current in the circuit and disclose s itself in the form of diminished current (N. Banthia and Pigeon, 1992), Equation 3.

$$I = \frac{V - Vp}{R}$$ Equation 3

It follows that in this case at least two various values of the applied voltage should be applied to determine the two unknowns VP and R. However, the best approach is via using alternating currents.

The impact of polarization is because of the movement of free ions in the concrete-CNTs sensor and causes a gradual increment in the electrical resistance of the cement-based sensors during the measurement (Baoguo Han *et al.*, 2012).

In this research, an alternating current circuit with two probes electrodes as this is presented in Figure 12 is applied.

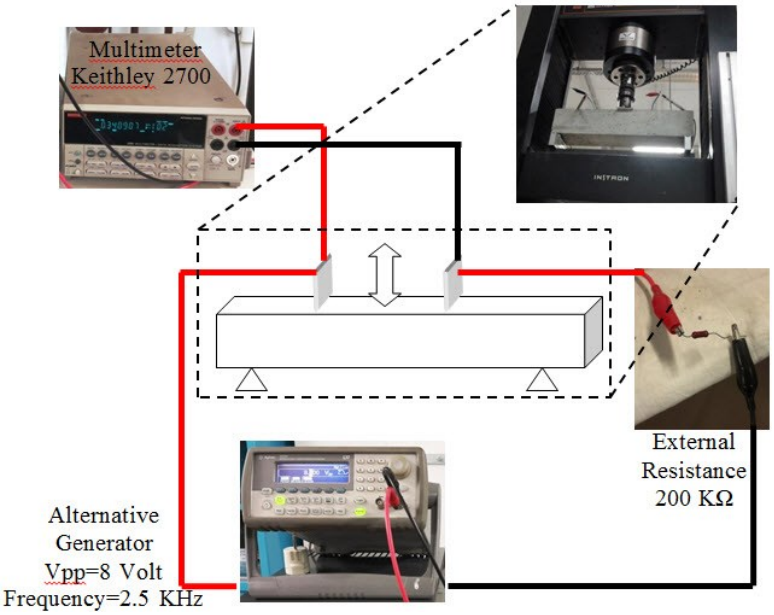

Figure 12- Three-point bending experiment under static and dynamic loading and experiment circuit setup

In this approach, the impact of polarization is considered by introducing a capacitor in series or parallel with the resistance, and Equation 4 takes the form (N. Banthia and Pigeon, 1992).

$$Z = \frac{V}{R}$$ Equation 4

Where Z is the system impedance in Ohms. Also, Z and R are related as:

$$Z = \frac{R}{\sqrt{(1 + \omega^2 C^2 R^2)}}$$ Equation 5

And ω=2πf, where f is the applied frequency in cycle per second (Hz), and C is the capacitance in farads. This can be seen that by increasing frequency, we can eliminate the impact of the capacitor. Usually, alternative voltage (AV) is plotted versus frequency, and the frequency in which the AV gets a higher number is calculated (Figure 13). At this frequency Z approaches R (Vossoughi, 2004) see Equation 5.

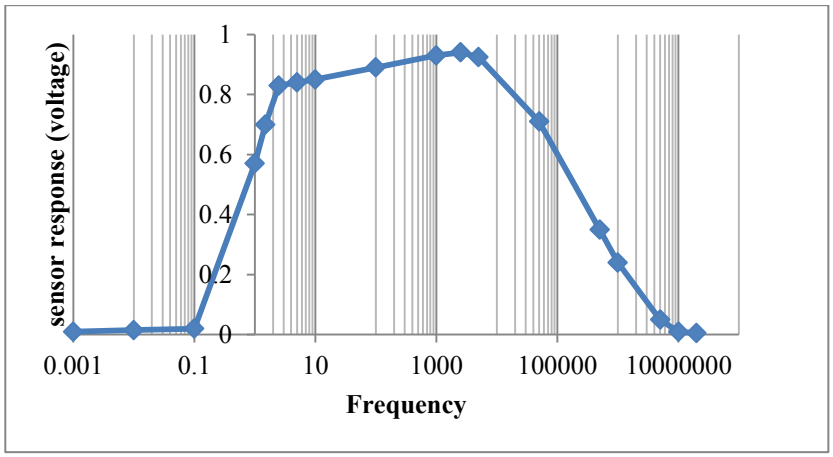

Figure 13- alternative voltage (AV) versus frequency

So to omit polarization effect, alternative generator with the value of Vpp = 8 Volts and the frequency of 2.5 kHz was applied to nullify this phenomenon. The cement-based sensor response in this circuit is the potential difference across the two ends of the cement-based sensor (Vs) that is evaluated by a multimeter (Keithley 2700 series) at regular intervals. Considering the circuit presented in this can be verified that by using a constant resistance (e.g. Rc=200 kΩ) in the circuit and also by measuring the potential difference across the two ends of the cement-based sensor, the electrical resistance of the cement-based sensors (RS) can be calculated at any point in time (See Equation 6 and Equation 7).

$$Vg=Vs+Vc \qquad \text{Equation 6}$$

$$Vs = Vg\frac{Rs}{Rs+Rc} \qquad \text{Equation 7}$$

Vg: Potential difference of the generator,
Vs: Potential difference between the head of concrete sensor,
Vc: Potential difference of the exterior resistance (constant resistance),
Rs: Resistance of the cement-based sensor,
Rc: Constant resistance (200 kΩ).

Chapter 4 Results and discussion

4.1 Abstract

For casting the concrete-CNTs sensors, some parameters are important, such as the number of CNTs, species of surfactant, dispersion quality etc. To appraise these parameters, the dispersion quality of multi-walled carbon nanotubes in the aqueous phase and cement mix was examined using Ultraviolet-Visible Spectrophotometry (UV-VIS), Scanning Electron Microscopy (SEM) and mechanical experiments for compressive and flexural strength. After finding the proper approach and surfactant to cast the concrete sensor, the optimum number of MWCNTs should be determined. To appraise the influences of the main parameters affecting concrete-CNTs sensors performance, diverse criteria in static and dynamic loading patterns were defined such as sensitivity of the cement-based sensor (Se), the standard deviation of the prediction error, repeatability (Re), cross-correlation (CC) and hysteresis (SSE). These criteria help to find proper number of MWCNTs to have the best cement-based sensor function that is consistent with conventional concrete in mechanical properties. After casting the proper cement-based sensor, the next step is exploring the influences of traffic loads on the pavement and model the cement-based sensor attitude, and to do so concrete-CNTs sensors were examined under various values of limited dynamic loads (10 cycles). In addition, to study the response of the concrete-CNTs sensor under the traffic loading and find out the destruction mechanism and crack propagation, unlimited fatigue experiments were run up to failure.

4.2 Dispersion phase

The degree of dispersion of MWCNTs in aqueous media has been inquired using the UV−vis spectra of the dispersions (Rausch, Zhuang and Mader, 2010). Individualized MWCNTs are active in the UV−vis region and show specification bands corresponding to additional absorption because of 1D Van Hove singularities (Yu *et al.*, 2007; Sohrabi and Nayeri, 2014). However, bundled MWCNTs are hardly active in the wavelength region between 200 and 1200 nm (Yu *et al.*, 2007; Sohrabi and Nayeri, 2014). So, this is notable to compare the number of individually dispersed MWCNTs in the solution via the absorption intensity.

Step 1: The UV−vis spectra of aqueous MWCNTs dispersions using various systems are shown in Figure 14. According to Figure 14, the maximum absorbance was obtained for SDS/DTAB mixture, indicating high dispersion of MWCNTs. The dispersion of MWCNTs with SDS, NaDDBS and TX_100/NaDDBS solutions were low compared to SDS/DTAB mixture. So, by mixing anionic and cationic surfactants, a higher dispersion of MWCNTs can be achieved at a lower concentration of surfactants. Also, all other parameters such as the sonication time and power, MWCNTs quantity etc. were held constant during the test. This has been remembered that the solution was diluted three times its original volume with pure water to gain high resolution spectra. So, the absolute values of the absorbance are higher than the outcomes shown in Figure 14, but relatively, these outcomes are reliable. Also, based on the experiment procedure, the solution without surfactant was not stable and the MWCNTs were completely sedimented after centrifugation, so that after dilution step, the absorbance result was near zero.

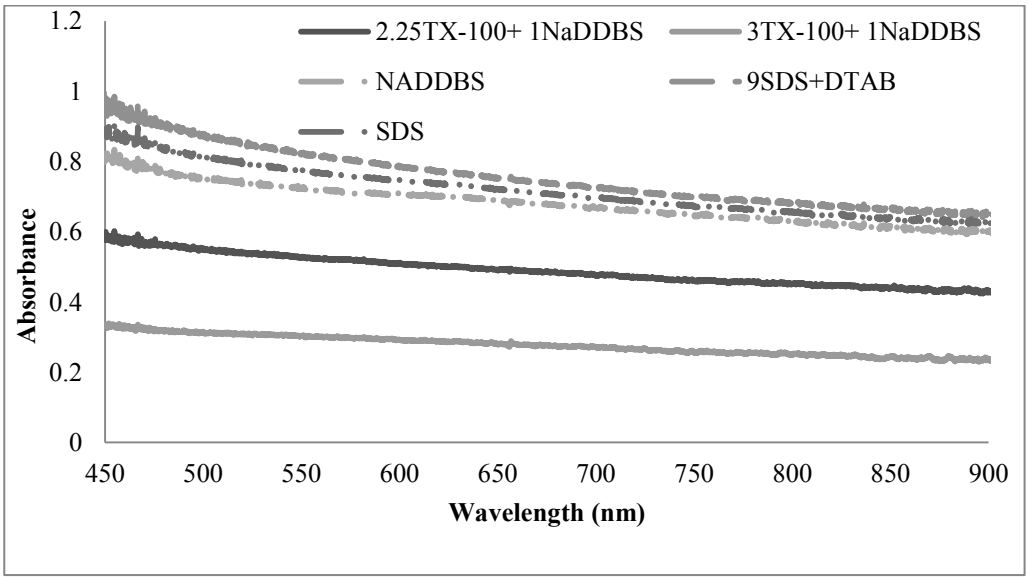

Figure 14- UV−vis spectra of an aqueous (0.05 wt%) MWCNTs dispersion using various surfactants.

The outcomes demonstrated that when a mixture of water, dispersed MWCNTs and the surfactant material is applied to make concrete, the mechanical specifications of concrete are severely diminished because of the foam resulting from the surfactant in the concrete mixing process. Figure 15 explains the impact of not using an antifoam in the concrete mixing. In this case, the defoamer, Tributyl Phosphate, can be applied to resolve this problem. So far, the exact mechanism of the antifoams is not truly understood (Barber, 2005). Nevertheless, the general function of the antifoams is that they disrupt the stability of the liquid films in the foam, increasing the rate of the liquid drainage and thus enhancing foam destruction (Winterburn and Martin, 2012). Azhari, observed that methylcellulose (that has an air-entraining impact and increases the number of porosity) and Tributyl phosphate antifoam

(that has the ability to reduce the number of porosity) cause a change in the quantity of the void phase (Azhari and Banthia, 2012).

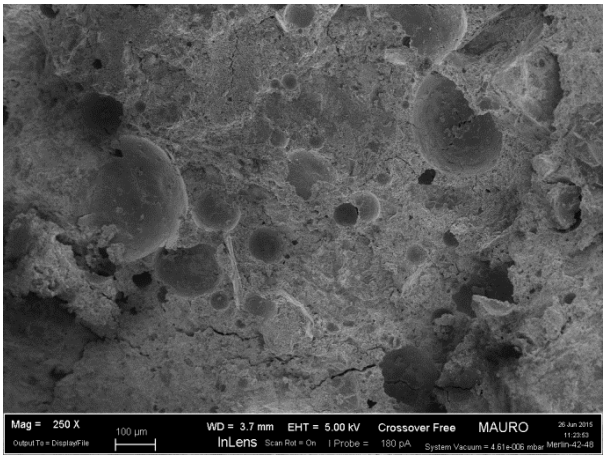

Figure 15- Air bubbles in the concrete with SDS as the surfactant in the absence of defoamer.

Figure 16 explains the impact of using Tributyl Phosphate antifoam (0.02 wt%) on the concrete mixing process when SDS is applied as the surfactant.

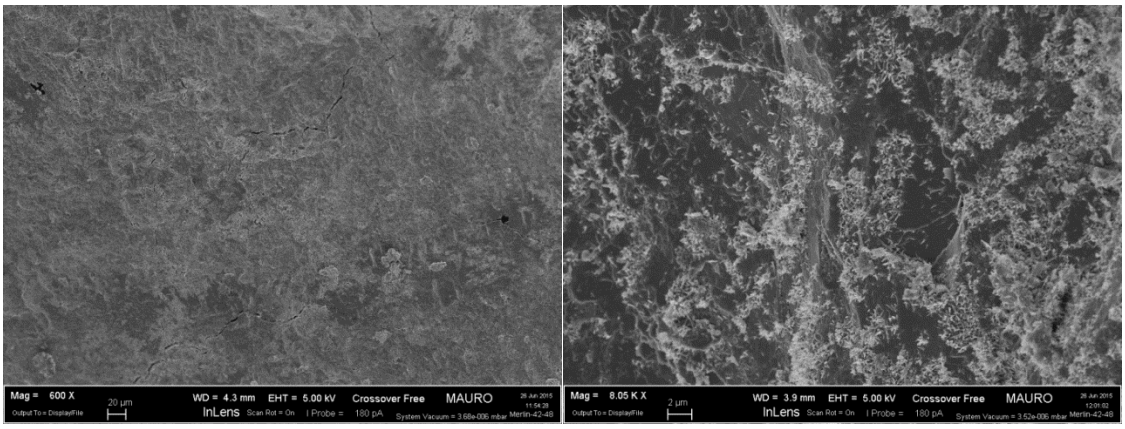

Figure 16- Concrete reinforced with 0.05% wt MWCNTs with SDS as the surfactant and Tributyl Phosphate defoamer.

Comparing the SEM micrographs (Figure 15, Figure 16) demonstrates that the elimination of the antifoam in the concrete mixing process outcomes in a lot of unwanted air bubbles and may reduce the mechanical specifications of concrete. This can also be observed that air bubbles reduction can boost MWCNTs dispersion uniformity in the concrete mixture. The compressive and flexural experiment outcomes on the concrete specimens containing 0.05 wt% MWCNTs and 0.02 wt% antifoam are explained in Figure 17 and Figure 18.

As can be seen in Figure 17 and Figure 18, the mechanical specifications of concrete reinforced with 0.05 wt% MWCNTs and containing various types of surfactant as well as, 0.02 wt% antifoam are promoted with respect to plain concrete, as the dispersion quality of MWCNTs is increased. The maximum compressive and flexural stresses that are related to SDS and DTAB surfactant composition with a mixing ratio of 9:1, are improved by 60.3% and 51.2%, respectively respect to conventional concrete (without MWCNTs). So, this was evidence that the composition of SDS/DTAB resulted in the best dispersion capability.

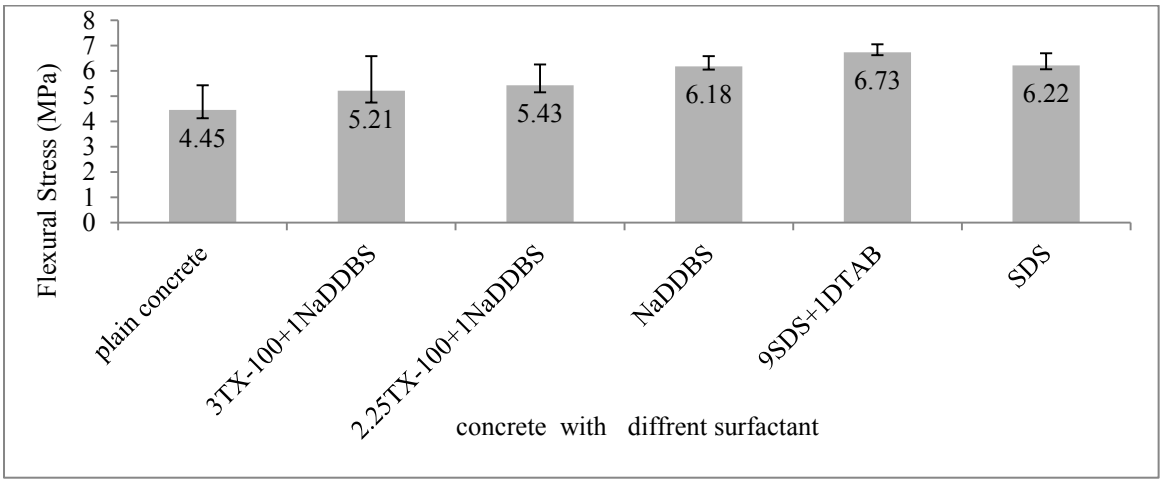

Figure 17- Modulus of rupture of concrete specimens containing 0.05 wt% MWCNTs and various surfactants.

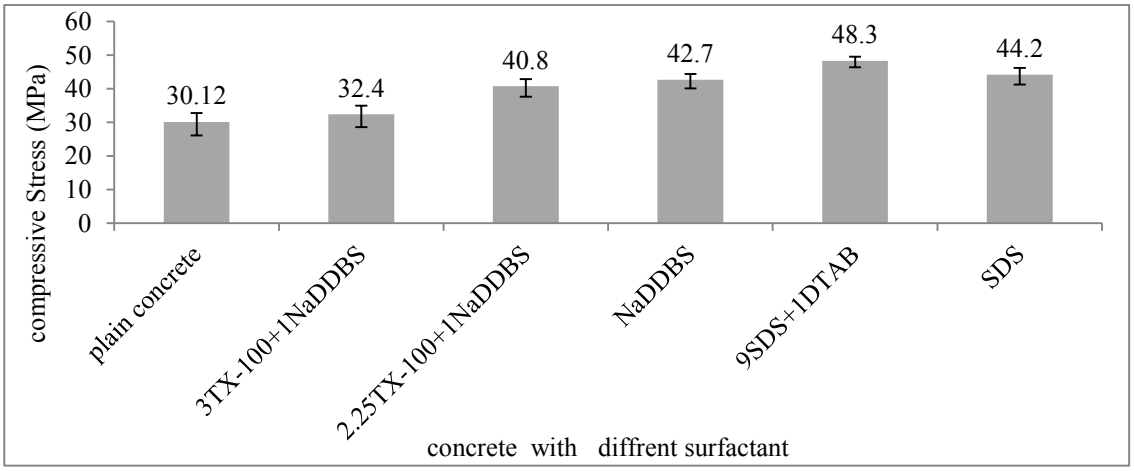

Figure 18- the compressive strength of concrete specimens containing 0.05 wt% MWCNTs and various surfactants.

Step 2: Another approach to resolving the problem of unwanted air bubbles in the concrete mixing process without the application of defoamers is the use of a surfactant compatible with concrete. One of the approaches indicated here is to apply compounds that eliminate the number of water needed in the mixture such as plasticizers and superplasticizers (B. Han *et al.*, 2012; Sun, Yu and Han, 2014; Han, Ding and Yu, 2015). In this research,

various amounts of polycarboxylate based superplasticizer were applied to disperse MWCNTs in the water. The UV−vis spectra of aqueous MWCNTs dispersions using various concentrations of polycarboxylate are evaluated to determine their optimum concentration (C_{opt}). As shown in

Figure 19, the increment in SP-C concentrations up to the concentration of 0.5 wt% leads to the increment in the absorbance intensity; however, further increases in SP-C concentrations cause the reduction in absorbance intensity. Thus, the value of C_{opt} for SP-C is determined to be 0.5 wt%. So, this is assumed that most SP-C in the suspensions adsorbed onto the surfaces of the MWCNTs. Further increment in SP-C concentrations above the C_{opt} outcomes in wasting materials and may cause undesired results. As regards, the new surfactant (superplastisizer) is compatible with concrete and doesn't require the application of a defoamer, the unwanted air bubbles are less, as shown in Figure 20. However, UV-Vis experiment outcomes have shown that the dispersion power of DTAB/SDS mixtures is higher than that of the superplasticizer. As shown in Figure 20 by an black ring, dispersion quality of MWCNTs dispersed with a superplasticizer is not proper and there is the agglomeration of MWCNTs in concrete.

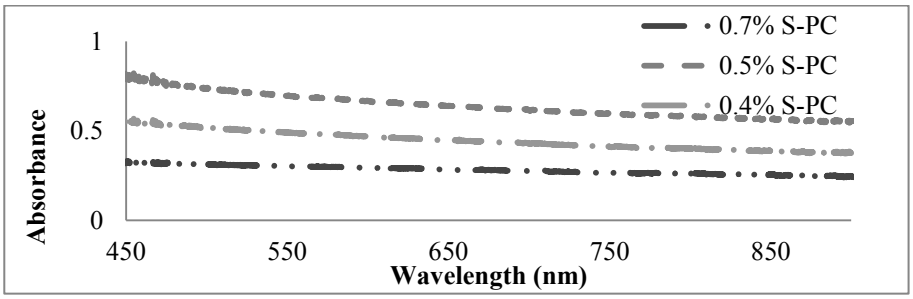

Figure 19-UV−vis spectra of an aqueous(0.05 wt%) MWCNT dispersion using various concentrations of SP-C.

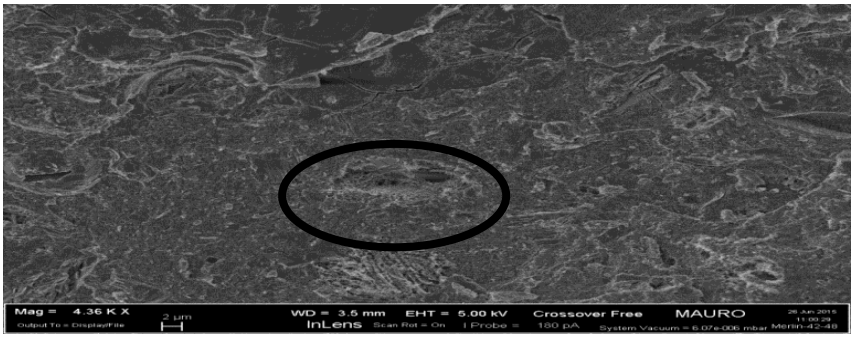

Figure 20- Concrete reinforced with 0.05% wt MWCNTs dispersed with superplastisizer in the absence of defoamer.

Step 3: Based on the outcomes presented in Figure 14, the composition of SDS+DTAB (9SDS+1DTAB) fabricated mildly better outcomes in dispersing multi-walled carbon nanotubes than SDS alone. To minimize the cost of the new surfactant composition that will be applied in large amounts in the process of casting smart concretes and, because of the ratio between SDS and DTAB is also challenging when this surfactant combine with SP-C, SDS is substituted with a composition of SDS+DTAB to boost SP-C surfactant effect. So, to obtain a high dispersion ability, the dispersing power of SP-C/SDS mixtures as new surfactant composition was investigated. To compare the dispersing power of SP-C/SDS mixtures, the UV−vis spectra of aqueous MWCNTS dispersions for various ratios of SP-C/SDS mixtures were evaluated. As shown in Figure 21, decreasing the ratio SP-C/SDS in the aqueous solution, the absorbance in the specification wavelength region changes to higher values, indicating that the number of individually dispersed MWCNTs is increased. Hence, according to our experimental results, the maximum dispersion is obtained with the ratio of 5 for SP-C/SDS mixtures. The outcomes demonstrated that the composition of these two surfactants could extend the new composition that can disperse MWCNTs in the aqueous phase much higher than each one did alone with the same dosage. The synergic impact of these two surfactants is because of attractive interactions between these surfactant molecules when dispersing MWCNTs in aqua phase.(Tan and Resasco, 2005; Luo, Duan and Li, 2009).

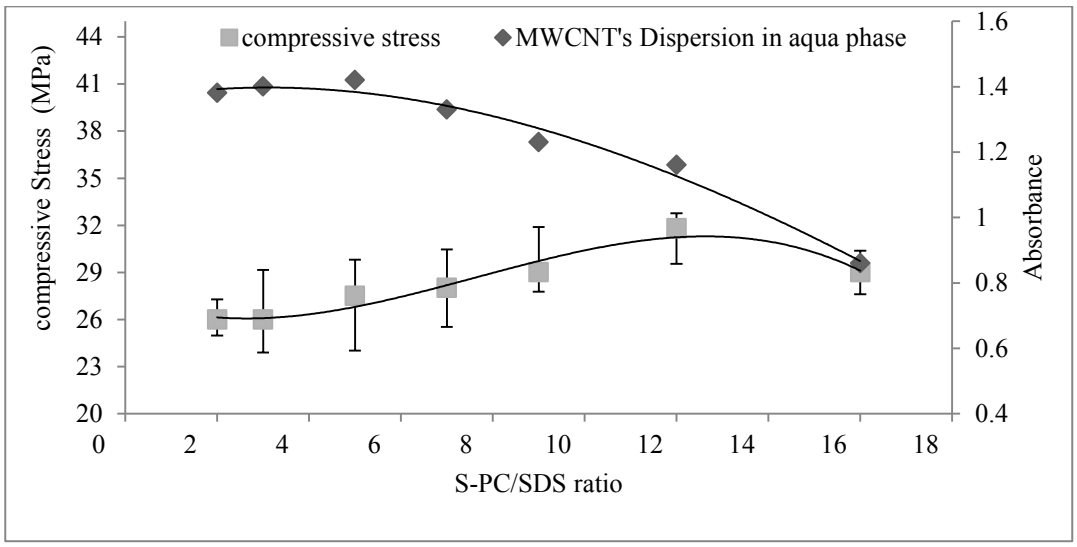

Figure 21- The impact of various mixing ratios of SP-C to SDS on the dispersion quality of MWCNTs in the aqueous phase and the compressive strength of specimens containing MWCNTs.

To appraise the influences of the new surfactant composition on the mechanical specifications of concrete six specimens ($5\times5\times5cm^3$) were cast and after 28 days curing, were examined according to ASTM C39 standard. The outcomes showed that the compressive

strength of concrete varies from -10% to +33% of the conventional concrete compressive strength (30 MPa) as the ratio of SP-C to SDS is reduced, Figure 21. As regards the number of foam formed in the concrete is increased as the number of SDS is increased this, in turn, would cause the decline in the mechanical specifications of the concrete. So, considering the intended purpose of making concrete containing MWCNTs, the optimum ratio of SP-C/SDS should be concerned. If the goal is to make concrete with the maximum strength, the ratio of SP-C/SDS equal to 12 is suggested, but if the goal is to make concrete containing the largest number of well-dispersed MWCNTs, the ratio of SP-C/SDS equal to 5 may be suggested. A ratio of SP-C/SDS equal to 9 is declared when making concrete with similar specifications to the conventional concrete (without MWCNTs) is concerned.

In order to compare the number of dispersion of MWCNTs, turbidity measurements of colloidally stable dispersed MWCNTs solutions containing pure surfactants, superplasticizer and mixtures of DTAB/SDS, NaDDBS/TX-100 and SP-C/SDS are performed. The UV and turbidity outcomes of all systems are shown in Figure 22 and **Table 6**.

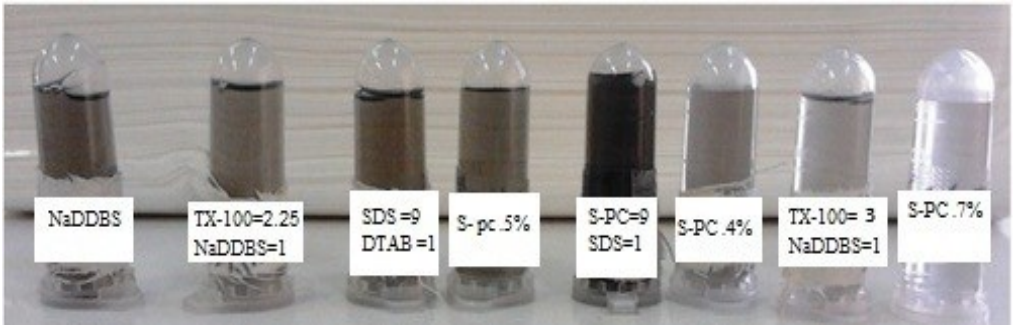

Figure 22- Comparing MWCNTs dispersion in aqua phase using turbidity meter.

Table 6- The turbidity of water containing MWCNTs using various surfactants

Surfactant	*Absorbance (out of 5)*	*Turbidity (NTU)*
SDS/DTAB(9:1)	0.76	1320
SDS	0.71	1086
NaDDBS	0.68	579
TX-100/NaDDBS(3:1)	0.28	27.6
TX-100/NaDDBS(2.25:1)	0.48	245
Superplasticizer (0.4 wt*%)	0.29	89.7
Superplasticizer (0.5 wt*%)	0.65	376
Superplasticizer (0.7wt*%)	0.45	187
Superplasticizer/SDS(9:1)	1.23	1835

As can be seen from the Figure 22, the mixture containing the composition of superplasticizer and the SDS with a mixing ratio of 9:1 respectively, by weight of cement shows the best dispersion ability than the other systems.

4.2.1 Summary of dispersion phase

In this part, a new surfactant composition compatible with concrete formulation is indicated to avoid unwanted air bubbles created during mixing process in the absence of an antifoam and to gain the uniform and the maximum possible dispersion of multi walled carbon nanotubes (MWCNTs) in aqua phase and subsequently in concrete. UV-visible spectroscopy and turbidimetry as the measurement criteria in the aqueous phase, and compressive and flexural strengths as the concrete function criteria, were applied to appraise various types of surfactants influence on MWCNTs dispersion. To gain this goal, three steps have been defined: (1) concrete was made with various types and the number of surfactants containing a constant number of MWCNTs (0.05 wt%) and the air bubbles were eliminated with a proper defoamer. The outcomes demonstrated that compressive and flexural strengths are improved by 60% and 50%, respectively respect to plain concrete. (2) Finding a compatible surfactant with concrete combinations and eliminating unwanted air bubbles in the absence of common antifoam is of fundamental importance to significantly increment concrete mechanical properties. In this step, the outcomes demonstrated that the poly carboxylate superplasticizer (SP-C) (as a compatible surfactant), dispersed MWCNTs worse than SDS/DTAB (sodium dodecyl sulphate / Dodecyltrimethylammonium bromide) but unwanted air bubbles were removed, so the antifoam can be omitted in the mixing process. (3) To solve the problem, a new compatible surfactant composition was developed and various ratios of surfactants were examined and appraised by means of function criteria above remarked. The outcomes demonstrated that the new surfactant composition (SDS and SP-C with the ratio of 1:9 respectively) can disperse MWCNTs around 24% more efficiently than the other surfactant compositions. Moreover, this has enough compatibility with the concrete to omit antifoam in the mixing process and to maintain the concrete mechanical specifications pretty constant.

4.3 Evaluation of the function of the concrete-CNTs sensors

In this research, concrete-CNTs sensors containing various amounts of MWCNTs were examined both statically and dynamically. According to previous studies, the cement-based sensors should have several specifications such as repeatability, proper sensitivity to the force changes applied to the specimen, the appropriate cross-correlation between the applied force (input) and the cement-based sensor response (electrical resistance (R) or potential difference (ΔV)), and the minimum hysteresis (Han et al. 2011; Han, Ding, et al. 2015). As can be seen in **Table 4**, because of the nature of loading and the responses of the cement-based sensors to the applied load, a variety of criteria were defined to appraise the function and behaviour of cement-based sensors in static and dynamic loading.

4.3.1 Static loading

Under static loading, determining the species of surfactant and the number of MWCNTs to create an appropriate cement-based sensor is defined as the objective of testing. According to this, two criteria including the sensitivity of the cement-based sensor and the sum of absolute error were defined. Sensitivity is generally the ratio between a small change in electrical signal to a small change in physical signal (Wilson, 2005). Sensitivity can be characterized by such parameters as the maximum magnitude of fractional change in electrical resistance ($\max|\Delta R/R_0|$), force sensitivity coefficient ($(\Delta R/R_0)/F$), stress sensitivity coefficient ($(\Delta R/R_0)/\sigma$), or strain sensitivity coefficient ($(\Delta R/R_0)/\varepsilon$), also called gage factor) (Han, Yu and Ou, 2015). The sensitivity of the cement-based sensor indicates the changes in the electrical resistance of the cement-based sensor per unit change in the flexural stress of the concrete specimen. To omit the dimension of the flexural stress, the sensitivity criterion is defined as showed in Equation 8 and is called Normalized stress sensitivity coefficient. Obviously, the bigger the changes are, the higher the cement-based sensor measurement precision is under low stress. So, the slope of the changes in the electrical resistance of the cement-based sensor versus the concrete specimen stress is presented in Figure 23. The stress at failure (σ_{max}), that is called module of rupture (MOR), is presented in Figure 24 as cement-based sensor sensitivity criteria. The outcomes showed that the higher the slope is, the higher the sensitivity of the cement-based sensor is.

$$\text{Normalized stress sensitivity coefficient (Se)} = \frac{\frac{\Delta R}{R0}}{\frac{\sigma}{MOR}} \qquad \text{Equation 8}$$

$\frac{\Delta R}{R0}$: Fractional change in electrical resistance.

$\frac{\sigma}{MOR}$: Normalized Flexural Stress (the ratio of the flexural stress over the modulus of rupture).

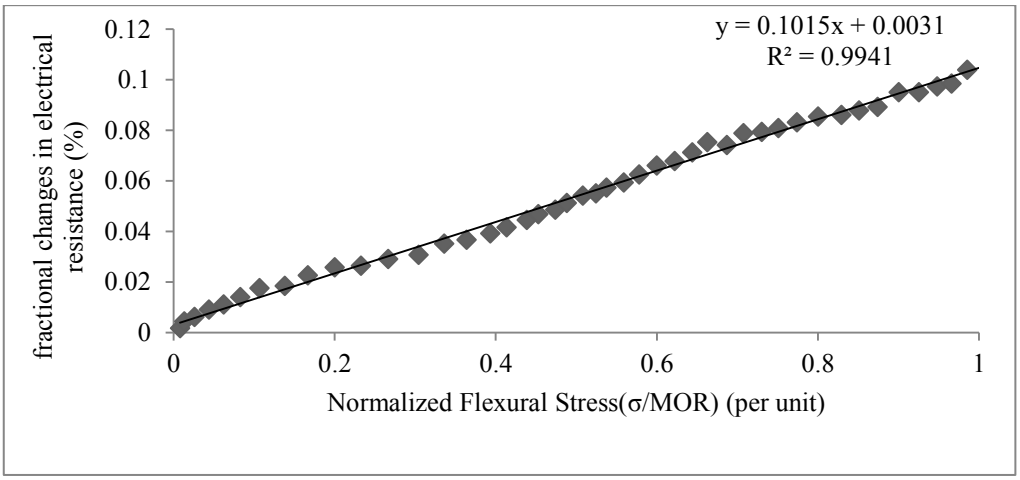

Figure 23- The cement-based sensor responses containing 0.1% CNTs

Analysing the sensitivity of the various cement-based sensors in Figure 24, this may be drawn that the cement-based sensors containing the superplasticizer and SDS as surfactant are more sensitive than the cement-based sensors that only contain the superplasticizer because of the efficient dispersion of MWCNTs in the concrete mixture. Given that the sensitivity of the cement-based sensor containing 0.15% MWCNTs is higher than the cement-based sensor containing 0.1% CNTs, the proper number for creating a sensitive cement-based sensor is 0.15% of MWCNTs based on this criterion. Han et al.(Han *et al.*, 2011) cast cement-based sensors having favourable function parameters such as a sensitivity of 0.911 kΩ/MPa when the stress was varied from 0 to 10 MPa. Compared to Han study, the procedure to determine the sensitivity was completely various in this study because of using the Equation 8 instead of the gage factor formula.

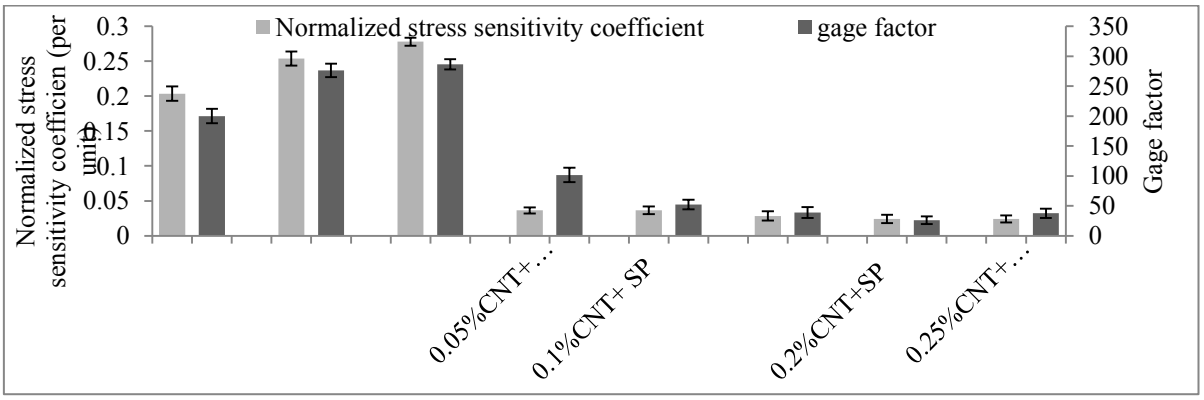

Figure 24- The Normalized stress sensitivity coefficient and gage factor of the various cement-based sensors

Another criterion defined in the static loading pattern is the linearity, defined as the maximum deviation from a best straight line matched to output data (Wilson, 2005). In this research, linearity is defined so that the deviation from best-fitted line presented in Figure 25

can be calculated according to Equation 9. The sum of absolute errors that represents the evaluation of data deviation using the predicted value (that can be obtained from the fitted equation by linear regression technique) is defined as follows:

$$\text{Sum Of Absolut Errors} = \sum \left| Yi - Y\hat{} \right| \qquad \text{Equation 9}$$

Y_i= the number of change in the output resistance of the cement-based sensor at a specific stress.

Y^*= the number of change in the output resistance obtained from the fitted equation to the cement-based sensor at a specific stress.

The wider the deviation in the outputs of the cement-based sensor against the way in which the force is applied is, the higher this criterion is, so the cement-based sensor that has a less deviated data set and is closer to the linear form because of the constant loading rate is more accurate.

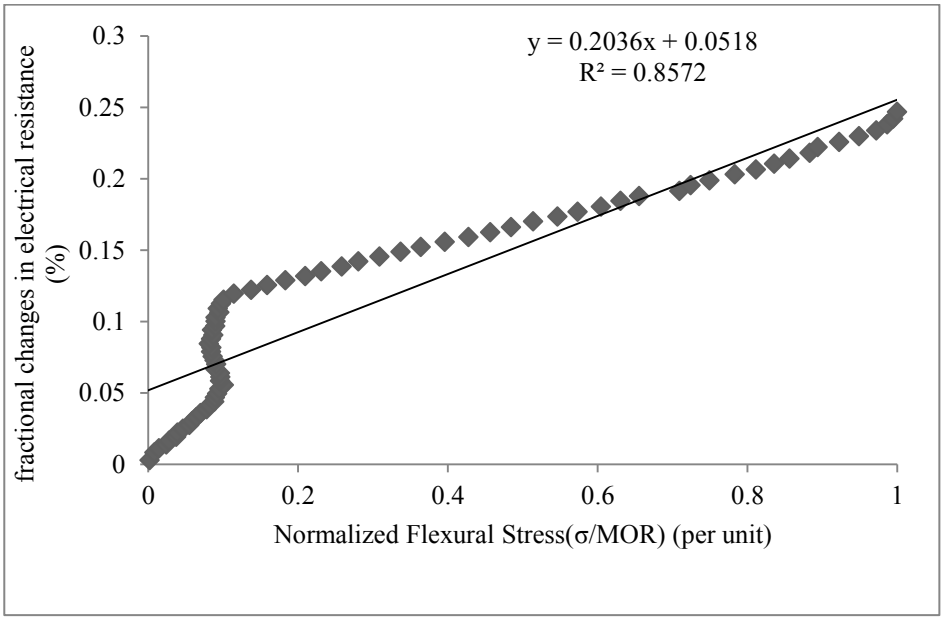

Figure 25- The cement-based sensor responses containing 0.05% MWCNTs

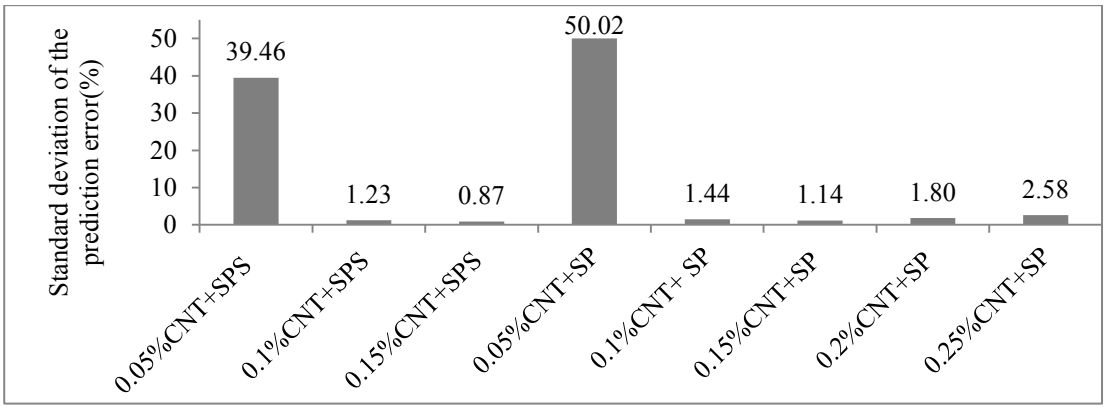

Figure 26- Standard deviation of the prediction error for evaluating the linearity of the cement-based sensor.

According to Figure 26, this can be seen that the total deviation of the observed data (the output of the cement-based sensor) and the estimated values (obtained from the fitted graph by linear regression technique) are the least possible with the number of 0.15% of CNTs. So, this can be claimed that 0.15% of MWCNTs that is dispersed by superplasticizer and SDS as surfactant has a less deviated data set and this is the closest to the linear form. This criterion showed that the small number of MWCNTs (0.05 wt%) cannot result in linear cement-based sensors but with higher amounts of CNTs, a linear cement-based sensor is fabricated so that there is not notable variation between the others cement-based sensors containing more CNTs.

4.3.2 Dynamic loading

Unlike the static loading, loading rate is variable in the dynamic loading, and the same goes for the cement-based sensor's response. As remarked above, MWCNTs are not truly dispersed in the cement-based sensor with the application of superplasticizer alone. So, in the dynamic loading, the cement-based sensors were created using superplasticizer and SDS at the ratio of 9 to one ($\frac{\text{superplasticizer}}{\text{SDS}} = 9$). After determining the species of surfactant and its impact on the cement-based sensor response, the impact of various levels of ultrasonic dispersion energy (dispersion quality) on the function of the cement-based sensors in the stage of dispersing MWCNTs in the aqueous phase is inquired using diverse function criteria (see **Table 4**). As remarked above, the sensitivity of the cement-based sensor response is defined as the slope of the stress-response (changes in the electrical resistance) graph of the cement-based sensor assuming a linear behaviour for it. The sensitivity of various cement-based sensors manufactured at various dispersion energy levels and various percentages of MWCNTs is explained in Figure 27.

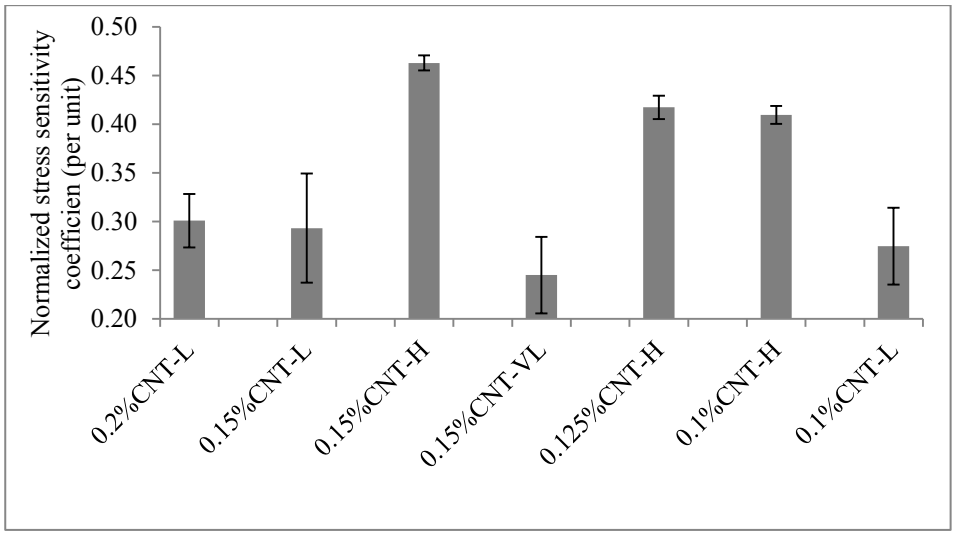

Figure 27- Sensitivity of the cement-based sensor under dynamic loading

Figure 27 shows that the ultrasonic energy level applied for the dispersion of MWCNTs plays a decisive role in the sensitivity of cement-based sensors. In fact, the energy consumed for the dispersion of MWCNTs improves their dispersion quality. According to this, some reports have shown that too high dispersion energy will cause the destruction of MWCNTs and eliminate their aspect ratio, and too much CNT incorporation will result in agglomeration. So, optimum dispersion energy level requires achieving maximum dispersion quality(Frmyr, Hansen and Olsen, 2012; Han, Yu and Ou, 2015). Compared to the outcomes shown in Figure 24, based on this study experiment method, increasing the dispersion energy from low level to high level can boost cement-based sensors sensitivity. Also, the outcomes in Figure 27 indicate that for a constant number of MWCNTs (0.15 wt%) increasing the sonication time effectively increases the MWCNTs dispersion and tends to increment the sensitivity. However, after the dispersion quality as the key point in cement-based sensor function reaches the maximum, the number of MWCNTs has a notable impact on making concrete more conductive. The outcomes show that the cement-based sensor created with 0.15% of MWCNTs and high ultrasonic dispersion energy has the highest sensitivity among the cement-based sensors.

The repeatability is defined as the similarity of the output at the given point from one cycle to another (Wilson, 2005). In fact, the repeatability of a cement-based sensor indicates to what extent the responses of a cement-based sensor at various loading and unloading cycles by applying a fixed-magnitude force, are similar (See Figure 28). In this research, this criterion is called the internal repeatability and is defined according to Equation 10. The higher this criterion is, the better the cement-based sensor is created because of the similarity in the behaviour of the cement-based sensor at various loading cycles.

$$\text{Internal repeatability} = 1 - \frac{|((\text{H2} - \text{H1}) * 100)|}{|(\max(\text{H2}, \text{H1}))|} \quad \text{Equation 10}$$

H_i: the minimum and maximum range of cement-based sensor responses in time of the dynamic experiment as shown in Figure 28.

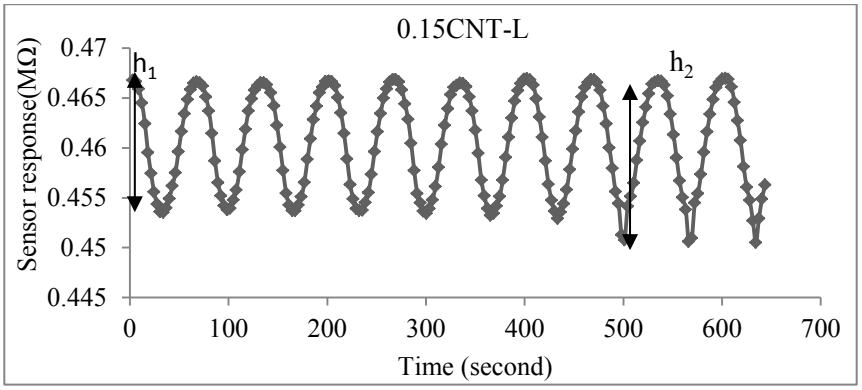

Figure 28- The definition of repeatability of the cement-based sensor

In another definition of this criterion, the repeatability of the cement-based sensor must have a constant value for the cement-based sensor responses (for a linear behaviour of the cement-based sensor) or must follow a specific function as various force levels are applied to the cement-based sensor. This criterion is defined as Equation 11:

$$\text{External repeatability} = \frac{\text{proportion of forces } (\frac{F_{i+1}}{F_i})}{\text{proportion of cement} - \text{based sensor responses } (\frac{R_{i+1}}{R_i})} \quad \text{Equation 11}$$

This means that if the applied force is doubled, the desired cement-based sensor response must be doubled. So, this can be argued that the cement-based sensor has a linear behaviour. The closer this criterion is to one, the more linear the cement-based sensor behaviour is, but this does not mean that the cement-based sensors that have values more than 1 are not good cement-based sensors. These cement-based sensors do not have a linear behaviour, but may have a systematic non-linear behaviour, so this criterion shows only the linearity of each cement-based sensor.

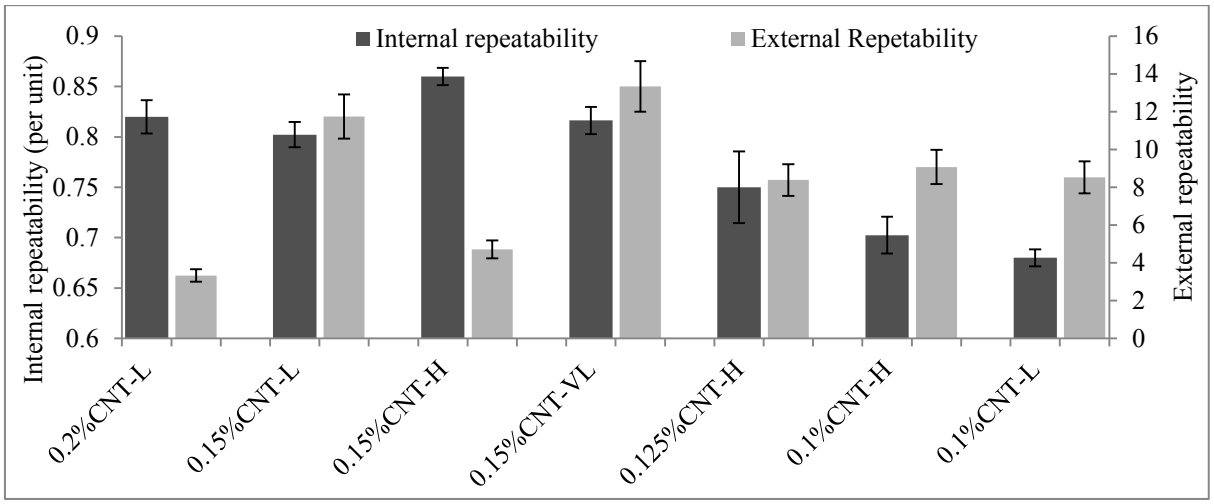

Figure 29- Internal and exterior repeatability of the cement-based sensors

As can be seen from Figure 29, the internal repeatability of a cement-based sensor is highly dependent on the ultrasonic dispersion energy level and on the dispersion quality of MWCNTs in the concrete, and partially dependent on the number of MWCNTs in the concrete. The number of MWCNTs being constant, for example, 0.15 wt%, suggests that using less energy in the dispersion process leads to more changes in the cement-based sensor response between two various cycles at the consequent loading cycles. Given the outcomes of these two criteria, this can, So, be concluded that using more MWCNTs in the cement-based sensor and applying more energy to uniformly disperse MWCNTs in the mixture, these two criteria are improved.

The outcomes showed that the exterior repeatability of the cement-based sensors is improved by increasing the number of MWCNTs implying that the cement-based sensor behaviour is linear. On the other hand, this can be concluded that the dispersion energy does not have as much impact as the number of MWCNTs on this criterion.

Another criterion defined in the evaluation of the dynamic behaviour of the cement-based sensor is the cross-correlation. Cross-correlation is a signal analysis technique with the goal of determining the similarity function of two signals based on the step by step movement of one of them toward the other one (Graham, 1970; Demčenko, Visser and Akkerman, 2016). In this research, the cross-correlation is applied to determine the similarity function between the force in a process of loading and unloading and the response of the cement-based sensor that may not be completely fitted to the force pattern because of the noise.

If the cement-based sensor wave response being identical to the wave force in case of shape and trend, this causes the maximum value of the cross-correlation to be one. So, the closer the

maximum value of the cross-correlation function is to one, the more similar the response is to the applied force.

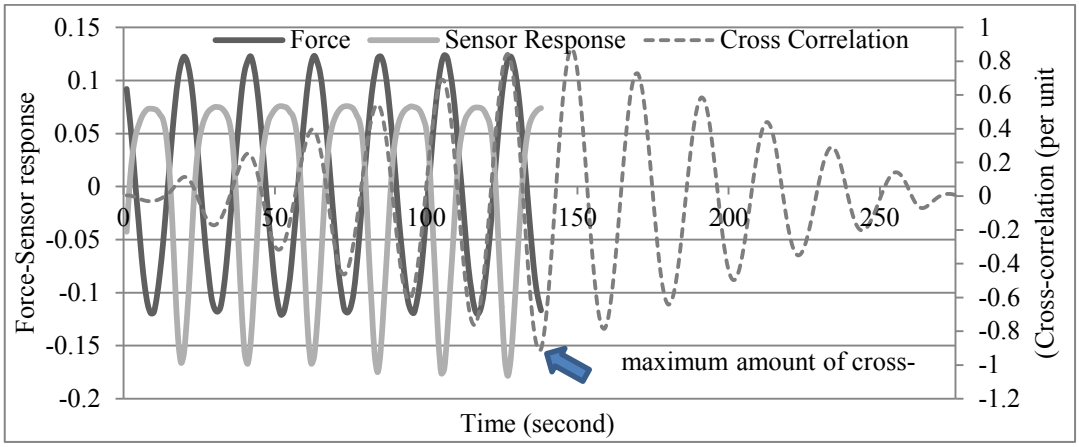

Figure 30- Normalized vector of the force, the response of the cement-based sensor and the cross-correlation function of the cement-based sensor 0.15CNT-VL

As Figure 30 explains, the response of the 0.15CNT-VL cement-based sensor has some irregularities in the loading and particularly unloading peaks because of the improper dispersion of CNTs. So, the value of 0.87 for the cross-correlation function represents the difference between the force and the response of the cement-based sensor in general and in detail too.

Based on cross-correlation function analysis, that is observed in Figure 30, the maximum value arises exactly at the end of signal time history (in the middle of Figure 30). The interpretation of this finding indicates that the maximum number of similarity between these two vectors is the time difference equal to zero (where two vectors have no shift (T) and they are completely opposite to each other). Figure 31 gives a schematic representation of the average of the maximum cross-correlation value of various cement-based sensors.

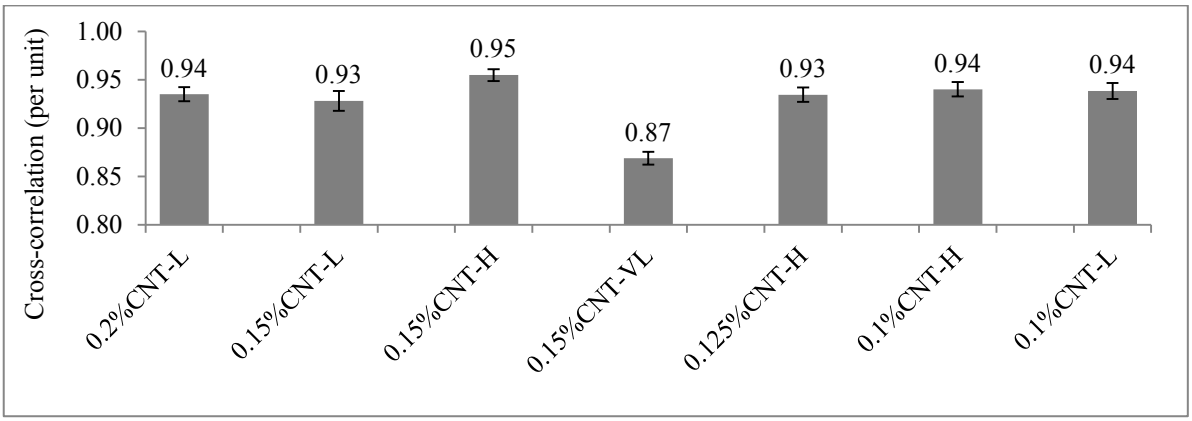

Figure 31- Cross-correlation of cement-based sensors

The outcomes suggest that the responses of most cement-based sensors have a relatively high similarity with the applied force, apart from the 0.15CNT-VL cement-based sensor in which very little energy is applied for the dispersion of CNTs. Obviously; the 0.15CNT-H cement-based sensor has the highest cross-correlation between the force and the response of the cement-based sensor. Based on the outcomes obtained by calculating the cross-correlation criterion, the maximum value of the cross-correlation function is obtained at the zero shift (T=0, the phase difference (T) between the cement-based sensor responses versus the force applied to the cement-based sensor) for all cement-based sensors, meaning that there is no phase difference between the response of the cement-based sensor and the applied force. According to this criterion, the combined impact of the number of MWCNTs and above all, the dispersion energy is obvious in this criterion. However, because of the lack of sensitivity of this criterion to the changes in the number of CNTs, this can be claimed that this criterion is not adequate to determine the optimum number of MWCNTs in the mixture.

Another criterion applied in this research for the analysis of the cement-based sensor output is the hysteresis. In the hysteresis-free systems, the outputs can be predicted based on the inputs at any point in time. In the systems with hysteresis, the system outputs not only depend on the inputs but also depend on the internal state of it, so this is difficult to predict the outputs based on the inputs at any point in time accurately. The hysteresis is obtained from measuring the inelastic quality of the instrumentation system components (sensor) and the number of hysteresis is called the hysteresis error. Han et al., run a study on piezoresistive concrete-CNTs sensors and declared that the number of hysteresis has a pronounced impact on the cement-based sensor. They defined the hysteresis as the difference of outputs corresponding to the same input during input decreasing and input increasing (Han *et al.*, 2011). This definition is very similar to the definition of internal repeatability and this seems inappropriate to appraise the hysteresis. As Figure 32 explains, the output of the cement-based sensor (in kΩ) versus the normalized applied force (normalized force is defined as the ratio of the sinusoidal applied forces with various magnitudes (from 0.2 to 0.7 and 0.2-1.2 kN) during the three points bending experiment over the maximum force (Fmax=0.7, 1.2 kN)) graph is plotted for 10 loading and unloading cycles.

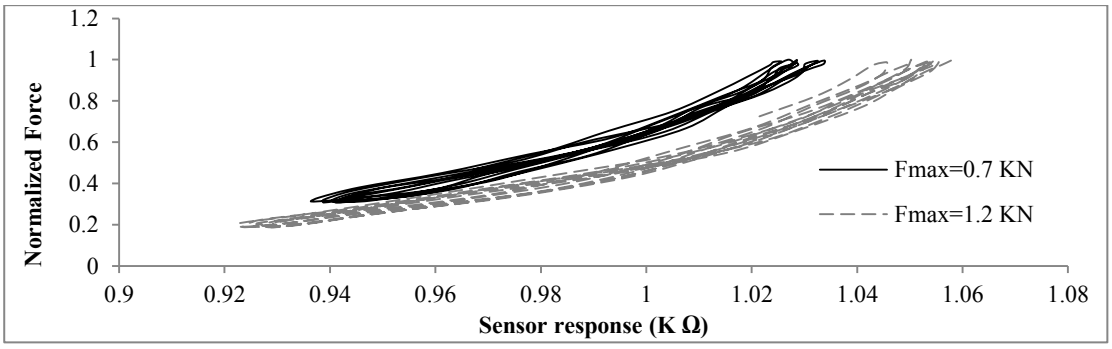

Figure 32- The output of the cement-based sensor versus the applied normalized force

One ideal cement-based sensor should not behave differently during loading and unloading cycles and may not have hysteresis in loading and unloading process. However, this was observed that all concrete-CNTs sensors with various percentages of MWCNTs and various dispersion qualities have hysteresis. The criterion defined in the study to appraise the number of hysteresis has to simultaneously appraise the changes in the cement-based sensor motion during a loading and an unloading cycle, as well as various loading and unloading cycles. So, assuming that the best line is fitted to the force-sensor response (voltage) dataset using the regression technique, the data deviation may be defined as the deviation from the response of an ideal cement-based sensor. In fact, the total number of deviation represents the total number of hysteresis during loading and unloading cycles. As a cement-based sensor has more hysteresis when loading, the output of cement-based sensor deviation from the best-fit line (assuming an ideal cement-based sensor) is higher. As a result, the sum of squared Error (SSE) value in the regression analysis can be defined as a criterion to show the hysteresis. Figure 33 explains the hysteresis of the inquired cement-based sensors.

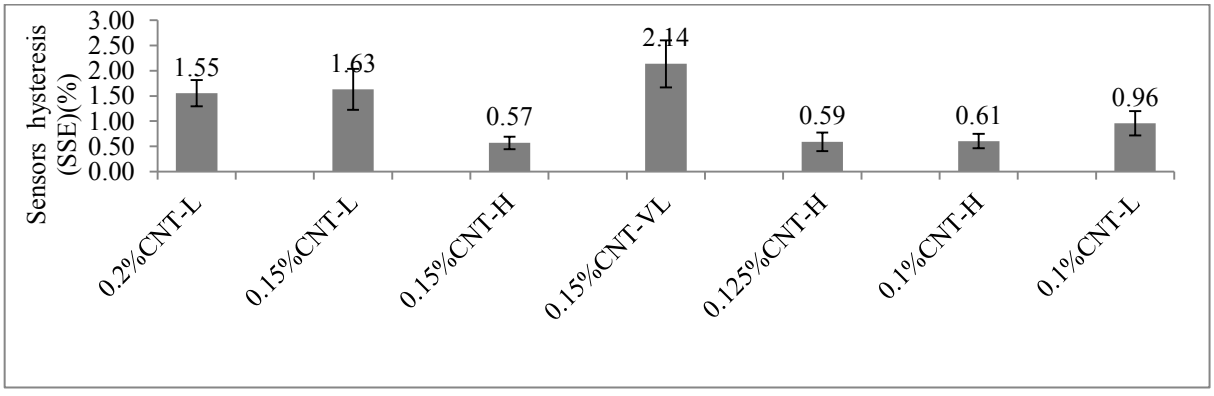

Figure 33- The hysteresis of the cement-based sensors

Regarding this criterion, the ultrasonic dispersion energy of MWCNTs has a pronounced impact on decreasing the hysteresis and increasing the precision of the cement-based sensor predictions. For instance, for a constant number of MWCNTs (0.15 wt%), the variation in

dispersion energy levels can significantly influence the hysteresis. The outcomes suggest that as the number of MWCNTs changes from 0.1% to 0.15% by weight of cement, there is no notable reduce observed in the hysteresis. Thus, according to this criterion, 0.1% of well-dispersed MWCNTs may be adequate to create a cement-based sensor with an acceptable hysteresis.

4.3.3 Summary of concrete-CNTs sensor function phase

One of the most notable and economical species of cement-based sensors is the concrete-CNTs sensor that is manufactured by mixing conductive fibers (such as multi-walled carbon nanotubes (CNTs)) with concrete. Two main parameters affecting the function of concrete-CNTs sensors are the number of MWCNTs and their dispersion quality in the mixture with regard to the combined influences of the surfactant composition and quantity and of the MWCNTs dispersed with various level of energy. The goal of this study is to appraise the influences of the main parameters affecting concrete-CNTs sensor function using diverse criteria in static and dynamic loading regime such as sensitivity of the cement-based sensor (Se), the standard deviation of the prediction error, repeatability, cross-correlation and hysteresis (SSE). The dynamic criteria such as sensitivity, internal repeatability, cross-correlation and hysteresis demonstrated that the dispersion energy levels for the dispersion of MWCNTs have a major impact on enhancing the function of the cement-based sensor than the number of CNTs, while the repeatability indicated, contrariwise, that the number of MWCNTs has a major impact on the function of the cement-based sensor compared to the dispersion `quality (energy level) of CNTs. On the whole, the cement-based sensor fabricated with 0.15 wt% (by weight of cement) CNTs, superplasticizer (SP) and sodium dodecyl sulfate (SDS) as a surfactant using the maximum energy level (ultrasonic bath for 2 hours and 90 minutes of probe's ultrasonication) revealed to offer the best function both in the static and dynamic load regime.

4.4 A study on behaviour of cement-based sensors response

4.4.1 Analysis of concrete-CNTs sensor function under dynamic loading pattern

Although diverse previous study studies have introduced haversine loading pattern as a model close to the wheel load pattern [Yoder and Witczak 1975], but applying this form of loading because of its complexity for its definition to the device applied In this research was not possible. Thus, according to diverse sources [AASHTO 1993] that knows a sinusoidal loading pattern as a good approximation to simulate the wheel load to the pavement, In this research, a sine wave was applied to apply the dynamic loading during tests. The dynamic

load experiment was applied by Universal Testing Machine (UTM) from MTS with 25-ton capacity. The dynamic load experiments were applied to concrete-CNTs sensors in two modes. In the first, to investigate the cement-based sensor response and to determine the optimum number of MWCNTs, the experiment cycles were limited (10 cycles) with low frequency 0.05 Hz. In the second mode, after finding the optimum number of MWCNTs, the main samples were cast to experiment the fatigue response of the cement-based sensors to simulate the accumulative destruction propagation in concrete and detect the destruction in concrete along the oscillation time by concrete-CNTs sensor self sensing property. The second mode was unlimited and continued up to failure.

The outcomes in dynamic loading experiments on concrete-CNTs sensors show a various behaviour between the unloading and loading. Arrows shown in Figure 34 show the peaks of unloading wave. As can be seen, the peaks in sine wave are completely various between unloading and loading. because of three-point bending experiment approach that this has not the jaw to guide the sample in the process of unloading, the speed of sample in recovery is less than the speed in unloading. So, these differences can be explained.

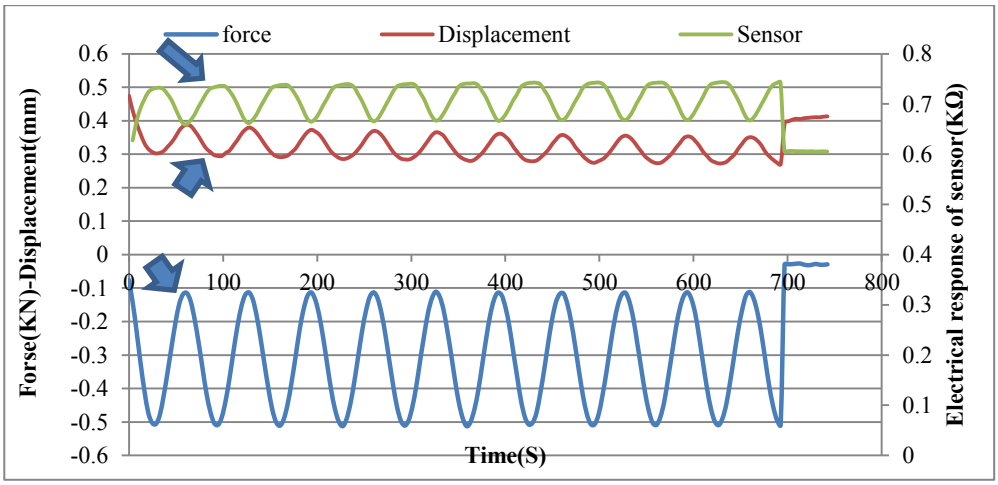

Figure 34- Electrical response of the cement-based sensor, the cement-based sensor movement and applied force against the time

Also, when the trend of displacement and the electrical response of the cement-based sensor are inquired along time, this can be seen that the delay in returning at unloading stage causes a slight irreversible deformation in the sample in each cycle and So So a falling trend in displacement along time is disclosed.

In order to determine the number of force applied to the concrete sensors, the cement-based sensors behaviour should be analyzed under dynamic loading and model their response. As regards the sinusoidal loading pattern is known to be a good approximation to simulate the wheel load on the pavement. Moreover, given that the determination of the load peak has critical importance in pavement analysis. In this research, the half wave model is

defined to show the force range from minimum to maximum by averaging the corresponding data during 10 cycles. To omit the impact of residual deformation during the test, the cement-based sensor responses were filtered with MATLAB software to de-trend it.

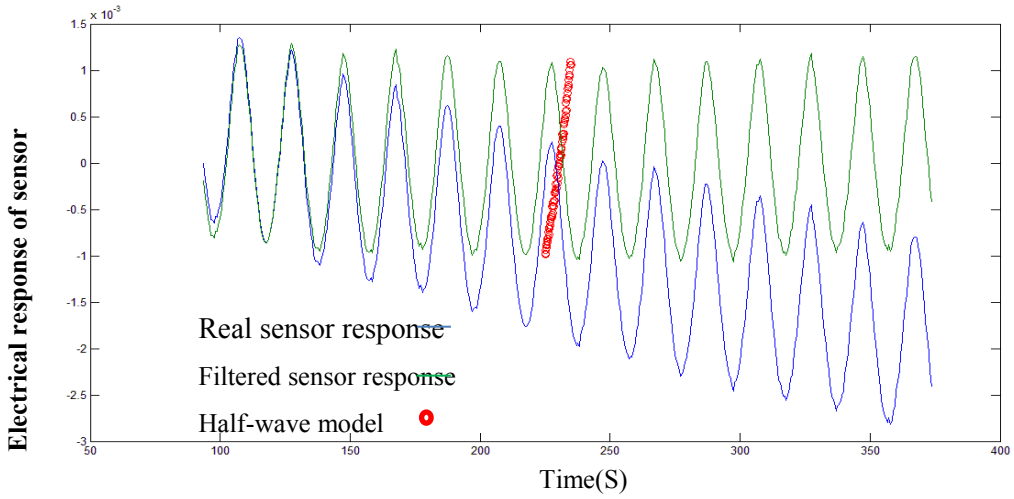

Figure 35- The production of the Half-wave model

This process is presented in Figure 35. The blue line is cement-based sensor response raw data and the green one shows this after filtration. The red line also is the average data between 10 cycles that is called half wave model.

The half wave model for a concrete-CNTs sensor in various load magnitudes (0.7, 0.9, 1.5, 2, 2.5, 3 KN) are presented in Figure 36.

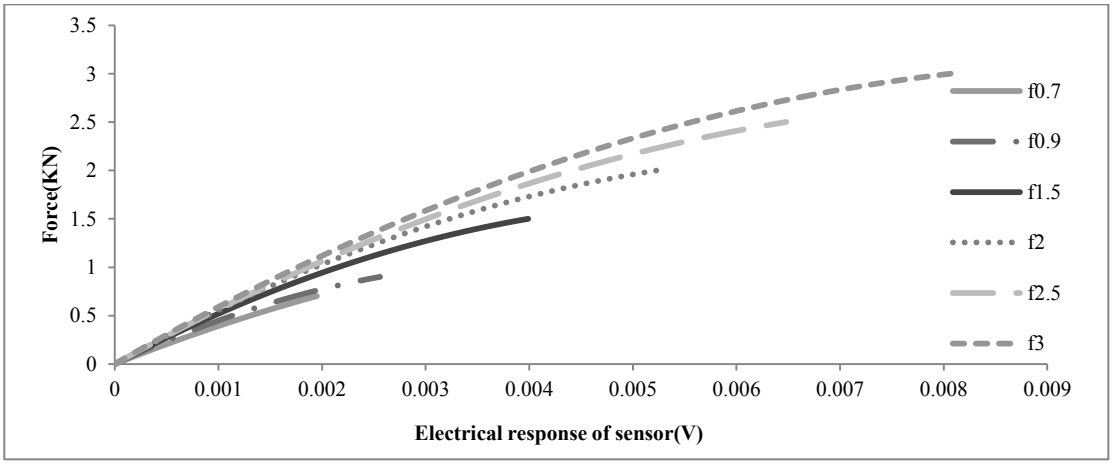

Figure 36- half-wave model of the cement-based sensor response versus exterior force levels.

It can be observed that the response of the cement-based sensor at various levels of exterior force are not the same and have some unconformities. This means that the slope of

the response of the cement-based sensor–force curve, is varied according to the maximum force applied to the cement-based sensor and this has no fixed amount.

Investigation of electrical and displacement concrete-CNTs sensor response demonstrates that the electrical cement-based sensor's response over the time in comparison to the displacement trend during the loading and unloading cycle is less dependent to the residual deformation. So, as this is presented in Figure 36 this may seem that concrete-CNTs sensor with a downward trend cannot be considered as ideal cement-based sensor compared by common electro-mechanical sensors. However, if the electrical sensor response in 10 cycles is plotted versus concrete-CNTs sensor deformation as in Figure 37, this can be observed that the slope of concrete-CNTs sensor deformation downward trend is much higher than the slope of electrical sensor response. This means that the electrical sensor response shows the real attitude of concrete-CNTs sensor and obviously, this downward trend is not its defect.

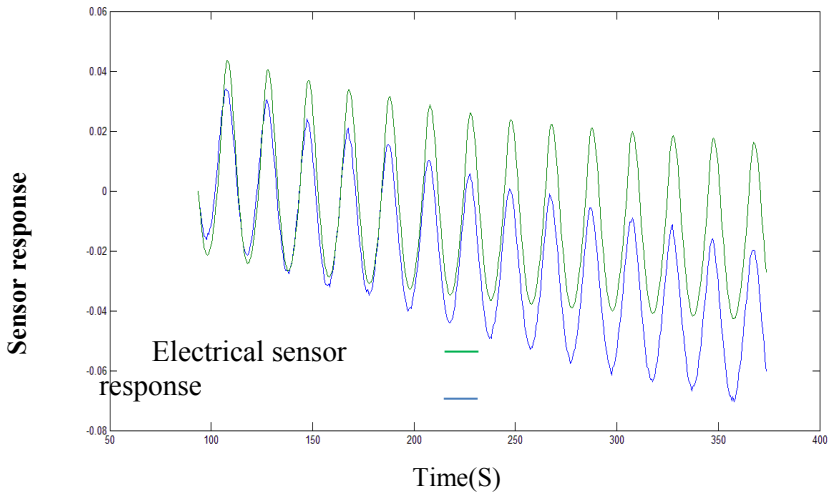

Figure 37- comparing the downtrend concrete-CNTs sensor displacement with sensor electrical response trend.

If CS is defined as ratio of between two slops, the slope of sensor displacement trend to slope of electrical sensor response trend, in various exterior loading magnitudes as presented in Figure 38, this can be observed that the higher level of the force is, the lower CS is. this means, in high level of the exterior forces applied to the concrete sensor, the electrical and mechanical behavior of the sensor are close to each other. So, this feature can increment the possibility to apply the electrical sensor response to estimate the concrete displacement and apply the sensor as piezoresistive sensor.

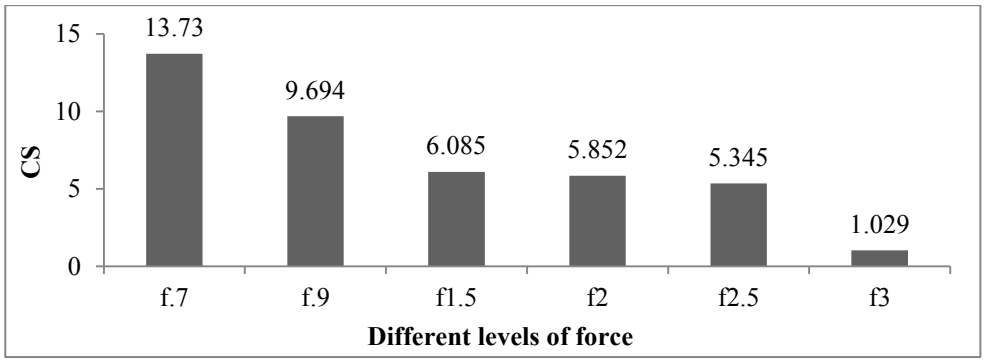

Figure 38- comparing the proportion of the slope of sensor displacement trend to slope of electrical sensor response trend (CS) in various levels of applied load.

4.4.2 Modelling of sensor response

The purpose of this part is formulation of concrete-CNTs sensor to estimate the number of force applied to the sensor based on electrical sensor response. This finding will be very important to estimate maximum exterior force applied by vehicle wheel load on to the pavement, based on electrical sensor response embedded in. The result will help to change electrical sensor response to load history and will be applied in analytical approach to model remaining life of the pavement based on sensor response presented in the next part of this chapter. To gain the goals two approaches, consisting of analytical approach based on regression technique and graphical based approach, have been developed.

4.4.2.1 First approach based on regression technique

In this approach electrical sensor response (voltage) versus exterior force (KN) is plotted in the Figure 39. as regards the behaviour a particular sensor is non-constant at diverse levels of exterior force, this can be concluded, in a constant loading speed (frequency), with changing in maximum force (Fmax), the proportion of the slope of the electrical sensor response ($tg\beta_i$) to slope of applied force ($tg\alpha_i$) and the maximum response of the sensor (Smax) is varied. So, this could be written in Equation 12:

$$Fmax=f(\frac{tg\alpha_i}{tg\beta_i},Smax) \quad \text{Equation 12}$$

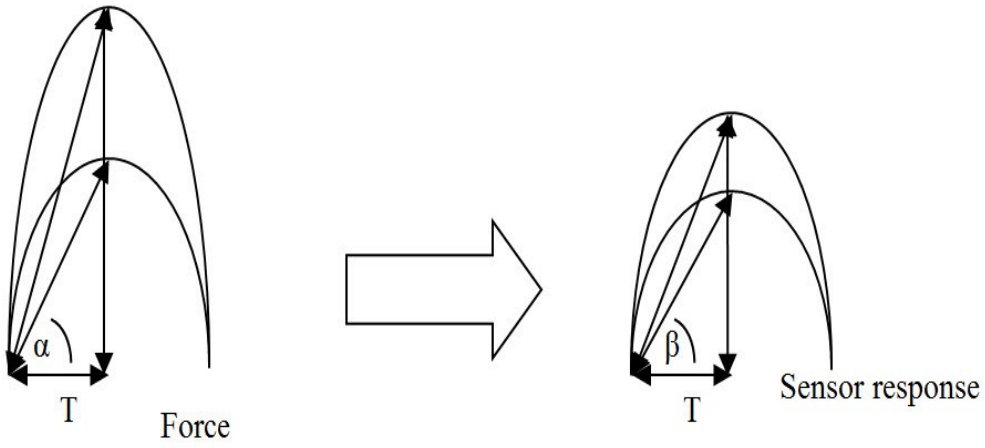

Figure 39- comparing the variation of the slope of the sensor response wave versus the slope of the force wave

Since the purpose the sensor usage is calculating the applied maximum force based on electrical sensor response and this is important parameters to analysis the pavement. So, by regression technique the relationship between the maximum force and the electrical response of the sensors can be modelled. The Figure 40 shows this relationship with high precision based on the number of R^2adj. and the final model is presented in **Table 7**.

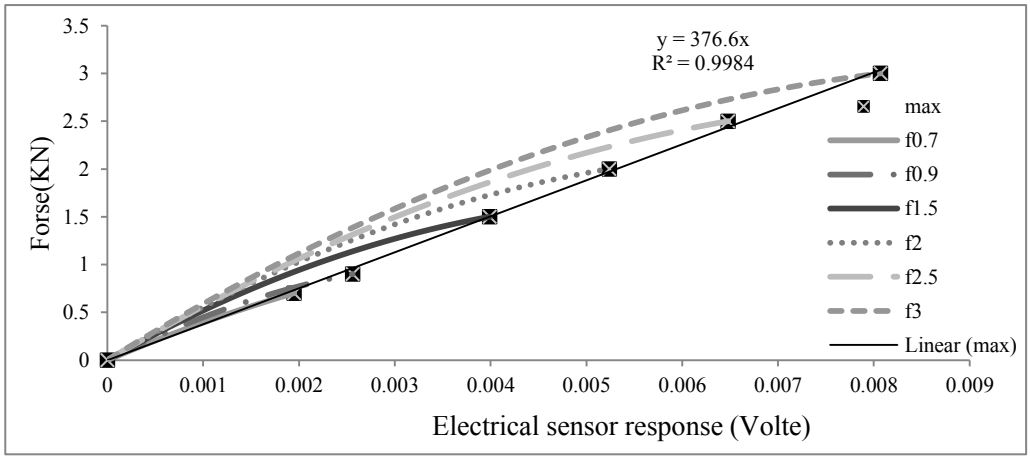

Figure 40- the half-wave model of concrete-CNTs sensor based on regression technique.

Table 7- the sensor half-wave model and its coefficients

f(x) = p1*x + p2		**Equation**
p1 = 376.6	p2 = 0	R-square: 0.9984

4.4.2.2 Second approach based on graphical analysis

If at any load levels, the slope of force wave and sensor response wave presented in Figure 41, calculated based on Equation 13 and Equation 14 and, plotted in Figure 42, this could be observed that the relationship between these two slops shows the proper relationship between maximum force and maximum electrical sensor response.

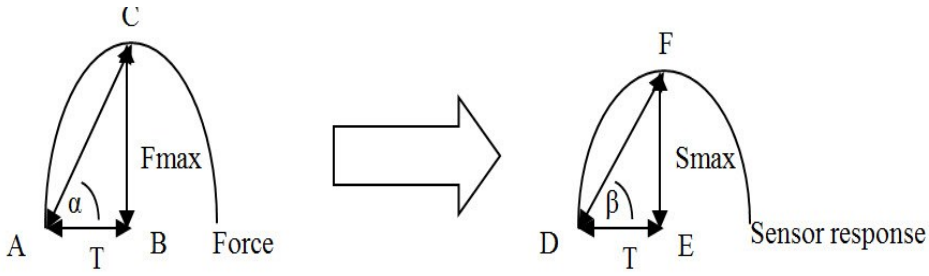

Figure 41- the graphical analysis of the sensor response.

$$\mathrm{tg}\alpha_{\mathrm{i}} = \frac{Fmax_i}{T} \qquad \text{Equation 13}$$

$$\mathrm{tg}\beta_{\mathrm{i}} = \frac{Smax_i}{T} \qquad \text{Equation 14}$$

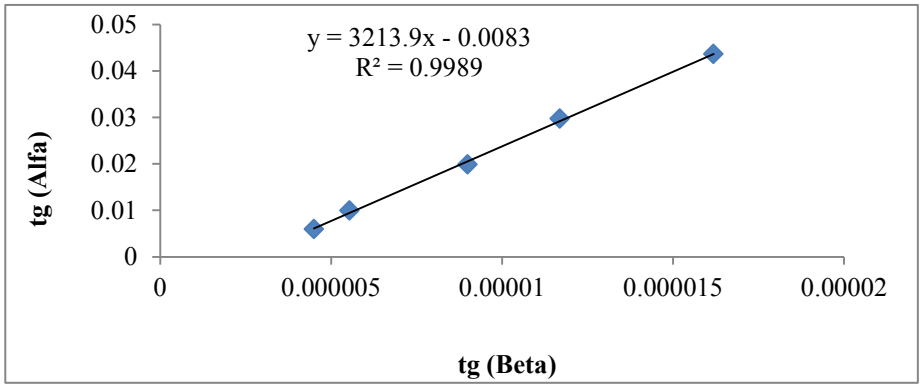

Figure 42- the relationship between the slope of force wave $\mathbf{tg\alpha_i}$ and sensor response wave $\mathbf{tg\beta_i}$

Based on relationship presented in Figure 42 and assumption a constant time T between sensor response wave and force wave, the following trigonometric relationship can be extracted.

$$\mathrm{Fmax}_i = \frac{\mathrm{tg}\alpha_{\mathrm{i}}}{\mathrm{tg}\beta_{\mathrm{i}}} \times Smax_i \qquad \text{Equation 15}$$

In Equation 15 the Smax can be evaluated by sensor and the $tg\beta_i$ and $tg\alpha_i$ coefficients can be calculated by calibrating the sensor before using this in real pavement in controlled lab experiment with known various levels of the force. Finally, the Fmax (maximum exterior load that is applied by vehicle wheels) can be calculated from Equation 15.

4.5 Fatigue Analysis

In this section, before determine the remaining life of Portland cement concrete pavement based on the response of the sensor in laboratory scale, the fatigue life of concrete-CNTs sensors should be calculated. If a notable relationship between the electrical consistent concrete-CNTs sensor outputs with fatigue life of conventional concrete Portland cement concrete pavement embedded in, can be extracted, this can be applied to correlate sensor response to remaining life of the pavement. Based on our limitation in time, budget and lack of fatigue field experiment instrumentations, fatigue experiment in lab scale is substituted with field tests. Based on this limitation, according to previous literature, Portland cement association (PCA)(Griffiths and Thom, 2007; Slabs, Pavement and Equations, 2014), three points bending fatigue experiment performed on cube samples that were consistent sensors. Running fatigue experiments on these species of concrete samples that have had self sensing ability and also same mechanical specifications with conventional concrete in a controlled lab situations, help to gather electrical and mechanical responses of the concrete in a fatigue test. These finding help to investigate these two types of concrete-CNTs sensor response simultaneously.

4.5.1 Testing procedure

In order to define the concrete fatigue experiment settings, 6 samples were broken under standard three-point bending stress to estimate the module of rapture (MOR) of the concrete samples. The outcomes are presented in **Table 8**.

Table 8- Flexural strength of concrete beam under three points bending test

No.	Width (mm)	Span (mm)	Height (mm)	Moment (N.M)	Moment of inertia (mm^4)	Failure force (K.N)	Bending stress (Mpa)	Average of bending stress(Mpa)	Standard deviation of bending stress (Mpa)
1	71.0	250	75.5	324896	2546349	5.20	4.82	4.58	0.029
2	70.3	250	75.9	293229	2561530	4.69	4.34		
3	70.6	250	75.4	303333	2521956	4.85	4.53		
4	70.1	250	75.2	310174	2484221	4.96	4.69		
5	70.8	250	74.9	295069	2479120	4.72	4.46		
6	71.6	250	75.8	316597	2598600	5.07	4.62		

Test outcomes in terms of experimental fatigue life are also reported in Table 9.

Table 9- Input parameters and fatigue experiment results

No.	Width (mm)	Span (mm)	Height (mm)	Moment (N.M)	Moment of inertia (mm^4)	Stress Level (S)	Bending stress (Mpa)	Failure force (K.N)	Stress Ratio (R)	Minimum Load (K.N)	Fatigue life (N)
1	71.7	250	71.9	254504	2220877	90	4.1	4.07	0.25	1.02	2493
2	72	250	73.9	269985	2421501			4.32		1.08	102
3	71.5	230	72.4	257336	2261208			4.48		1.12	1116
4	72.8	250	73.2	267837	2379487			4.29		1.07	4398
5	72.3	250	72.8	263099	2324616			4.21		1.05	896
6	71.8	250	73.1	263437	2337197			4.21		1.05	2983
7	72.2	250	75.4	250522	2579111	80	3.7	4.01		1.00	15034
8	72.2	250	74.8	246550	2518029			3.94		0.99	23835
9	71.6	250	74.6	243196	2477127			3.89		0.97	12538
10	71.5	250	72.9	231914	2308380			3.71		0.93	37347
11	71	230	75.3	245705	2526167			4.27		1.07	10002
12	70.5	230	75	242034	2478516			4.21		1.05	15460
13	70.8	230	75.1	213249	2499032	70	3.2	3.71		0.93	1765284
14	70.8	230	74.6	210419	2449450			3.66		0.91	893465
15	71.6	230	73.9	208821	2408048			3.63		0.91	1136824
16	71.9	230	75.4	218296	2568394			3.80		0.95	439581
17	72	250	73.9	209988	2421501			3.36		0.84	259879
18	69.1	230	73	196651	2240090			3.42		0.86	2500000

4.5.2 Fatigue analysis

In general, there are two groups of fatigue equations to model the fatigue life of concrete. Fatigue single logarithmic equations in the form: ($S = \alpha - \beta$. Log N) and the pair logarithmic equations ($\log S = \log \alpha - \beta \times \log N$) that S, is defined as stress level and N shows the fatigue life of concrete.

Fatigue function is dependent, the two main parameters (α and β). The parameter α reflects the maximum value of fatigue curve. The larger the α quantity is the major value of fatigue graph and ultimately the better function of fatigue is. The coefficient β is defined as the slope of fatigue model. Larger amounts of this parameter, suggest that concrete is more sensitive to stress changes.

Now fatigue single logarithmic equation is widely applied , but fatigue pair logarithmic equation is more complete and precise than the single one(Bennett, 1980; Daghash, Tarefder and Taha, 2015). In this research, both single and pair logarithmic equations are applied to analyse the concrete fatigue performance. Base on concrete beam fatigue experiment results,

the fatigue life model is calibrated and the model coefficients present in **Table 10** also. The model is shown in Figure 43.

Table 10- Single logarithmic fatigue life model (S-log N)

Fatigue life model form	**S= a-b*log(N)**
coefficients	a =107.6 (102.3, 112.8) b =2.707 (2.21, 3.204)
Regression parameters	SSE: 128.7 R-square: 0.8928 Adjusted R-square: 0.8861 RMSE: 2.836

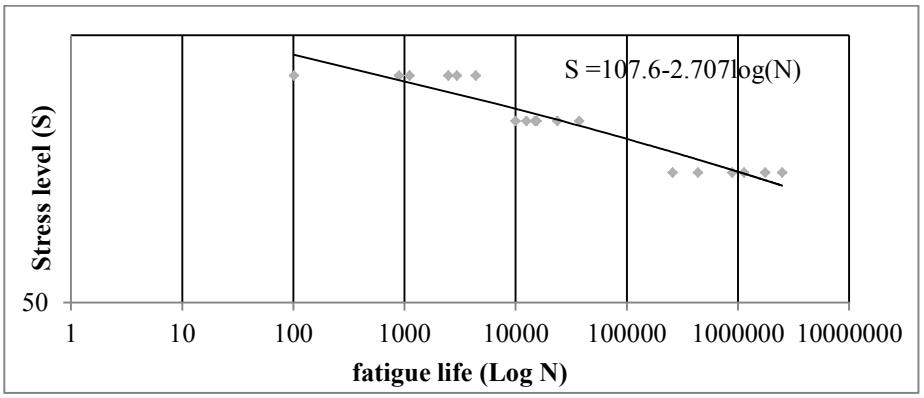

Figure 43- fatigue life model (S-log N) of concrete-CNTs sensors 0.15CNT-0.5 SPS

4.5.3 Statistical analysis of fatigue life model

In the process of modeling, the three stages of verification, calibration and validation are defined.

4.5.3.1 Verification

At this stage, various methods and techniques of problem solving and modelling will be considered (Trucano *et al.*, 2006). In the process of modelling a phenomenon, there are some assumptions that may cause solving methods to deal with an approximation. The purpose of this step is identifying possible modelling techniques. To this end, referring to previous study researches According to this is quite instructive. In this research by examining past research in the field of formulation of fatigue equation, linear regression techniques in diverse forms

as presented in Figure 4 were evaluated. Initial investigation showed that the linear form (S = a × Log N + b) and power (S = a × Log N^b + c) is being applied more.

4.5.3.2 Model calibration

The approach of finding the best correlation between the model outputs and actual outcomes is called calibration. Also, calibration can be intended as parameters adjustment so that maximum compatibility between the model and the observed data exist [87]. One of the statistical methods of calibration is linear regression [88]. In particular, the calibration technique of minimizing the root mean square error between the predicted values and the observed data to calculate the model coefficients is the one applied in linear regression.

4.5.3.3 Validation

The set of techniques that show the correspondence between predicted values and actual values of the model is called validation. The concept of verification is more general than the concept of validation. Validation is the concept that the outcomes taken after the implementation of the system match with the outcomes that are the aim for making the system (doing the right work) [87]. However, verification means the full compliance of the system with the description of the system (doing this right). To experiment the validity of models, diverse criteria are applied such as a goodness of fit (R^2adj), model coefficients significance experiment (t-test and F-test) and the graph presenting values derived from models against actual values. Another approach to experiment the validity of a model is separation of experiment data (Ort´uzar and G.Willumsen, 2011). Part of the data (e.g. 80% data) presented in **Table 11** is applied to calibrate the model (model training) and the rest (20% data), is applied for validation of the model (model testing).

Table 11- separating experiment data for model validation

Description	Gradient of electrical sensor response graph (G)	Fatigue life (N)	Stress level
Model training	18.9	2493	90
	100.37	101.63	90
	22.06	1116	90
	12.95	4398	90
	37.89	896	90
	6.1	12538	80
	5.84	37347	80
	9.01	10002	80
	5.47	15460.13	80
	0.93	893465	70

	0.734	1136824	70
	1.536	439581	70
	1.76	259878.9	70
	0.4	2500000	70
Model testing	19.03	2983	90
	5.04	15034.18	80
	4.9	23835	80
	0.56	1765284	70

According to the literature, linear regression forms presented in Figure 4 were the most applied among other forms. So, these two forms of linear and power models presented in Figure 44 and Figure 45 respectively were fitted to 80 percent of data to train the models in confidence interval 95% and the models specifications are presented in **Table 12**.

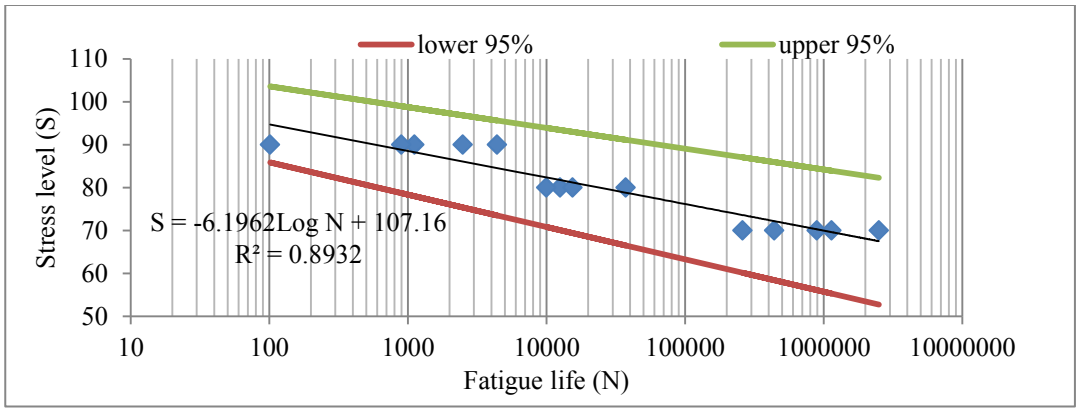

Figure 44- calibration of linear regression model with the form S = a *LogN + b

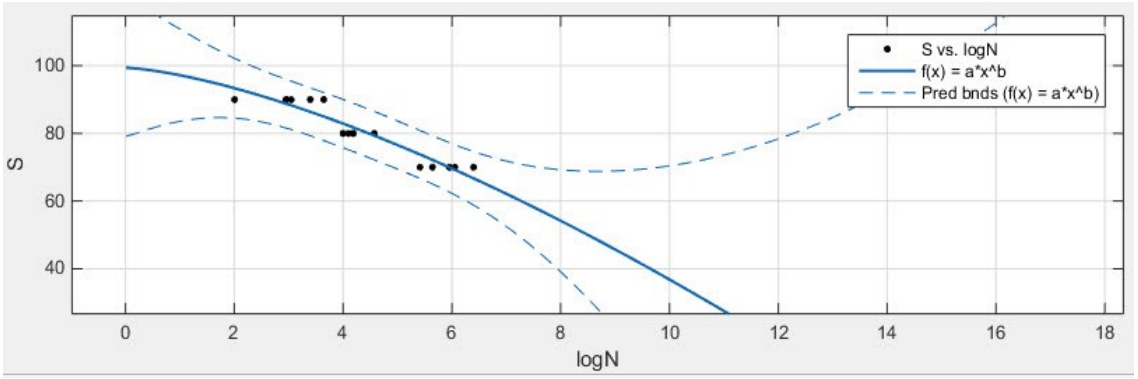

Figure 45- calibration of linear regression model with the form $S = a*LogN^b + c$

The outcomes showed the model that has the less root mean square error and p-value (lower than 0.05 at the confidence level 95%) has the most precise estimation [31]. Accordingly, the linear fatigue model has better goodness of fit and lowers RMSE than the power one. These two forms are very close together in terms of validation and T-test and F-test validate the model coefficients significance.

Table 12- various models validation

Fatigue life model form	**S= a-b*log(N)**	**S=a*(LogN)^b+c**
coefficients	a =107.6 (102.3, 112.8) b =2.707 (2.21, 3.204)	a =-2.191 (-9.636, 5.253) b =1.456 (-0.1063, 3.017) c =99.38 (80.27, 118.5)
Regression parameters	SSE: 128.7 R-square: 0.8928 Adjusted R-square: 0.8861 RMSE: 2.836	SSE: 101.1 R-square: 0.8989 Adjusted R-square: 0.8805 RMSE: 3.032

4.5.4 Graphical model validation by using the new data set

To validate the model by using graphical technique as shown in Figure 46, 20 percent of the data (N) are applied as input in the model that is calibrated by extra 80 percent of the data set. The model estimation (S') is shown in the graph in figure 46 against the actual values (corresponding to 20% of the data values (S)). The closer fitted line to Y=X is, the less differences between actual values and model outcomes are and the more data validity are. This approach is presented in Figure 46 to show the validation of two forms of linear and power model.

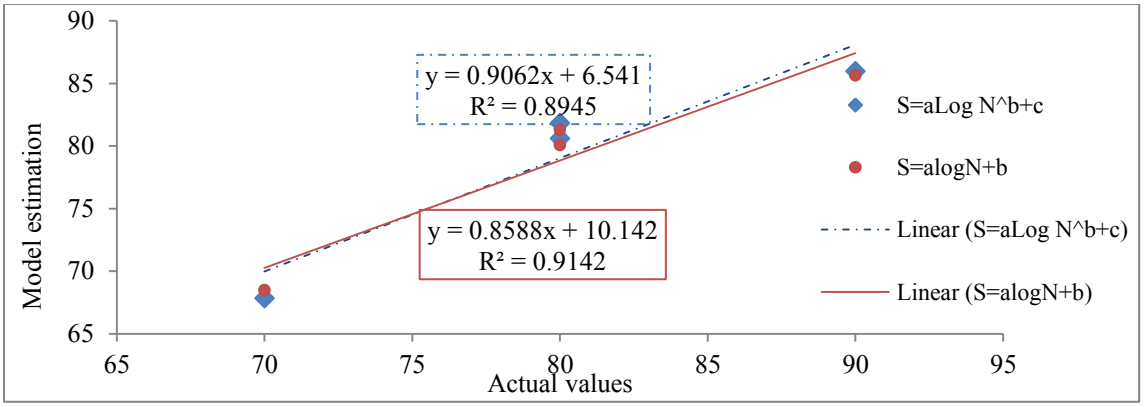

Figure 46- compares the model estimation by actual values in two forms of linear and power model.

As shown in Figure 46, the coefficient of power model is more similar to Y=X than linear model but the goodness of fit is vice versa. In the validation process of models, the model with lower standard error shows the minimum dispersion between actual and

predictive values [31]. So, the linear form model that has better goodness of fit than the power one, is here judged as the best validation model form.

4.5.5 Validation based on comparison with outcomes of previous studies

Another way to validate the model is comparing its result with the previous studies [89]. Accordingly, by comparing these study outcomes with the outcomes of Lee et.al. presented in Figure 3 which is emanated from statistical analysis on nine previous studies on fatigue experiment results, this was figure out that reinforced concrete containing 0.15% carbon nanotube by weight of cement has a major fatigue life compared to plain concrete. And higher percentage of fibres in concrete will increment fatigue life of concrete. Also, the similarities between our outcomes and the average of fatigue outcomes which is summary of 8 various studies in fatigue life of fibre concrete presented by Lee et al. presented in Figure 47 demonstrate that our outcomes have high reliability compared with outcomes provided by previous research.

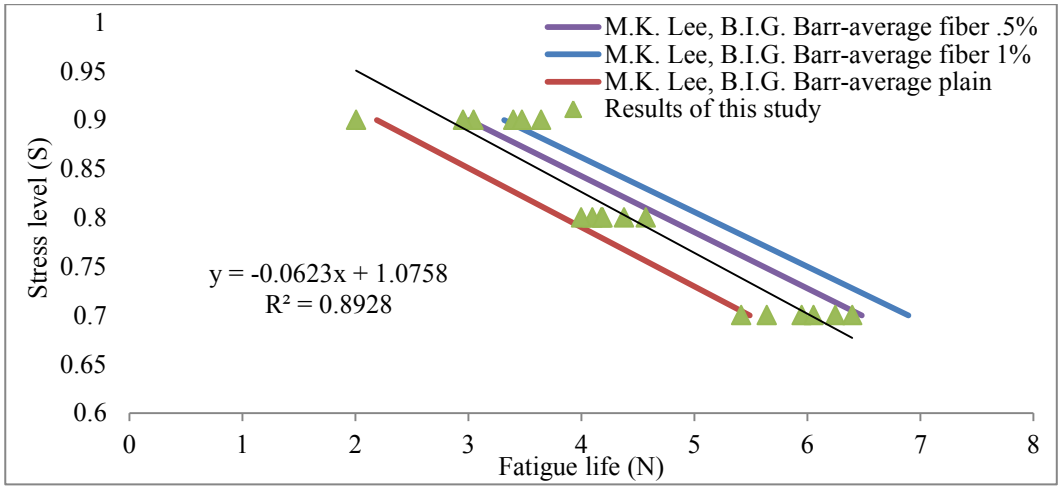

Figure 47- validation of our outcomes with respect to the average outcomes of several studies [48].

4.5.6 Interpretation of sensor behaviour under fatigue loading

As the outcomes in Figure 34 show, when a sinusoidal loading pattern is applied to the concrete-CNTs sensor beam, the electrical sensor outputs shape is the same as the exterior loading pattern. But when a large number of loading cycles is applied a new trend can be observed as shown in Figure 48. This trend is linear up to the failure of the concrete sensor.

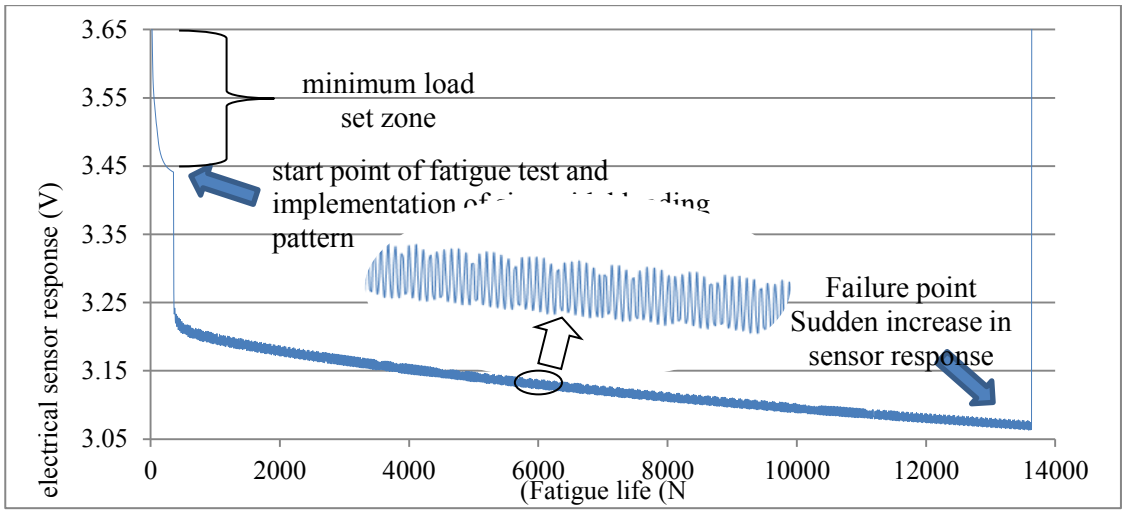

Figure 48- the interpretation of the sensor behaviour in the fatigue test

This phenomenon was observed in all the sensors examined under dynamic load. To find a possible correlation between the various sensors response trend with the same composition (0.15 CNT-0.5 SPS) with the various levels of stress (S), the outcomes are shown in Figure 49.

Based on the outcomes presented in figure 49, the G_i is defined as slopes of the fitted line by linear regression technique on response of the sensor versus the logarithm of the number of cycles until failure.

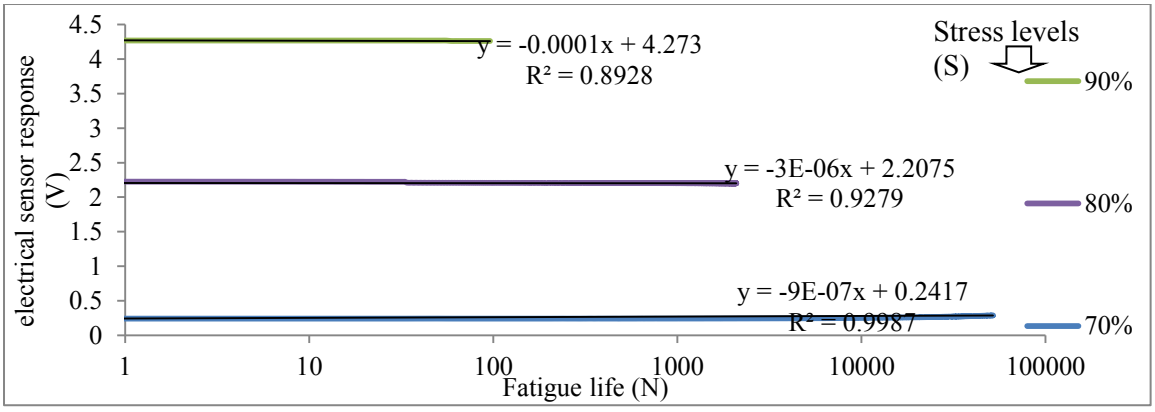

Figure 49- the relationship between stress levels and various sensors response trend under fatigue.

Figure 50 present proper correlation between Log (G_i) versus various levels of Log stress (S_i). This can be observed that there are goodish correlation between these two parameters with R^2adj.=0.88.

This correlation is quite valuable because this can correlate the material specifications of concrete beam that is stress levels in a fatigue life model (S-Log (N)) with electrical specifications of concrete beam under the fatigue loading pattern.

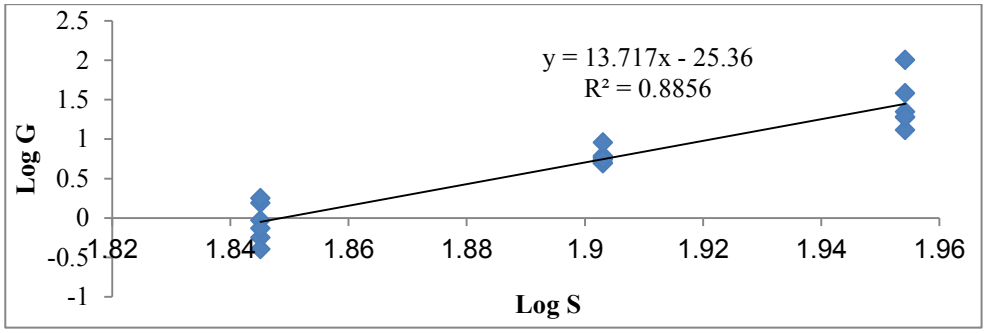

Figure 50- the relationship between the slopes of the response of the sensor (G) in fatigue experiments with various levels of stress (S).

Based on the Figure 50 this can be concluded that the higher the levels of stress (S) is the major slope of the sensor response is and the less the number of loading cycles up to failure is. In this research, the concept of G has been defined for the first time as the slope of a sensor's response that reflects the destruction created in a pavement because of one pass of vehicle load. Based on this finding, log (G)-log (N) was applied instead of traditional S-log(N) fatigue graphs (Goodman curves), based on the electrical sensor response with a linear regression approach and the outcomes were shown in Figure 51.

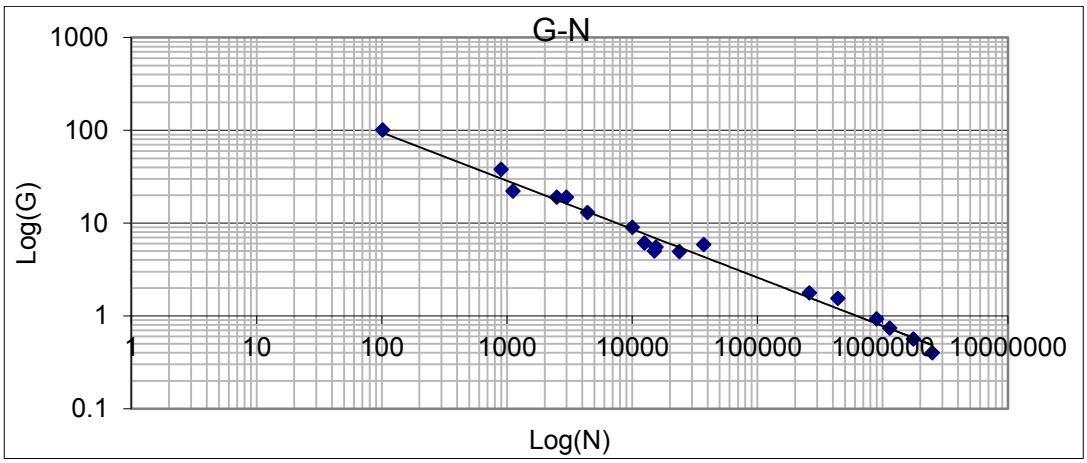

Figure 51- relationship between stress magnitude and slope of baseline resistance under fatigue in 0.15 CNT-0.5 SPS.

In order to model the equation presented in Figure 51 and according to the linear form fatigue equation in the previous section, four linear forms were appraised in **Table 13** and **Table 14**.

Table 13- Fatigue model in form of G-Log (N)

Fatigue life model form	**G = log(a)-b×log(N)**	**G = a-b×log(N)**
coefficients	a=160.5 (109.6, 211.4) b =64.25 (42.09, 86.41)	a =5.011e+10 (-4.384e+12, 4.485e+12) b =5.653 (-32.86, 44.17)
Regression parameters	SSE: 2843 R-square: 0.7025 Adjusted R-square: 0.6839 RMSE: 13.33	SSE: 8523 R-square: 0.108 Adjusted R-square: 0.05226 RMSE: 23.08

Table 14- Fatigue model in form of Log (G)-Log (N)

Fatigue life model form	**Log(G)= log(a)-b×log(N)**	**Log(G) = a-b×log(N)**
coefficients	a = 12.77 (11.57, 13.96) b = 4.881 (4.359, 5.403)	a =3.498e+05 (-6.97e+04,7.693e+05) b =4.881 (4.359, 5.403)
Regression parameters	SSE: 1.576 R-square: 0.9609 Adjusted R-square: 0.9585 RMSE: 0.3138	SSE: 1.576 R-square: 0.9609 Adjusted R-square: 0.9585 RMSE: 0.3138

4.5.7 The correlation between stress magnitude and slope of baseline resistance

After determining the proper linear form for the slope of the sensor response versus number of cycles at failure in the previous section, the selected linear form is compared with power form in Figure 52 and Figure 53 respectively to appraise the proper model form.

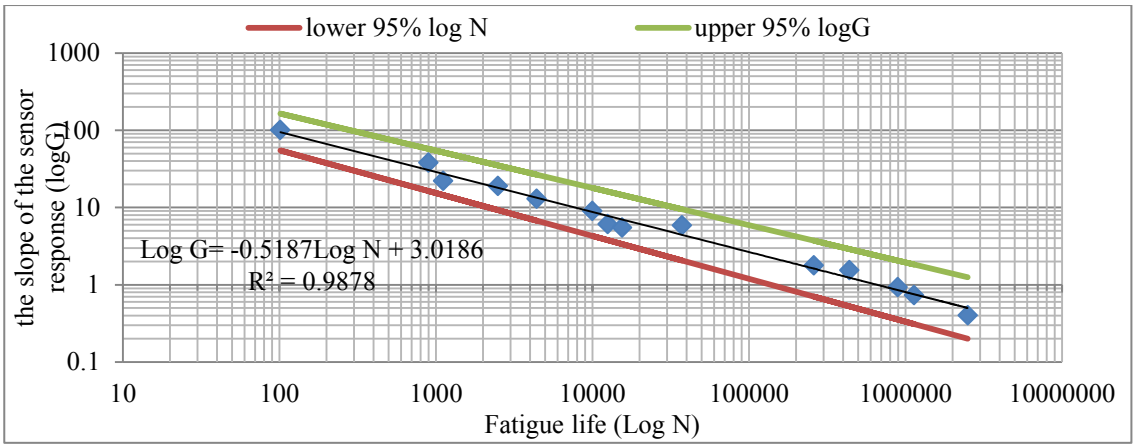

Figure 52- calibration of linear regression model in form of Log G =a×LogN+b

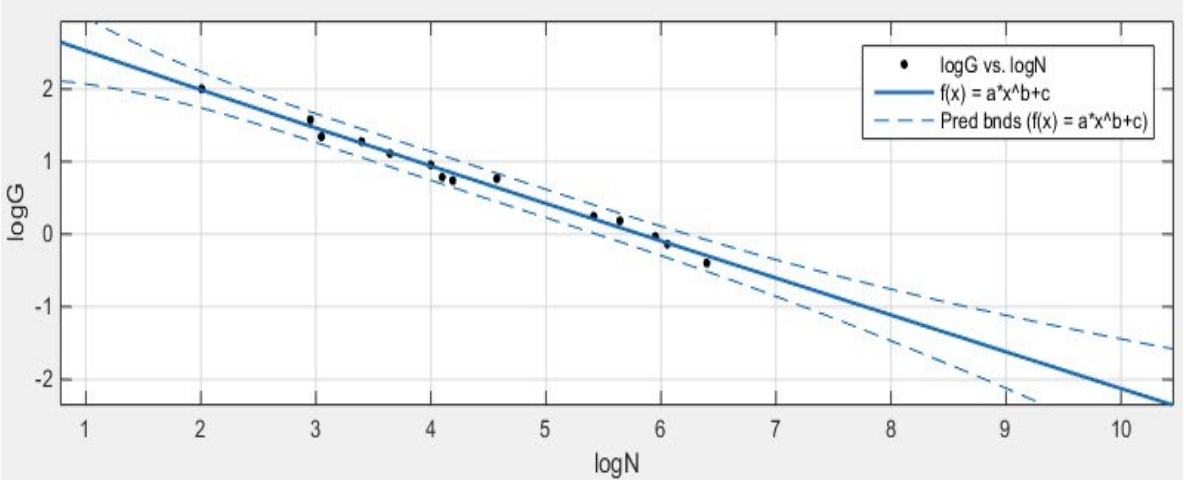

Figure 53- calibration of linear regression model in form of Log G=a×LogN^{b}+c

Investigation of linear and power forms of the slope of the sensor response against fatigue life models shows that the data distribution is very minor and both forms of linear and power have high goodness of fit. The outcomes demonstrated that all the data are located in the range of notable level of 95% and the two forms are very similar in terms of shape. Also, these two forms are statistically analysed and the outcomes are presented in **Table 15**.

Table 15- models validation in the two forms of linear and power

Fatigue life model form	**Log G =a×LogN+b**	**Log G =a×LogN^{b}+c**
coefficients	a = -0.56 (-1.203, 0.0835) b =0.9689 (0.5053, 1.432) c =3.086 (2.035, 4.137)	a = -0.5187 (-0.555, -0.4824) b = 3.019 (2.853, 3.184)
Regression parameters	SSE: 0.07725 R-square: 0.9878 Adjusted R-square: 0.9856 RMSE: 0.0838	SSE: 0.07739 R-square: 0.9878 Adjusted R-square: 0.9868 RMSE: 0.08031 P-value:7.52E-13

According to the outcomes of T and F test, all the models coefficients have the proper validity. The linear form show higher goodness of fit than the power form so the linear form is accepted to formularize the correlation between the slope of the sensor response and fatigue life.

4.5.8 Graphical model validation by using the new data set

To validate the linear and power forms of models calibrated by 80% of data set, the graphical technique is shown in Figure 54 using 20 percent of the data (N) and the model estimation (S') is shown in the graph against the actual values (corresponding to 20% of the data values (S)). Accordingly, because the linear form has a constant coefficient closer to zero and

variable coefficient closer to one than the power form model and having better goodness of fit, the linear form is the most reliable form considered in the modeling process.

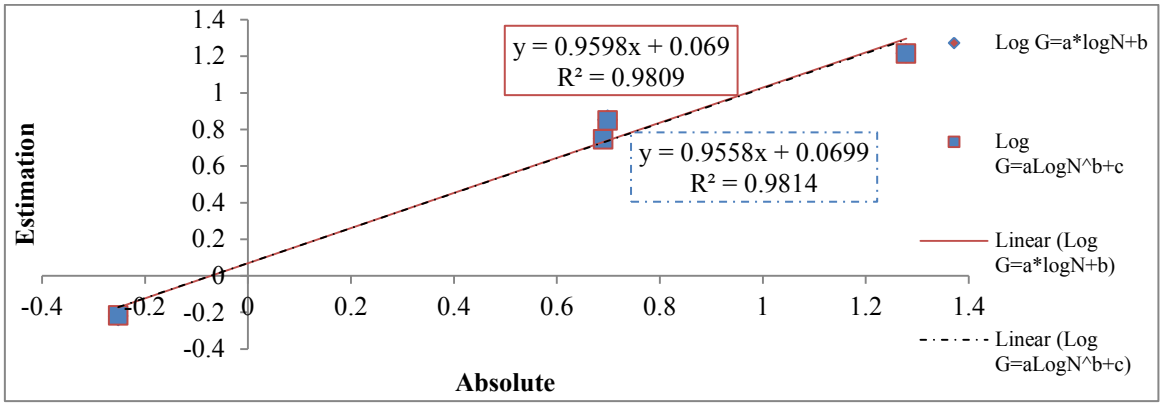

Figure 54- comparing absolute and estimation values of two forma of linear and power and models.

4.5.9 Determination of the remaining life of the pavement

In order to determine the equation that can estimate the remaining life of the pavement, In this research a hypothesis is made that Portland cement concrete pavement life is equal to fatigue life of concrete beam in lab experiments under sinusoidal loading. Following this hypothesis, two approaches (sensor and detector) are recommended below.

4.5.9.1.1 First approach (sensor approach)

In this approach, electrical sensor outputs change to maximum exterior force applied to the sensor Based on a model shown in Figure 43. In the next step, the number of maximum exterior loads (n), categorized in various magnitudes (i). In the following, the stress in various parts of the Portland cement concrete pavement can be calculated by AASHTO or PCA stress equations for each load categories (i). Using module of rupture (MOR) which is accessible for Portland cement concrete pavement, make this possible to calculate the stress level ($s = \frac{\sigma}{MOR}$). By using stress level as input value in the fatigue life model which is presented in Figure 43 (S=107.6-2.707×log (N)), the maximum number of repetitions until the failure (N) for each load categories (i) can be calculated.

According to Equation 2 cited by AASHTO-1986 to estimate the remaining life of pavement based on pavement structural performance. The number of destruction arising from any of each forces categories (di) with passing number of (n_i) applied on the concrete-CNTs sensor by vehicle wheels, will be achieved by dividing n_i to N_i. By accumulating d_i for all

force categories (i), the total relative destruction is calculated. If relative destruction is close to one failure arises. The Portland cement concrete pavement remaining life can be calculated by subtracting the relative destruction thus obtained from the unity. In the below paragraph, this approach is described as sample for one of the Westergaard equation which is applied for evaluation stress in middle of concrete slab. This is clear that the final result obtained must be validated by field tests.

Using Equation 15, the maximum force can be derived from the sensor response via $Smax_i$. If the Equation 15 is replaced in Westergaard equation (Equation 16), the critical stress is measurable based on the sensor response, which is presented in Equation 17.

$$\sigma_i = \frac{\alpha_1 P_i}{h^2}\left(\alpha_2 Log\left(\frac{l}{a}\right) + \alpha_3\left(\frac{a}{l}\right) + \alpha_4\right) \quad \text{Equation 16}$$

$$P_i = \frac{tg\alpha_i}{tg\beta_i} \times Smax_i$$

$$\sigma_i = \frac{\beta_1 Smax_i}{h^2}\left(\alpha_2 Log\left(\frac{l}{a}\right) + \alpha_3\left(\frac{a}{l}\right) + \alpha_4\right) \quad \text{Equation 17}$$

In these equations αi are coefficients in Westergaard equation that change according to the load on the slab.

After calculation of the stress based on sensor output, the model shown in the **Table 10** can be placed in Equation 2 to appraise relative destruction presented in Equation 18 for all load categories.

$$\text{Relative damage} = \sum_{i=1}^{c} \frac{n_i}{N_i}$$

$$S = 107.6 - 2.707 \times \log(N)$$

$$s = \frac{\sigma i}{MOR}$$

$$\text{Total destruction for all load categories} = \sum_{i=1}^{c} \frac{n_i}{10^{(36.57 - .3298\frac{\sigma_i}{MOR})}}. \quad \text{Equation 18}$$

C is the number of various Load categories.

If the relative destruction is subtracted from one, the Equation 19, which represents the remaining life, is achieved.

$$\text{Remaining life} = 1 - \sum_{i=1}^{c} \frac{n_i}{10^{(36.57-.3298\frac{\sigma_i}{MOR})}}.$$ Equation 19

4.5.9.1.2 Second approach, the approach of the detector

As S-N graphs are applied to design and determine the thickness of a pavement, the G-N graph presented in **Table 14** with respect to the definition of G that is destruction unit per cycle load, can be applied to determine the level of destruction to the structure - that sensor is embedded in - under the specific load cycles.

For example, if a specific load is applied to a structure, based on the various load magnitudes, the G value is varied. So, with measuring G of the sensor response under the specific load, and using G-N model, which is developed in Figure 51, the fatigue life of the pavement (N) can be calculated under that specific load category. On the other hand, the sensor can count the number of load repetitions on the pavement (n). The pavement remaining life is obtained by subtracting the partial number of load repetitions applied to the pavement up to now (n) from the total fatigue life (N) in accordance to Equation 20:

RL=N-n Equation 20

RL= remaining life by assuming a constant load pattern

n= the number of load applied to the pavement from the first time up to now

N= fatigue life of the pavement

By replacing the equation presented in **Table 14** to Equation 20, remaining life (in years or number of applied load) is calculated based on sensor response in Equation 21.

$$RL = 10^{(13.3-1.821\text{Log}(G))}\text{-}n$$ Equation 21

Remaining life of the pavement at constant load pattern is presented in Equation 22 as a percentage of total pavement life.

$$RL = (1 - \frac{n}{10^{(13.3-1.821\text{Log}(G))}}) \times 100$$ Equation 22

If the loading pattern on pavement varied over times, the above equation is not helpful. To generalize the concept of remaining life model to real world where loads are varied over time, a solution is breakdown the time history into sub-segments (t_i) to gain a constant (G_i) in each segment, as in Figure 55.

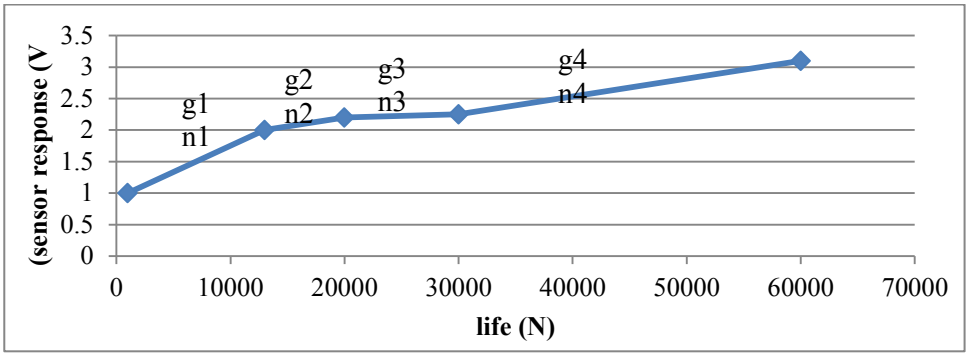

Figure 55- sensor response changes generated by random changes in intensity of traffic passing via a way and the process of braking down.

In this case, the Equation 2 extracted PCA applied to calculate the accumulative destruction in each part. Placing the equation presented in **Table 14** in this Equation 2 generate the new Equation 23 to estimate the total destruction based on sensor response under the traffic flow.

$$\text{Total damage} = \sum_{i=1}^{c} \frac{n_i}{10^{(13.3-1.821\text{Log}(G_i))}}$$ Equation 23

Like previous approach, if the relative destruction is subtracted from one, the Equation 24 which represents the remaining life is achieved.

$$\text{Remaining life} = 1 - \sum_{i=1}^{c} \frac{n_i}{10^{(13.3-1.821\text{Log}(G_i))}}$$ Equation 24

C is the number of segments of the sensor response curve.

Chapter 5 Results and conclusion

In this research, the composition of SDS and superplasticizer was introduced as a new surfactant composition to effectively disperse MWCNTs in the aqueous phase whereas the mechanical specifications of reinforced concrete were similar to the ones of plain concrete. In addition, the following conclusions may be drawn from this study.

The mechanical specifications of concrete are improved with the apply of an antifoam and as the number of MWCNTs remains constant (0.05 wt%) the compressive and the flexural strengths of concrete containing MWCNTs are improved by 60.3% and 51.2% respectively respect to plain concrete.

Omitting Tributyl phosphate as the defoamer, some little foam is fabricated in concrete because of SDS presence in the compatible surfactant composition and this causes a reduction of concrete mechanical specifications respect to the concrete with the defoamer. Then, a higher SDS number leads to a higher dispersion quality in the aqueous phase, but also more unwanted air bubbles in concrete and a higher reduction of the concrete mechanical specifications too.

The optimum dosage of superplasticizer as the surfactant is 0.5 wt% to gain the maximum dispersion of MWCNTs in the aqueous phase when the number of MWCNTs is 0.05 wt%.

The composition of SDS/DTAB or SP-C/SDS causes a synergic impact while dispersing MWCNTs in water.

A composition of superplasticizer and SDS with a mixing ratio of 9:1 respectively, by weight of cement is declared when this is required to make concrete with similar specifications to the plain concrete.

A composition of superplasticizer and SDS with a mixing ratio of 12:1 respectively, by weight of cement is declared when making concrete with higher compressive strength is targeted.

A composition of superplasticizer and SDS with a mixing ratio of 5:1 respectively is declared when the largest number of well-dispersed MWCNTs in the aqueous phase is required.

The dynamic criteria such as sensitivity, internal repeatability, cross-correlation and hysteresis demonstrated that the dispersion energy levels for the dispersion of MWCNTs create a major impact on enhancing the specifications of the sensor than the changes in the number of CNTs. The exterior repeatability has just shown a various result because of intrinsic difference in its definition than the others.

For the same level of energy, increasing MWCNTs from 0.1% to 0.15% by weight of cement showed that sensitivity and repeatability function criteria were boosted and cross correlation and hysteresis did not show notable changes.

The dynamic criteria demonstrated that apart from the hysteresis that presents 0.1% of MWCNTs as the proper number for creating a precise sensor, the other criteria suggest 0.15% of MWCNTs as the proper number for sensors manufacturing.

The static criteria showed that the quality of the dispersion (using proper surfactant material) and the number of MWCNTs are efficient on the sensitivity and the standard deviation of the prediction error, respectively.

Considering the above-stated criteria, 0.15% of MWCNTs by weight of cement using superplasticizer and SDS as a surfactant to gain proper dispersion quality, are the best choices to create a sensor with the maximum sensitivity and the minimum standard deviation of the prediction error.

Based on the cross-correlation, this was figure out that the phase difference (T) between the sensor responses versus the force applied to the sensor is equal to zero for all sensors with various amounts of MWCNTs and various dispersion qualities.

The outcomes demonstrated that the maximum exterior load applied on the sensor (Fmax) is linearly correlated to the maximum response of the sensor (Smax) via a constant coefficient tagα/tagβ, in which tagα is defined as the slope of the Force vs. Time graph and tgβ is defined as the slope of the Sensor's response vs. Time curve. So, this can be concluded that the application of the indicated concrete-CNTs sensors for piezoresistive applications is feasible and the sensors can appraise the load with of high-goodness of fit (R^2adj.> 0.99).

An alternative data processing log (G)-log (N) was applied instead of traditional S-log (N) fatigue graphs (Goodman curves), based on the electrical sensor response with a linear regression approach and the outcomes were verified by statistical tests.

The outcomes demonstrated that the resistance increment showed the occurrence of damage. So that the major the stress magnitude, the larger and the less reversible is, the

damage-induced resistance reduce. The study demonstrated that there is a proper relationship between stress magnitude and baseline resistance, which is modelled in Figure 50.

In this research, the concept of G has been defined for the first time as the slope of a sensor's response that reflects the destruction created in a pavement because of one pass of vehicle load.

References

36-RDL, R. C. (1984) *Long term random dynamic loading of concrete structures*, *Matériaux et Construction*. doi: 10.1007/BF02474050.

AASHTO (1993) *AASHTO GUIDE FOR DESIGN OF PAVEMENT STRUCTURES 1993*. Washington D.C.: American Association of State Highway and Transportation Officials.

Adresi, M., Hassani, A., Tulliani, J.-M., Lacidogna, G. and Antonaci, P. (2016) 'A study on the main factors affecting the performance of self-sensing concrete', *Advances in Cement Research*, pp. 1–14. doi: 10.1680/jadcr.15.00147.

Astm:C192/C192M-13 (2013) 'Standard Practice for Making and Curing Concrete Test Specimens in the Laboratory', *ASTM International*, 4, pp. 1–8. doi: 10.1520/C0192.

ASTM C78 (2012) 'Standard Test Method for Flexural Strength of Concrete (Using Simple Beam With Center-Point Loading)', *ASTM International, West Conshohocken, PA*, pp. 12–14. doi: 10.1520/C0293.

ASTMC136/C136M-14 (2014) *Standard Test Method for Sieve Analysis of Fine and Coarse Aggregates*, *ASTM International, West Conshohocken, PA*.

ASTMC39/C39M-04a (2004) 'Standard Test Method for Compressive Strength of Cylindrical Concrete Specimens', *ASTM International, West Conshohocken, PA*.

Azhari, F. and Banthia, N. (2012) 'Cement-based sensors with carbon fibers and carbon nanotubes for piezoresistive sensing', *Cement and Concrete Composites*. Elsevier Ltd, 34(7), pp. 866–873. doi: 10.1016/j.cemconcomp.2012.04.007.

Baeza, F. J., Galao, O., Zornoza, E. and Garcés, P. (2013) 'Multifunctional cement composites strain and damage sensors applied on reinforced concrete (RC) structural elements', *Materials*, 6(3), pp. 841–855. doi: 10.3390/ma6030841.

Barber, W. (2005) 'Anaerobic Digester Foaming; Causes and Solutions.pdf', in *Proceedings of the Water Environment Federation, WEFTEC 2002: Session 51 through Session 60*, p. 303–310(8).

Behnia, A., Chai, H. K. and Shiotani, T. (2014) 'Advanced structural health monitoring of concrete structures with the aid of acoustic emission', *Construction and Building Materials*. Elsevier Ltd, 65, pp. 282–302. doi: 10.1016/j.conbuildmat.2014.04.103.

Bennett, E. W. (1980) 'Fatigue of plain concrete in compression under varying sequences of two-level programme loading', *International Journal of Fatigue*, 78(4), pp. 171–175.

Bontea, D.-M., Chung, D. D. L. and Lee, G. C. (2000) 'Damage in carbon fiber-reinforced concrete, monitored by electrical resistance measurement', *Cement and Concrete Research*, 30(4), pp. 651–659. doi: 10.1016/S0008-8846(00)00204-0.

Camponeschi, E., Florkowski, B., Vance, R., Garrett, G., Garmestani, H. and Tannenbaum, R. (2006) 'Uniform directional alignment of single-walled carbon nanotubes in viscous polymer flow', *Langmuir*, 22(4), pp. 1858–1862. doi: 10.1021/la052714z.

Chang, D. Il and Chai, W. K. (1995) 'Flexural fracture and fatigue behavior of steel-fiber-reinforced concrete structures', *Nuclear Engineering and Design*, 156(1–2), pp. 201–207. doi: 10.1016/0029-5493(94)00946-V.

Chen, B. and Liu, J. (2007) 'Damage in carbon fiber-reinforced concrete, monitored by both electrical resistance measurement and acoustic emission analysis', *Construction and Building Materials*, 22, pp. 2196–2201.

Chen, P.-W. and Chung, D. D. L. (1993) 'Carbon fiber reinforced concrete for smart structures capable of non-destructive flaw detection', *Smart Materials and Structures*, 2(1), pp. 22–30. doi: 10.1088/0964-1726/2/1/004.

Chen, P.-W. and Chung, D. D. L. (1996) 'Carbon fiber reinforced concrete as an intrinsically smart concrete for damage assessment during static and dynamic loading.pdf', *ACI Materials Journal*, 93(4), pp. 341–350.

Chen, S. J., Collins, F. G., Macleod, A. J. N., Pan, Z., Duan, W. H. and Wang, C. M. (2011) 'Carbon nanotube–cement composites: A retrospect', *The IES Journal Part A: Civil & Structural Engineering*, 4(4), pp. 254–265. doi: 10.1080/19373260.2011.615474.

Chung, D. D. L. (1995) 'Strain sensors based on the electrical resistance change accompanying the reversible pull-out of conducting short fibers in a less conducting matrix', *Smart Materials and Structures*, 4(1), p. 59. Available at: http://stacks.iop.org/0964-1726/4/i=1/a=009.

Chung, D. D. L. (1998) 'Self-monitoring structural materials', *Materials Science and Engineering: R: Reports*, 22(2), pp. 57–78. doi: 10.1016/S0927-796X(97)00021-1.

Coleman, J. N., Khan, U., Blau, W. J. and Gun'ko, Y. K. (2006) 'Small but strong: A review of the mechanical properties of carbon nanotube–polymer composites', *Carbon*, 44(9), pp. 1624–1652. doi: 10.1016/j.carbon.2006.02.038.

Cui, S., Canet, R., Derre, A., Couzi, M. and Delhaes, P. (2003) 'Characterization of multiwall carbon nanotubes and influence of surfactant in the nanocomposite processing', *Carbon*, 41(4), pp. 797–809. doi: 10.1016/S0008-6223(02)00405-0.

D'Alessandro, A., Rallini, M., Ubertini, F., Materazzi, A. L. and Kenny, J. M. (2016) 'Investigations on scalable fabrication procedures for self-sensing carbon nanotube cement-matrix composites for SHM applications', *Cement and Concrete Composites*, 65(November

2015), pp. 200–213. doi: 10.1016/j.cemconcomp.2015.11.001.

Daghash, S. M., Tarefder, R. and Taha, M. M. R. (2015) 'A New Class of Polymer Concrete with Improved Fatigue Strength Using Carbon Nanotubes Conference', in, pp. 377–382. doi: 10.1007/978-3-319-17088-6.

Demčenko, A., Visser, H. A. and Akkerman, R. (2016) 'Ultrasonic measurements of undamaged concrete layer thickness in a deteriorated concrete structure', *NDT and E International*, 77(2016), pp. 63–72. doi: 10.1016/j.ndteint.2015.09.005.

Du, H., Quek, S. T. and Pang, S. D. (2013) 'Smart multifunctional cement mortar containing graphite nanoplatelet', *Sensors and Smart Structures Technologies for Civil, Mechanical, and Aerospace Systems*, 8692(APRIL 2013), pp. 1–10. doi: 10.1117/12.2009005.

Dyke, C. A. and Tour, J. M. (2004) 'Overcoming the Insolubility of Carbon Nanotubes Through High Degrees of Sidewall Functionalization', *Chemistry - A European Journal*, 10(4), pp. 812–817. doi: 10.1002/chem.200305534.

Frmyr, T. R., Hansen, F. K. and Olsen, T. (2012) 'The optimum dispersion of carbon nanotubes for epoxy nanocomposites: Evolution of the particle size distribution by ultrasonic treatment', *Journal of Nanotechnology*, 2012(Article ID 545930), p. 14. doi: 10.1155/2012/545930.

Fu, X. and Chung, D. D. L. (1996) 'Self-monitoring of fatigue damage in carbon fiber reinforced cement', *Cement and Concrete Research*, 26(1), pp. 15–20. doi: 10.1016/0008-8846(95)00184-0.

Fu, X., Ma, E., Chung, D. D. L. and Anderson, W. A. (1997) 'Self-monitoring in carbon fiber reinforced mortar by reactance measurement', *Cement and Concrete Research*, 27(6), pp. 845–852. doi: http://dx.doi.org/10.1016/S0008-8846(97)83277-2.

Galao, O., Baeza, F. J., Zornoza, E. and Garcés, P. (2014) 'Strain and damage sensing properties on multifunctional cement composites with CNF admixture', *Cement and Concrete Composites*. Elsevier Ltd, 46(2014), pp. 90–98. doi: 10.1016/j.cemconcomp.2013.11.009.

Gopalakrishnan, K., Bjorn Birgisson, P. T. and (Eds.), and N. O. A.-O. (2011) *Nanotechnology in Civil Infrastructure A Paradigm Shift*. Springer-Verlag Berlin Heidelberg. doi: 10.1007/978-3-642-16657-0.

Graham (1970) 'Theory of cross-correlation of signal and idler in parametric oscillators', *Physics Letters A*, 32(6), pp. 373–374.

Griffiths, G. and Thom, N. (2007) *Concrete Pavement Design Guidance Notes*. Taylor &Francis.

Han, B. (2006) *Properties, sensors and structures of pressure- sensitive carbon fiber*

cement paste. Dissertation for the Doctor Degree in Engineering. Harbin Institute of Technology. Harbin Institute of Technology, Harbin, China.

Han, B. . b, Yu, X. ., Zhang, K. ., Kwon, E. . and Ou, J. . d (2011) 'Sensing properties of CNT-filled cement-based stress sensors', *Journal of Civil Structural Health Monitoring*, 1(1–2), pp. 17–24. doi: 10.1007/s13349-010-0001-5.

Han, B., Ding, S. and Yu, X. (2015) 'Intrinsic self-sensing concrete and structures: A review', *Measurement*. Elsevier Ltd, 59, pp. 110–128. doi: 10.1016/j.measurement.2014.09.048.

Han, B. and Ou, J. (2007) 'Embedded piezoresistive cement-based stress/strain sensor', *Sensors and Actuators, A: Physical*, 138(2), pp. 294–298.

Han, B., Sun, S., Ding, S., Zhang, L., Yu, X. and Ou, J. (2015) 'Review of nanocarbon-engineered multifunctional cementitious composites', *Composites Part A: Applied Science and Manufacturing*. Elsevier Ltd, 70, pp. 69–81. doi: 10.1016/j.compositesa.2014.12.002.

Han, B., Yu, X. and Kwon, E. (2009) 'A self-sensing carbon nanotube/cement composite for traffic monitoring.', *Nanotechnology*, 20(44), p. 445501.

Han, B., Yu, X. and Ou, J. (2014) 'Chapter 5 - Sensing Properties of Self-Sensing Concrete', in *Self-Sensing Concrete in Smart Structures*, pp. 95–162. doi: http://dx.doi.org/10.1016/B978-0-12-800517-0.00005-8.

Han, B., Yu, X. and Ou, J. (2015) *Self-Sensing Concrete in Smart Structures*, *elsevier*. Elsevier B.V.

Han, B., Zhang, K., Yu, X., Kwon, E. and Ou, J. (2012) 'Electrical characteristics and pressure-sensitive response measurements of carboxyl MWNT/cement composites', *Cement and Concrete Composites*. Elsevier Ltd, 34(6), pp. 794–800. doi: 10.1016/j.cemconcomp.2012.02.012.

Han, B., Zhang, K., Yu, X., Kwon, E. and Ou, J. (2012) 'Fabrication of Piezoresistive CNT/CNF Cementitious Composites with Superplasticizer as Dispersant', *Journal of Materials in Civil Engineering*, 24(6), pp. 658–665.

Hanson, J. M., Antrim, J. D., Brown, E. I., Hiisdorf, H. K., Segner, E. P. and Hawkins, N. M. (1997) *Considerations for Design of Concrete Structures Subjected to Fatigue Loading Reported by ACI Committee 215*, *ACI 215R-74*.

Hilding, J., Grulke, E. a., George Zhang, Z. and Lockwood, F. (2003) 'Dispersion of Carbon Nanotubes in Liquids', *Journal of Dispersion Science and Technology*, 24(1), pp. 1–41. doi: 10.1081/DIS-120017941.

Horii, H., B, H. C. S. and Pallewatta, T. M. (1992) 'Mechanism of fatigue crack growth in concrete', *Cement and Concrete Composites*, 14(2).

Hou, T.-C. and Lynch, J. P. (2005) 'Conductivity-based strain monitoring and damage characterization of fiber reinforced cementitious structural components', *Proc. of SPIE Vol.*,

5765, pp. 419–429. doi: 10.1117/12.599955.

Hsu, T. T. C. (1984) 'Fatigue and microcracking of concrete', *Matériaux et Construction*, 17(1), pp. 51–54. doi: 10.1007/BF02474056.

Huali, J., Huicai, X. and Jinwei, L. (2003) 'The effect of fiber content on the mechanical properties and Pressure-sensitivity of CFRC', *CHINA BUILDING SCIENCE CORE PERIODICAL*, (12), pp. 21–32.

Ibarra, Y. S. De, Gaitero, J. J. and Campillo, I. (2005) 'ANALYSIS BY ATOMIC FORCE MICROSCOPY OF THE EFFECTS ON THE NANOINDENTATION HARDNESS OF CEMENT PASTES BY the introduction of nanotube dispersions', in *TNT2005*. Oviedo-Spain, pp. 2–3.

Islam, M. F., Rojas, E., Bergey, D. M., Johnson, A. T. and Yodh, A. G. (2003) 'High weight fraction surfactant solubilization of single-wall carbon nanotubes in water', *Nano Letters*, 3(2), pp. 269–273. doi: 10.1021/nl025924u.

Khare, R. and Bose, S. (2005) 'Carbon Nanotube Based Composites- A Review', *Journal of Minerals & Materials Characterization & Engineering*, 4(1), pp. 31–46. doi: Vol. 4, No.1.

Kim, H. K., Park, I. S. and Lee, H. K. (2014) 'Improved piezoresistive sensitivity and stability of CNT/cement mortar composites with low water-binder ratio', *Composite Structures*. Elsevier Ltd, 116, pp. 713–719. doi: 10.1016/j.compstruct.2014.06.007.

Kolluru, S. V, O'Neil, E. F., Popovics, J. S. and Shah, S. P. (2000) 'Crack Propagation in flexural fatigue of Concrete', *Journal of Engineering Mechanics*, 126(9), pp. 891–898. doi: 10.1061/(ASCE)0733-9399(2000)126.

Konsta-Gdoutos, M. S. and Aza, C. A. (2014) 'Self sensing carbon nanotube (CNT) and nanofiber (CNF) cementitious composites for real time damage assessment in smart structures', *Cement and Concrete Composites*. Elsevier Ltd, 53, pp. 162–169. doi: 10.1016/j.cemconcomp.2014.07.003.

Konsta-Gdoutos, M. S., Metaxa, Z. S. and Shah, S. P. (2010) 'Highly dispersed carbon nanotube reinforced cement based materials', *Cement and Concrete Research*. Elsevier Ltd, 40(7), pp. 1052–1059. doi: 10.1016/j.cemconres.2010.02.015.

Lee, M. K. and Barr, B. I. G. (2004) 'An overview of the fatigue behaviour of plain and fibre reinforced concrete', *Cement & Concrete Composites*, 26, pp. 299–305. doi: 10.1016/S0958-9465(02)00139-7.

Li, H., Zhang, M. and Ou, J. (2006) 'Abrasion resistance of concrete containing nano-particles for pavement', *Wear*, 260(11–12), pp. 1262–1266. doi: 10.1016/j.wear.2005.08.006.

Luo, J., Duan, Z. and Li, H. (2009) 'The influence of surfactants on the processing of multi-walled carbon nanotubes in reinforced cement matrix composites', *Physica Status Solidi (A) Applications and Materials Science*, 206(12), pp. 2783–2790. doi:

10.1002/pssa.200824310.

Mailhot, T., Bissonnette, B., Saucier, F. and Pigeon, M. (2001) 'Flexural fatigue behavior of steel fibre reinforced concrete before and after cracking', *Materials and Structures*, 34(6), pp. 351–359. doi: 10.1007/BF02486486.

Materazzi, A. L., Ubertini, F. and D'Alessandro, A. (2013) 'Carbon nanotube cement-based transducers for dynamic sensing of strain', *Cement and Concrete Composites*, 37(2013), pp. 2–11.

N. Banthia, S. D. and Pigeon, M. (1992) 'ELECTRICAL RESISTIVITY OF CARBON AND STEEL MICRO-FIBER REINFORCED CEMENTS', *Cement and Concrete Research*, 22, pp. 804–814.

Nasibulin, A. G., Koltsova, T., Nasibulina, L. I., Anoshkin, I. V., Semencha, A., Tolochko, O. V. and Kauppinen, E. I. (2013) 'A novel approach to composite preparation by direct synthesis of carbon nanomaterial on matrix or filler particles', *Acta Materialia*, 61(6), pp. 1862–1871. doi: 10.1016/j.actamat.2012.12.007.

NCHRP1-37A (2004) *PCC REHABILITATION DESIGN OF EXISTING PAVEMENTS*, *Transportation Research Board*. doi: 10.1007/s13398-014-0173-7.2.

O'Connell, M. J., Bachilo, S. M., Huffman, C. B., Moore, V. C., Strano, M. S., Haroz, E. H., Rialon, K. L., Boul, P. J., Noon, W. H., Kittrell, C., Ma, J., Hauge, R. H., Weisman, R. B. and Smalley, R. E. (2010) 'Band Gap Fluorescence from Individual Single-Walled Carbon Nanotubes', *SCIENCE*, 297(2002), pp. 593–596. doi: 10.1126/science.1072631.

Ort´uzar, J. de D. and G.Willumsen, L. (2011) *MODELLING TRANSPORT*. fourth. A John Wiley and Sons, Ltd., Publication.

Parveen, S., Rana, S. and Fangueiro, R. (2013) 'A Review on Nanomaterial Dispersion, Microstructure, and Mechanical Properties of Carbon Nanotube and Nanofiber Reinforced Cementitious Composites', *Journal of Nanomaterials*, 2013, pp. 1–19. doi: 10.1155/2013/710175.

Qu, J. and Han, B. (2008) 'Piezoresistive Cement-based Strain Sensors and Self-sensing Concrete Components', *Journal of Intelligent Material Systems and Structures*, 20(3), pp. 329–336.

Raithby, K. D. (1979) 'Flexural Fatigue Behaviour of Plain Concrete', *Fatigue & Fracture of Engineering Materials and Structures*, 2(3), pp. 269–278. doi: 10.1111/j.1460-2695.1979.tb01085.x.

Rausch, J., Zhuang, R. C. and Mader, E. (2010) 'Surfactant assisted dispersion of functionalized multi-walled carbon nanotubes in aqueous media', *Composites Part A: Applied Science and Manufacturing*. Elsevier Ltd, 41(9), pp. 1038–1046. doi: 10.1016/j.compositesa.2010.03.007.

Rosen, M. J. and Kunjappu, J. T. (2012) *Surfactants and Interfacial Phenomena*. John Wiley and Sons Ltd.

Saafi, M. (2009) 'Wireless and embedded carbon nanotube networks for damage detection in concrete structures.', *Nanotechnology*, 20(39), p. 395502. doi: 10.1088/0957-4484/20/39/395502.

Sendeckyj, G. P. (2001) 'Constant life diagrams — a historical review', *International Journal of Fatigue*, 23(4).

Shah, S. P., Konsta-Gdoutos, M. S., Metaxa, Z. S. and Mondal, P. (2009) 'Nanoscale modification of cementitious materials', *Nanotechnology in Construction 3*, pp. 125–130. doi: 10.1007/978-3-642-00980-8_5.

Sharifi, M. (2012) *the investigation of the interaction of the surfactants with carbon nanotube structures*. Tarbiat Modares University.

Shi, Z. Q. and Chung, D. D. L. (1999) 'Carbon fiber-reinforced concrete for traffic monitoring and weighing in motion', *Cement and Concrete Research*, 29(3), pp. 435–439. doi: 10.1016/S0008-8846(98)00204-X.

Shvartzman-Cohen, R., Levi-Kalisman, Y., Nativ-Roth, E. and Yerushalmi-Rozen, R. (2004) 'Generic approach for dispersing single-walled carbon nanotubes: The strength of a weak interaction', *Langmuir*, 20(15), pp. 6085–6088. doi: 10.1021/la049344j.

Singh, S. P. and Kaushik, S. K. (2000) 'Flexural fatigue life distributions and failure probability of steel fibrous concrete', *Materials Journal*, 97(6), pp. 658–667.

SIXUAN, H. (2012) *MULTIFUNCTIONAL GRAPHITE NANOPLATELETS (GNP) REINFORCED CEMENTITIOUS COMPOSITES HUANG SIXUAN (B . Eng ., Tsinghua University) A THESIS SUBMITTED FOR THE DEGREE OF MASTER OF ENGINEERING*. B. Eng., Tsinghua University.

Slabs, O. F. C., Pavement, E. C. and Equations, F. (2014) 'Fatigue and Static Testing of Concrete Slabs', *TRANSPORTATION RESEARCH RECORD*, (99).

Sohrabi, B. and Nayeri, N. (2014) 'Dispersion of Carbon Nanotubes Using Mixed Surfactants: Experimental and Molecular Dynamics Simulation Studies', *The Journal of Physical Chemistry B*, 118, pp. 3094–103.

Sun, M., Liew, R. J. Y., Zhang, M.-H. and Li, W. (2014) 'Development of cement-based strain sensor for health monitoring of ultra high strength concrete', *Construction and Building Materials*. Elsevier Ltd, 65(2014), pp. 630–637. doi: 10.1016/j.conbuildmat.2014.04.105.

Sun, S., Yu, X. and Han, B. (2014) 'Sensing Mechanism of Self-Monitoring CNT Cementitious Composite', *Journal of Testing and Evaluation*, 42(1), p. 20120302. doi: 10.1520/JTE20120302.

Tan, Y. and Resasco, D. E. (2005) 'Dispersion of single-walled carbon nanotubes of narrow diameter distribution', *Journal of Physical Chemistry B*, 109(30), pp. 14454–14460.

doi: 10.1021/jp052217r.

Trucano, T. G., Swiler, L. P., Igusa, T., Oberkampf, W. L. and Pilch, M. (2006) 'Calibration, validation, and sensitivity analysis: What's what', *Reliability Engineering and System Safety*, 91(10–11), pp. 1331–1357. doi: 10.1016/j.ress.2005.11.031.

Ubertini, F., Materazzi, A. L., D'Alessandro, A. and Laflamme, S. (2014) 'Natural frequencies identification of a reinforced concrete beam using carbon nanotube cement-based sensors', *Engineering Structures*. Elsevier Ltd, 60(2014), pp. 265–275.

Vaisman, L., Wagner, H. D. and Marom, G. (2006) 'The role of surfactants in dispersion of carbon nanotubes', *Advances in Colloid and Interface Science*, 128–130(2006), pp. 37–46. doi: 10.1016/j.cis.2006.11.007.

Vossoughi, F. (2004) *Electrical Resistivity of Carbon Fiber Reinforced Concrete*. Department of Civil Engineering, University of California, Berkeley, CA 94720.

Wang, X., Wang, Y. and Jin, Z. (2002) 'Electrical conductivity characterization and variation of carbon fiber reinforced cement composite', *JOURNAL OF MATERIALS SCIENCE*, 7, pp. 223–227.

Wen, S. and Chung, D. D. . (2001) 'Electric polarization in carbon fiber-reinforced cement', *Cement and Concrete Research*, 31, pp. 141–147.

Wen, S. and Chung, D. D. L. (2002) 'Cement-based materials for stress sensing by dielectric measurement', *Cement and Concrete Research*, 32(9), pp. 1429–1433.

Wen, S. and Chung, D. D. L. (2006) 'Self-sensing of flexural damage and strain in carbon fiber reinforced cement and effect of embedded steel reinforcing bars', *Carbon*, 44(8), pp. 1496–1502. doi: 10.1016/j.carbon.2005.12.009.

Wen, S. and Chung, D. D. L. (2007) 'Double percolation in the electrical conduction in carbon fiber reinforced cement-based materials', *Carbon*, 45, pp. 263–267.

Wilson, J. (2005) *Sensor Technology Handbook*, *elsevier*. Chandler, Arizona, USA: Elsevier Ltd. doi: 10.1016/j.patrec.2005.01.006.

Winterburn, J. B. and Martin, P. J. (2012) 'Foam mitigation and exploitation in biosurfactant production', *Biotechnology Letters*, 34(2), pp. 187–195. doi: 10.1007/s10529-011-0782-6.

Xiao, H., Li, H. and Ou, J. (2011) 'Strain sensing properties of cement-based sensors embedded at various stress zones in a bending concrete beam', *Sensors and Actuators, A: Physical*. Elsevier B.V., 167(2), pp. 581–587. doi: 10.1016/j.sna.2011.03.012.

Xin Jiang, Torsten L. Kowald, Thorsten Staedler, R. H. F. T. (2006) 'Carbon nanotubes as a new reinforcement material for modern cement-based binders', in *2nd International Symposium on Nanotechnology in Construction*, pp. 209–213.

Xue, W., Wang, L., Wang, D. and Druta, C. (2014) 'Pavement Health Monitoring

System Based on an Embedded Sensing Network', *Journal of Materials in Civil Engineering*, 26(10), p. 4014072. doi: 10.1061/(ASCE)MT.1943-5533.0000976.

Yazdanbakhsh, A. (2012) *Production, Characterization, and Mechanical Behavior of Cementitious Materials Incorporating Carbon Nanofibers*.

Yoder, E. J. and Witczak, M. W. (1975) *Principles of Pavement Design*. second. John Wily.

Yu, J., Grossiord, N., Koning, C. E. and Loos, J. (2007) 'Controlling the dispersion of multi-wall carbon nanotubes in aqueous surfactant solution', *Carbon*, 45(3), pp. 618–623. doi: 10.1016/j.carbon.2006.10.010.

Yu, X. and Kwon, E. (2009) 'A carbon nanotube/cement composite with piezoresistive properties', *Smart Materials and Structures*, 18(5), p. 55010. doi: 10.1088/0964-1726/18/5/055010.

Yu, X. and Kwon, E. (2012) *Carbon Nanotube Based Self-sensing Concrete for Pavement Structural Health Monitoring*.

Zhang, B., Phillips, D. V and Wu, K. (1997) 'Further research on fatigue properties of plain concrete', *Magazine of Concrete Research*, 49(180), pp. 241–252. doi: 10.1680/macr.1997.49.180.241.